To the Graduate Council:

I am submitting herewith a thesis written by Rodney Howard Kingrea entitled "Comparison and Correlation of Meteorological Data on the Oak Ridge Reservation: Potential Impacts on Dispersion Modeling of Air Pollutants." I have examined the final copy of this thesis for form and content and recommend that it be accepted in partial fulfillment of the requirements for the degree of Master of Science, with a major in Environmental Engineering.

Wayne T. Davis

Wayne T. Davis, Major Professor

We have read this thesis
and recommend its acceptance:

Terry Miller

Gregory Reed

Accepted for the Council:

C W Minkel

Associate Vice Chancellor
and Dean of the Graduate School

COMPARISON AND CORRELATION OF METEOROLOGICAL DATA ON THE OAK RIDGE RESERVATION: POTENTIAL IMPACTS ON DISPERSION MODELING OF AIR POLLUTANTS

A Thesis

Presented for the

Master of Science

Degree

The University of Tennessee, Knoxville

Rodney Howard Kingrea

May 1993

ACKNOWLEDGMENTS

A sincere appreciation must be granted to Dr. Wayne Davis for significant guidance and technical assistance during the development and preparation of this thesis. In addition, the helpful technical review and critique by Dr. Terry Miller and Dr. Gregory Reed was also appreciated. Review for proper formatting by Ms. Ann Lacava was also very helpful and appreciated. The author also wishes to thank the following Martin Marietta Energy Systems, Inc., employees for their helpful technical review and assistance: Mr. Ron Sharp, Dr. Frank Kornegay, and Mr. Gary Worley. Meteorological data and other information provided by Mr. Sharp was invaluable.

A special appreciation must also be granted to his wife, Lisa Kingrea, for her patience and constant support throughout the development of this thesis.

ABSTRACT

Martin Marietta Energy Systems, Inc., manages three large installations for the Department of Energy (DOE) on the Oak Ridge Reservation (ORR): Y-12 Plant, Oak Ridge National Laboratory, and K-25 Site. The ORR is located in moderately complex terrain with a series of ridges and valleys separating the major facilities. These large and multi-faceted production and research facilities have historically evaluated air pollutant emissions independently. However, with increasing emphasis on risk-based health standards for hazardous air pollutants, it is becoming necessary to integrate the cumulative effects of emissions from each installation on all receptors around the ORR. Historic modeling on the ORR has used Industrial Source Complex (ISC) dispersion model, a straight-line Guassian model that assumes a uniform wind field.

This study compared meteorological data at four monitoring sites typically used for dispersion modeling on the ORR. Annual joint frequency data and hourly data were compared and correlated. Parameters evaluated included wind direction, wind speed, and stability category since these parameters are used directly in dispersion models. Review of annual frequency data found significant differences in wind direction between the sites, especially when the two towers at the Y-12 Plant were compared. It appears that the Y-12 Plant East tower is highly influenced by an adjacent flow-equalization basin and valley cross-roads. The evaluation of hourly data found that wind direction varied significantly from one site to another, especially during light winds and stable conditions. During high winds and neutral conditions, wind direction data compared more favorably. Although wind speed and stability category also showed some variation, the variations were not as significant as wind

direction.

Dispersion modeling of unit releases (1 g/s) using ISC was conducted for three hypothetical emission points at the Y-12 Plant, ORNL, and K-25 Site. In addition, a unit release was also modeled for the Toxic Substance Control Act Incinerator at the K-25 Site. Each emission point was modeled using each of the four sets of meteorological data. Therefore, actual modeling results served as another tool in comparing the difference in the combined effect of all meteorological parameters.

Annual and 1-hour average concentrations were evaluated because they represent the most commonly used averaging periods when evaluating hazardous air pollutants. For all emission points, maximum annual concentration varied by approximately a factor of two when using each of the meteorological data sets. Maximum 1-hour concentration varied from less than 10 percent to 30 percent, depending upon the meteorological data used. The magnitudes of maximum concentrations did not show as significant variation as the meteorological data. However, the locations of maximum concentration showed greater variability when using the different meteorological data. Locations of annual average concentrations were most greatly affected by the primary wind directions and proximity from the source to the ORR boundary. Locations of maximum 1-hour concentrations were significantly affected by the elevation of the receptor. In only one case, did maximum 1-hour concentration occur at the receptor nearest to the source. In all cases, maximum 1-hour concentration occurred at receptors near or above the stack height.

TABLE OF CONTENTS

LIST OF TABLES

LIST OF TABLES (continued)

LIST OF FIGURES

LIST OF FIGURES (continued)

FIGURE PAGE

LIST OF FIGURES (continued)

LIST OF FIGURES (continued)

LIST OF ABBREVIATIONS AND SYMBOLS

CONC	Concentration
DOE	Department of Energy
$\Delta T/\Delta Z$	Vertical Temperature Gradient
EPA	U.S. Environmental Protection Agency
g/s	Grams Per Second
ISCLT	Industrial Source Complex Long Term
ISCST2	Industrial Source Complex Short-Term Version 2
kg	Kilogram
KPOINT	Modeled release point for K-25 Site
KTSCA	Modeled release point for TSCA Incinerator
K25	K-25 Site Meteorological Tower
Lbs	Pounds
m	meter
OMDRAP	ORNL Meteorological Data Retrieval and Analysis Program
ORNL	Oak Ridge National Laboratory
ORR	Oak Ridge Reservation
σ_A	Standard Deviation of Horizontal Wind Direction
σ_y	Standard Deviation of Lateral Dispersion
σ_z	Standard Deviation of Vertical Dispersion
STAR	Stability Array Data
TSCA	Toxic Substances Control Act
$\mu g/m^3$	Microgram per cubic meter
XPOINT	Modeled release point for Oak Ridge National Laboratory
χ/Q	Concentration per Unit Emission ($\mu g/m^3$ per g/s)
X10	ORNL Meteorological Tower
YE	Y-12 Plant East Meteorological Tower
YPOINT	Modeled release point for the Y-12 Plant
YW	Y-12 Plant West Meteorological Tower

CHAPTER 1

INTRODUCTION

1.1 FACILITY DESCRIPTION

Martin Marietta Energy Systems, Inc., (Energy Systems) manages three large installations for the Department of Energy (DOE) on the Oak Ridge Reservation (ORR) near Oak Ridge, Tennessee: the Y-12 Plant, Oak Ridge National Laboratory (ORNL), and the K-25 Site. Each of these installations contain a number of highly complex and unique production and research facilities. Air pollutant emissions from these facilities include all of the criteria pollutants and a number of hazardous air pollutants, including radionuclides.

The Y-12 Plant's primary mission is fabrication of component parts for the nation's nuclear weapon arsenal and conducting related research and development activities. ORNL is a multipurpose research and development center in the physical, biomedical, and environmental sciences; nuclear and engineering technologies; and advanced energy systems. The K-25 Site, previously the Oak Ridge Gaseous Diffusion Plant, is now responsible for a variety of research and development activities including the development of atomic vapor laser isotope separation (AVLIS) technology for use in uranium enrichment. In addition, the K-25 Site serves as a center for a variety of waste management activities including the Toxic Substances Control Act (TSCA) Incinerator. The TSCA Incinerator is one of the few incinerators in the world permitted to burn radioactive hazardous waste (i.e., mixed waste).

1.2 SITE TOPOGRAPHY AND METEOROLOGY

The ORR consists of approximately 35,000 acres of federally owned land and is located in the Tennessee Valley between the Cumberland Mountains to the west and the Great Smokey Mountains to the east. The valley is approximately 60 to 70 km wide, has a mean elevation of approximately 300 m and is characterized by a series of ridges and valleys oriented from southwest to northeast. Ridges in the vicinity of the ORR typically rise 100 m above the valley bottoms. The valley floor generally descends from the northeast to the southwest along a 53 to 233 degree axis; however, some minor variations in slope and ridge alignment do occur. Each of the three major installations are located in three different valley bottoms. The Y-12 Plant is located in Bear Creek Valley; ORNL is located in Bethel Valley; and the K-25 Site is located in a wider but unnamed valley. The approximate widths of Bear Creek and Bethel Valley are 1.2 and 2.5 km, respectively. The K-25 Site is located in a valley approximately 3.8 km wide. Figure 1-1 provides a contour map of the Oak Ridge area [1].

Meteorology of the ORR is highly influenced by the valleys and ridges characteristic of the area. Specifically, the wind patterns in the area are largely controlled by the valley and ridge topography. Prevailing winds are generally up-valley (northeasterly) or down-valley (southwesterly). As a result of the valleys and ridges, the ORR has been characterized as moderately complex terrain [2]. In addition, the ORR is characterized by very light winds. Seventy-five percent of the time during 1991, the average wind on the ORR was less than 7.4 miles per hour (3.3 m/s) [3].

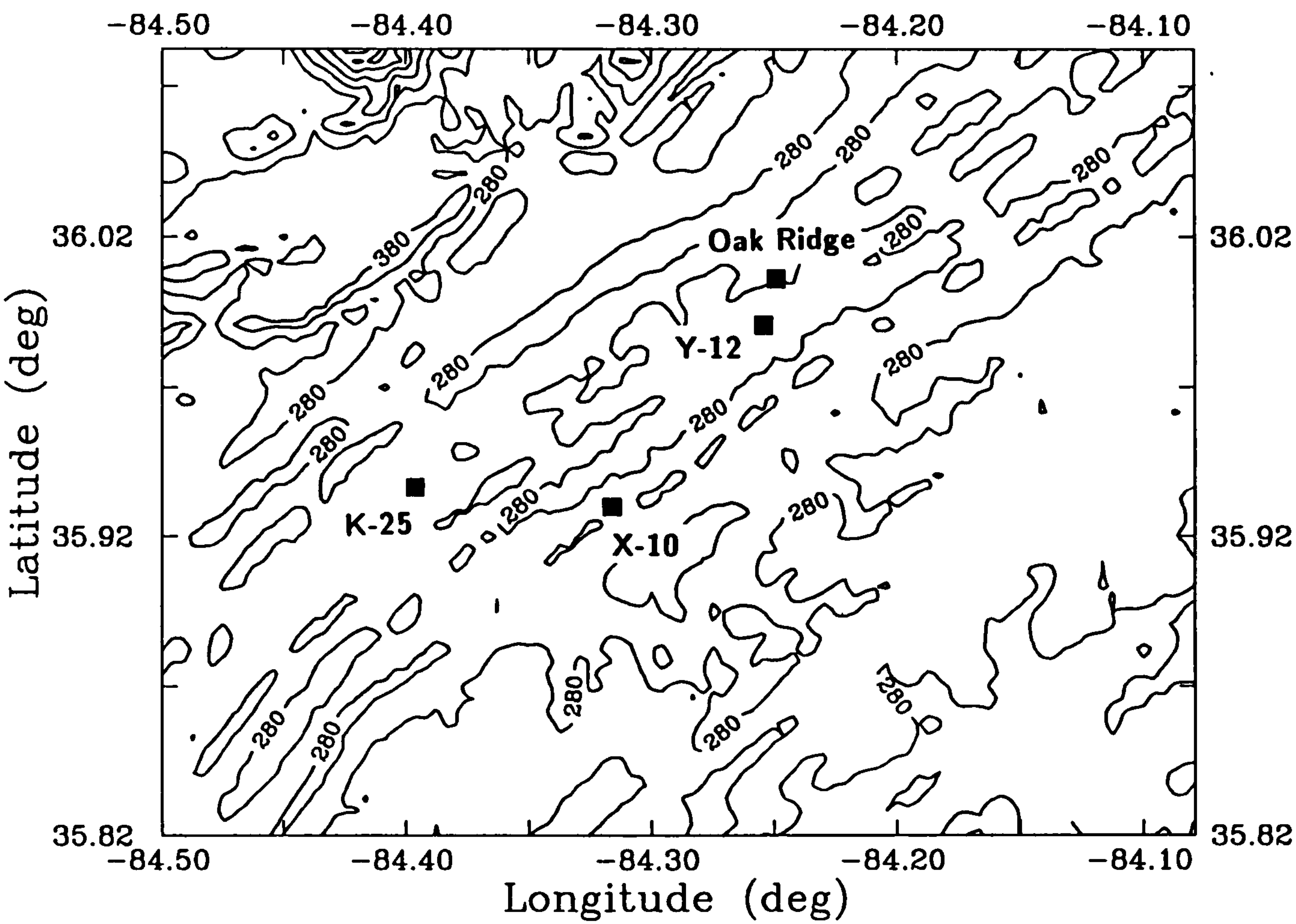

Figure 1-1: Contour Map of the Oak Ridge Area (Contours are in 100 m intervals).

Source: National Oceanic and Atmospheric Administration, "Preliminary Analysis of Wind Data from the Oak Ridge Site Survey," NOAA Publication ERL -193, February 1992, Atmospheric Turbulence and Diffusion Division, Oak Ridge, Tennessee, p. 5 [1].

1.3 BACKGROUND

Air quality planning on the ORR has historically been managed independently by the three major installations. With the exception of radionuclides, very few efforts have been made to integrate the effects of emissions from all of the installations. As a result, when conducting air dispersion modeling studies, it was necessary to only consider emissions from one installation at a time. However, in order to implement an integrated air quality management program, it is necessary to consider cumulative effects and impacts of emissions from all installations, particularly for hazardous air pollutants. As a result, it becomes more important to predict pollutant concentrations resulting from emissions from each installation at all receptors around the ORR as opposed to only those receptors in the immediate vicinity of the emission point.

For example, when estimating emissions and resulting concentration for a pollutant emitted from the K-25 Site, modelers in the past were only interested in the receptor with the maximum concentration which typically occurred close to the site. In this case, consideration was not given to lower concentrations of pollutants which may occur at farther distances. However, recognizing that more than one installation on the ORR may be emitting the same pollutant, it is necessary to consider cumulative concentrations at receptors which may be impacted by two or more sites. Therefore, it is also important to predict concentrations at receptors which may not be located immediately adjacent to the source.

Complex topography on the ORR makes selection of representative meteorological data difficult, especially when predicting concentrations at significant distances from the source. The regulatory models historically used on the ORR employ the straight-line gaussian equation and accept only one set of meteorological data per model run. As a result, the modeler must use judgement to select the meteorological data which is believed most representative.

1.4 OBJECTIVES

The objectives of this study are: (1) to compare, contrast, and correlate meteorological data on the ORR, and (2) to determine potential impacts on dispersion modeling of air pollutants using the different meteorological data. It is hopeful that this study can be used by those responsible for dispersion modeling on the ORR to better understand the effects of complex terrain on local meteorology and its potential impacts on pollutant dispersion modeling.

1.5 APPROACH

The approach used in accomplishing the stated objectives is briefly summarized below:

(1) A literature review was conducted of various statistical techniques typically used to characterize and compare meteorological data and to review and evaluate related research projects.

(2) Annual joint frequency and hourly meteorological data from selected meteorological towers on the ORR were compared, contrasted, and correlated using a variety of statistical techniques.

(3) Computer dispersion modeling using selected meteorological data on the ORR was conducted. Results of the modeling were used to highlight differences in meteorological data and to demonstrate the associated impacts on modeling of air pollutants in the ORR.

This study in no way establishes policy for the DOE or Energy Systems for the design and operation of ambient air monitoring programs or control of air pollutants. Instead, this report may be used by DOE and/or Energy Systems as an informational source and tool in establishing necessary policy and procedures. Further, it must also be noted that results of this study should not be used for regulatory compliance purposes since a number of simplifying assumptions were necessary to accomplish the stated objectives.

CHAPTER 2

LITERATURE REVIEW

2.1 STATISTICAL TECHNIQUES

In the analysis of earth science data, such as meteorological data, it is often necessary to compare two data sets or distributions. Comparison of two variables is referred to as bivariate analysis. In this study, different meteorological data sets will be compared, contrasted, and correlated using various statistical techniques. In addition, concentrations calculated from dispersion modeling using different meteorological data will also be compared. Listed below are the statistical tools which are used in this study.

2.1.1 Frequency Distributions

A common univariate statistical tool is the frequency distribution or cumulative frequency distribution. Frequency distribution is classification of the elements of a data set by a quantitative characteristic [4]. The frequency distribution simply provides the frequency (in percent) that a particular event occurs. For example, wind direction is commonly characterized by frequency distributions. In this case, the percentage of time that wind blowing from each of the 16 primary wind directions is provided in a table or diagram. Other methods of illustrating frequency distribution data include histograms and frequency polygons. Two or more frequency distributions can be readily compared and contrasted if they have the same class intervals and are both expressed in percent.

Frequency distribution data can also be expressed as cumulative frequency distribution data. In this case, the percentage of time that elements of a data set have values above or below certain levels are calculated. This technique is very effective in summarizing information and can be used as a tool in comparing multiple data sets. A line graph can be used to visually illustrate cumulative frequency distribution data.

2.1.2 Scatterplots

One of the most common graphical tools used in displaying relationships and correlation among two variables is a scatterplot. A scatterplot is an x-y graph of data where one variable is plotted on the x-axis and the second variable on the y-axis. By visual comparison, qualitative conclusions about the data sets can be made. Three general conclusions can be made. First, the data may be positively correlated which indicates that as one variable increases, the second variable also increases. Second, the data may be negatively correlated if one variable increases and the other decreases. And third, the data may be uncorrelated. In this case, there is no apparent relationship between the two variables. In addition to determining relative correlation, the scatterplot is an effective tool in identifying questionable or errant data [5]. It is common in scatterplots to provide a line which indicates perfect correlation. The line is typically at a 45 degree angle in the plot and can be used as a visual aid in determining relative degree of correlation and comparison of the data.

2.1.3 Correlation Coefficient

The correlation coefficient is a statistical tool which is used to quantify the relationship, or lack of relationship, between two variables. The correlation coefficient may be used to describe data provided in a scatterplot. The correlation coefficient (r) is calculated as follows [6]:

$$r = \sum_{i=1}^{n} \frac{(x_i - m_y)(y_i - m_y)}{n\sigma_x\sigma_y} \tag{2-1}$$

where: x_i = a data value for the first variable,

m_x = the mean of the first variable,

y_i = a data value for the second variable,

m_y = the mean of the second variable,

n = the number of data values,

σ_x = the standard deviation of the first variable, and

σ_y = the standard deviation of the second variable.

The correlation coefficient is actually a measure of how close two data sets fall on a straight line. When r = 1.0, the data is positively correlated and the scatterplot will be a straight line with a positive slope. When r = -1.0, the data is negatively correlated and the scatterplot will be a straight line with a negative slope. The higher the absolute value of the correlation coefficient, the better the correlation.

2.1.4 Linear Regression

Linear regression is a technique used to characterize data which is linearly related. The basic equation for a straight line is:

$$y = ax + b \tag{2-2}$$

where: a = slope of the line, and

b= the y-intercept.

The linear regression model allows for the estimation of the slope and y-intercept using the following equations:

$$a = r \frac{\sigma_y}{\sigma_x} \tag{2-3}$$

$$b = m_y - am_x \tag{2-4}$$

Data sets which are equivalent would have a correlation coefficient of one, a slope of one and a y-intercept of zero.

2.1.5 Statistics of Directional Data

In most cases, conventional statistical tools cannot be used for directional data such as wind direction. For example, it is inappropriate to employ conventional linear techniques to average wind directions of 359 degrees and 1 degree. The arithmetic mean would be 180 degrees; however, the actual mean value is zero degrees since the two angles are only separated by two degrees. Therefore, special consideration is needed for calculating mean and standard deviation of wind direction. These methods are briefly discussed below.

The mean wind direction can be obtained by assuming a unit vector (magnitude = 1.0 unit) and breaking the vector down into its u- and v- components. The u-component is typically east to west with east being positive, and the v-component is north to south with north being positive. For each component (u and v), the mean value of all the observations is calculated. The mean wind direction is then calculated by using conventional trigonometric functions to calculate the angle between the mean u- and v-components [7].

Standard deviation of the horizontal wind direction, σ_A, also requires special consideration. Several methods are available for calculation of σ_A ; however, the method outlined by Mardia [8] and discussed in *On-Site Meteorological Program Guidance for Regulatory Modeling Applications* [9] is described herein. The following notation convention is used: A_i = horizontal wind direction, measured clockwise from north, values restricted to between 001 and 360 (inclusive) and; n = number of measurements. Standard deviation of horizontal wind direction, σ_A, (in radians) is calculated by use of the following equations:

$$\sigma_A = \sqrt{-2\ln(R)} \tag{2-5}$$

where the parameters R, S_a, and C_a are defined below:

$$R = \sqrt{(S_a^2 + C_a^2)} \tag{2-6}$$

$$S_a = \left(\frac{1}{N}\right) \sum \sin(A_i) \tag{2-7}$$

$$C_a = \left(\frac{1}{N}\right) \sum \cos(A_i) \tag{2-8}$$

2.2 ATMOSPHERIC DISPERSION MODELS

The Industrial Source Complex (ISC) model has historically been used by DOE and state regulatory agencies for dispersion modeling studies on the ORR. The ISC model is based upon the straight-line, steady-state Gaussian plume equation with some modifications to predict ambient concentrations of pollutants given certain input parameters. The modified Gaussian equation used to predict concentration (χ) with Industrial Source Complex, Version 2 (ISCST2) is provided below: [10]:

$$\chi = \frac{QKVD}{2\pi u_s \sigma_y \sigma_z} \exp[-0.5 \left(\frac{Y}{\sigma_y}\right)^2] \qquad (2\text{-}9)$$

where: Y = cross-wind distance (m)

Q = pollutant emission rate (mass per time)

K = a scaling coefficient to convert to desired units

V = vertical term

D = decay term

σ_y, σ_z = standard deviation of lateral and vertical dispersion

u = mean wind speed (m/s)

The computer code allows various emission types to be modeled including point, area, and volume sources, and has algorithms to account for building downwash and stack-tip downwash effects. ISCST2 accepts hourly meteorological data to define conditions for plume rise, transport, and diffusion. Industrial Source Complex Long Term, Version 2 (ISCLT2) uses stability array data as meteorological input as discussed in Section 2.3.4.

Concentration and deposition estimates can be made for each source and for a variety of user specified averaging periods. ISC2 replaced the initial version of Industrial Source Code (ISC) model and includes improvements in computer code, user interface, and end user documentation [11]. ISC2 can be run with flat or simple terrain considerations. For this study, both ISCST2 and ISCLT2 were utilized. Hereforward, ISCST2 and ISCLT2 will be referred to as ISCST and ISCLT, respectively.

2.3 METEOROLOGICAL PARAMETERS

Three of the most important meteorological parameters used in applying the Gaussian equation are wind speed, wind direction, and atmospheric stability class. Each of these parameters is discussed below.

2.3.1 Wind Speed

Wind speed appears in the denominator of the Gaussian equation and determines the amount of initial dilution experienced by a plume. Therefore, concentration is inversely proportional to wind speed. Wind speed is also used in other equations for determining plume rise and downwash effects. In addition, wind speed is also used in some methods to determine atmospheric stability (see Section 2.3.3). Wind speed is measured directly using cup anemometers, propeller anemometers, or wind speed transducers. For most instruments, the minimum speed that can be accurately measured is 0.5 m/s. This speed is referred to as the threshold speed for the instrument. Wind measurement systems can typically measure wind speed to within plus or minus 0.2 m/s. [12].

Calm or light winds cause problems in modeling applications since the Gaussian equation assumes that concentration is inversely proportional to wind speed. Concentrations become unrealistically large when wind speeds less than 1 m/s are input into most models (i.e., concentration approaches infinity as wind speed approaches zero). For this reason, many Gaussian-based models substitute a 1.0 m/s wind speed for all wind speeds less than 1.0 m/s [13].

2.3.2 Wind Direction

Wind direction is defined as the orientation of the wind vector in the horizontal and ranges from one to 360 degrees. In conventional meteorological notation, wind direction is defined as the direction from which the wind is blowing. However, for the ISCST model, the direction input to the model is the direction toward which the wind is blowing. Meteorological input data used in ISCLT uses conventional meteorological notation. Throughout this report, conventional meteorological notation will be used.

Wind direction is a very important parameter because it determines the transport direction for the plume in Gaussian models. Wind direction is measured using wind vanes and wind direction transducers. The threshold speed for most wind direction devices is 0.5 m/s, and system accuracies are at least plus or minus 5 degrees [14]. Like wind speed, special consideration is needed for wind direction during calm wind conditions. During calm wind periods, wind direction cannot be accurately measured. Therefore, many models, including ISCST, set the wind direction equal to the value reported during the last non-calm hour [15].

Wind occurs as a result of pressure gradients caused by differential heating. Such differential heating and resulting pressure gradients can occur on both the local and global scale. Consider a pressure gradient which exists due to differential heating. In a non-rotating system, a parcel of air would be accelerated from high pressure to low pressure. However, since the earth is rotating, any parcel moving in the northern hemisphere will be deflected to the right due to the Coriolis force. For equilibrium to be achieved (i.e., the parcel moves at a constant velocity and does not accelerate), the pressure gradient force and the Coriolis force must be equal and in opposite directions. When this occurs, the wind direction is parallel to the isobars (lines of equal pressure) with low pressure to the left and high pressure to the right. The wind is known as the geostrophic wind and is illustrated in Figure 2-1 (a).

The geostrophic wind is an idealized situation and can only occur when frictional and centrifugal forces are not present (i.e, above the earth's boundary layer and when the isobars do not have curvature). Therefore, the geostrophic wind is used to approximate wind conditions above the earth's surface. However, from the surface to approximately 1 km, effects of surface friction cannot be ignored and result in additional forces that modify the wind direction. As an air parcel moves in the lower atmosphere, frictional forces tend to reduce its speed. Since the Coriolis force is directly proportional to wind speed, the equilibrium between the pressure gradient force and Coriolis force is disrupted. As a result, the pressure gradient force exceeds the Coriolis force and the wind blows across the isobars toward higher pressure. Figure 2-1 (b) provides a graphical illustration of the force diagram. The angle between the geostrophic (upper air) wind and surface wind depends upon stability and surface roughness and can range from approximately 10 degrees during unstable conditions to 35 degrees during very stable conditions [16].

2.3.3 Atmospheric Stability Category

Unlike wind speed and direction, atmospheric stability is not directly measured. Instead, various meteorological parameters are evaluated and stability class determined through pre-established guidelines and criteria. Pasquill-Gifford stability classes are identified

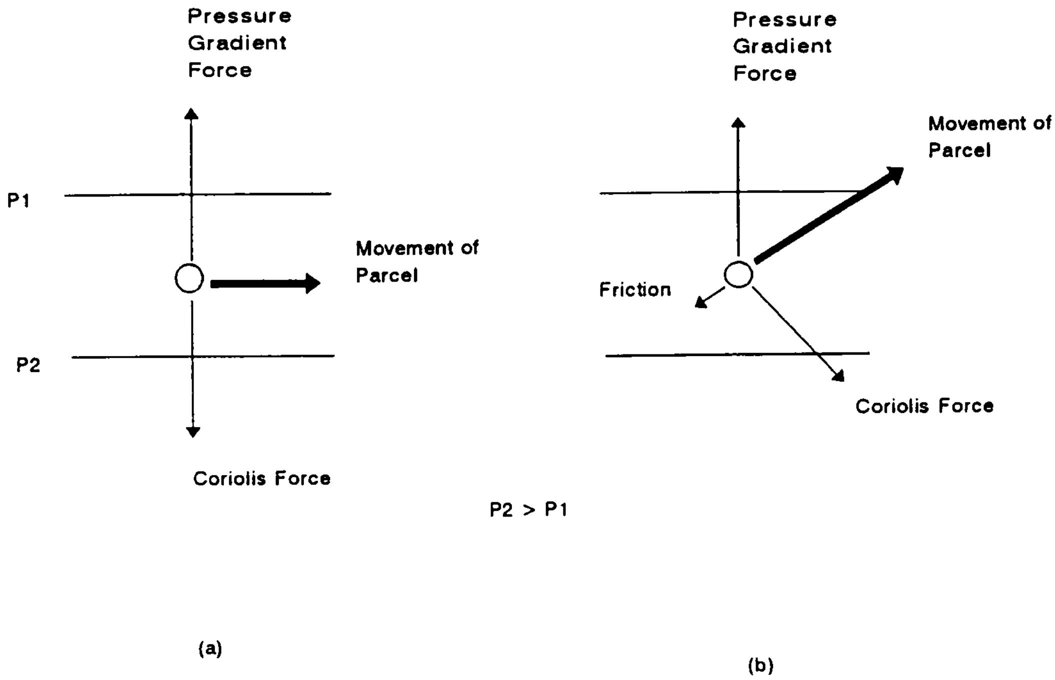

Figure 2-1: Diagram Showing Forces Acting on a Parcel of Air: (a) Above Earth's Surface without Friction (b) At Earth's Surface with Friction in the Northern Hemisphere

Source: Adapted from U.S. DOE, "Atmospheric Science and Power Production," DOE/TIC 27601, 1984, p. 44 [16].

as A, B, C, D, E, or F. Stability Class A is the most unstable and class F is the most stable. Stability class is important in the Gaussian equation because it effects the magnitude of the dispersion coefficients (σ_y and σ_z). ISCST uses various equations that approximately fit the Pasquill-Gifford curves to calculate σ_y and σ_z. These equations use coefficients which are a function of the atmospheric stability category [17].

On-Site Meteorological Program Guidance for Regulatory Compliance Modeling Applications recommends four methods of calculating atmospheric stability [18]:

(1) Turner's 1964 method using site-specific data which include cloud cover, ceiling height, and wind speeds;

(2) Standard deviation of vertical wind direction, σ_E, modified by wind speed;

(3) Standard deviation of horizontal wind direction, σ_A, modified by wind speed, and;

(4) Turner's 1964 method using site-specific wind speed with cloud cover and ceiling height from a nearby National Weather Site office.

Stability class is determined on the ORR by use of standard deviation of the horizontal wind direction, σ_A, and wind speed method (number 3 above). In this method, the stability category is determined by combining σ_A and wind velocity data. First, σ_A is used to determine an initial stability class by use of a table provided in the reference. The larger the value of σ_A, the more unstable the atmosphere. However, the initial stability class is adjusted to account for the time of day and wind speeds. For example, at nighttime, it would be unreasonable to expect an A stability; therefore, a high σ_A would be assigned a stability class of D, E, or F, depending upon the wind speed. Likewise, an A stability class would not be expected during high winds; therefore, under high wind speeds, the stability would be adjusted to lower stability classes depending upon the wind speed. For more details on the algorithm for determining stability class using this method, refer to reference 18.

2.3.4 Stability Array Data

ISCST uses hourly meteorological data, with some adjustments as described above, for input to the dispersion model. However, for ISCLT, the meteorological input file used to define the meteorological conditions is a joint frequency distribution. The joint frequency distribution data are commonly referred to as stability array (STAR) data. The frequency distribution defines the percentage of time during a given year that certain meteorological conditions exists.

The parameters included in the stability array are 16 primary wind direction sectors, six wind speed categories, and six stability classes. The wind direction sectors are constructed with the first 22.5 degree sector centered to represent winds from the north and increasing clockwise. The six wind speed categories are 0-3, 3-6, 6-10, 10-16, 16-21, and greater than 21 knots. For each wind speed category, ISCLT uses a mean wind speed. The default mean wind speed used by ISCLT for each of the six wind categories is 2.91, 4.86, 8.35, 13.21, 18.45, and 24.26 knots. The six Pasquill stability categories (A through F) are also utilized. The meteorological file therefore consists of 96 rows and six columns. The first 16 rows represent the frequency of winds from each of the 16 sectors for stability class A. The six columns for each row correspond to the frequency of time in each of the wind speed categories. The next 16 rows are for stability class B, and so forth.

2.4 RELATED RESEARCH PROJECTS

2.4.1 Coupling of Synoptic and Valley Winds

Doran and Whiteman performed a study to evaluate the coupling of upper air and surface winds in the Tennessee Valley [19]. The study identified four different mechanisms which control coupling of winds aloft and at the surface in the Tennessee Valley. Each of these mechanisms are discussed below and illustrated graphically in Figure 2-2.

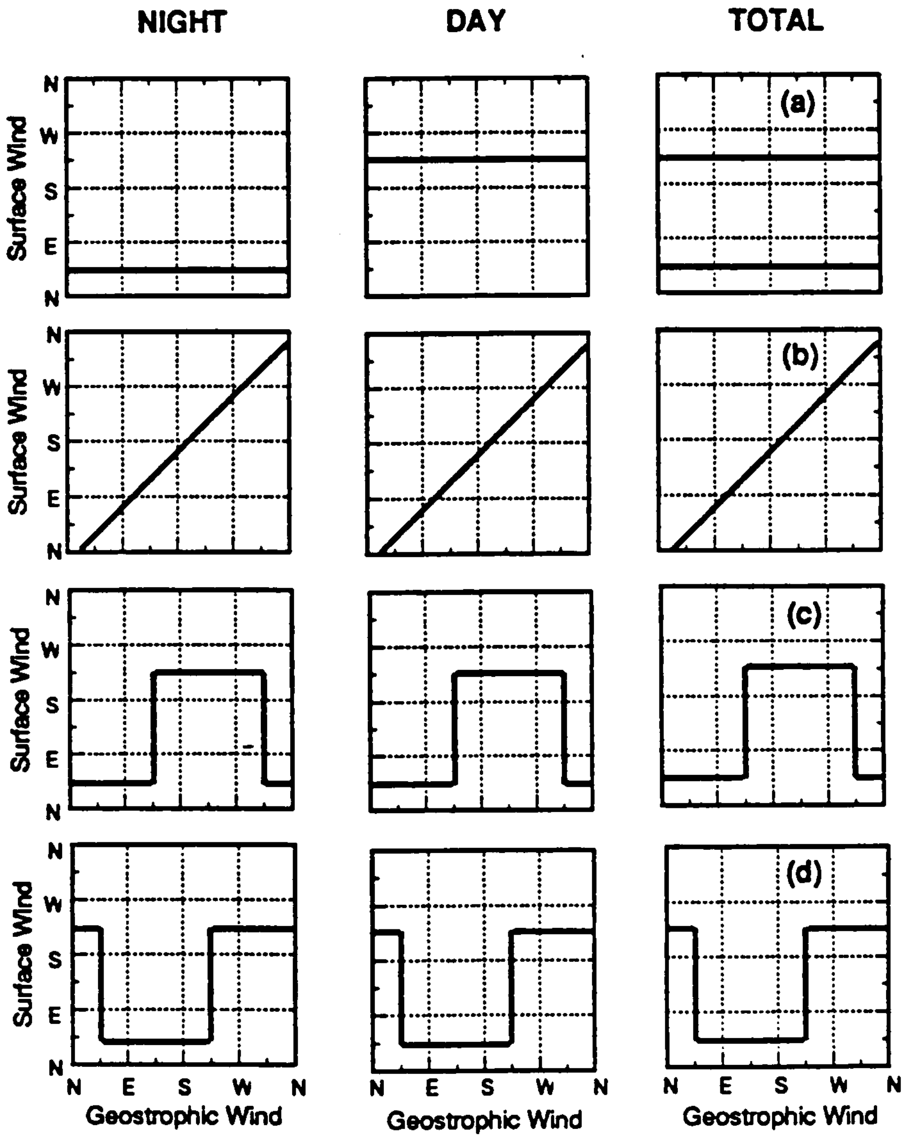

Figure 2-2: Joint Probability Distribution of Upper- and Surface-Level Winds from Four Possible Forcing Mechanisms: (a) Thermally Driven, (b) Downward Momentum Transport, (c) Forced Channeling, and (d) Pressure Driven Channeling

Source: Doran, J. C., Whiteman, C. D., "The Coupling of Synoptic Valley Winds in the Tennessee Valley," Presented at the Tenth Symposium on Turbulence and Diffusion, September 29 - October 2, 1992, Portland, Oregon [19].

The first mechanism considered was thermal forcing in which valley winds were produced by pressure gradients associated with temperature differences in the valley. For example, nighttime cold-air drainage can result in northeasterly (down-valley) flows; and, daytime heating may cause flows to occur from the southwest (up-valley). These conditions are more prevalent when upper-air winds are weak and not well defined.

The second mechanism evaluated was downward momentum transport of upper-air winds into the valley. In this case, upper air winds are strong and result in similar valley winds. However, because of frictional forces near the surface, ground-level winds may be approximately 25 degrees out of phase. This mechanism is most likely to occur in neutrally stratified conditions in wide, flat-bottomed valleys.

The third mechanism studied was forced mechanical channeling in which valley winds depend upon the sign and magnitude of the component of the upper wind projected along the valley axis. Valley wind would be either up-valley or down-valley depending on the direction of upper air flow. For example, upper-level winds between southeast and northwest would result in southwesterly winds in the valley; and upper-level winds between northwest and southeast would result in northeasterly winds in the valley. Valley winds change abruptly from southwest to northeast and northeast to southwest as upper air winds pass through northwest and southeast in the clock-wise direction, respectively.

The final mechanism, pressure driven channeling, was hypothesized by Gross and Wipperman [20]. Pressure channeling occurs when flow across a valley results in deceleration of the wind due to the increased cross-section width through which the air flows. The deceleration disturbs the equilibrium between the pressure gradient force and the Coriolis force by diminishing the latter. As a result, wind direction in the valley is controlled by the pressure gradient force resulting in winds from high to low pressure. However, since the wind is forced along the axis of the valley (like mechanical channeling), only the pressure gradient force component along the valley affects the wind direction. In this case, the relationship between upper- and lower-level winds is similar to mechanical forced channeling, except they occur 90 degrees apart.

2.4.2 Spatial Variability of the Wind Over Moderately Complex Terrain

From October 1989 until the end of 1990, the Atmospheric Turbulence and Diffusion Division (ATDD) of the National Oceanic and Atmospheric Administration (NOAA) conducted a study of wind fields around Oak Ridge, Tennessee [21, 22]. Twenty-eight meteorological towers were temporarily installed at various locations around and near Oak Ridge. Meteorological towers were located in three general areas: Cumberland Mountains, ridge-tops, and valley-bottoms. Although a number of parameters were evaluated, wind direction was the primary variable studied for a three-week period in November 1990. Both one-minute and 15-minute averages of wind speed and direction were recorded for the study. In most cases, the wind instruments were located 10 meters above the ground. Wind speeds below 0.5 m/s were not considered in the study because they were near or below the threshold of the wind direction instruments.

Vertical coupling of wind fields was evaluated by comparing wind observations at towers located in different terrain features (i.e., ridge-top winds compared to mountain-top winds). Figure 2-3 (a) and (b) provide scatterplots of 3 weeks of wind direction data for mountain-top wind direction versus ridge-top wind direction and ridge-top wind direction versus valley-bottom wind direction, respectively.

Figure 2-3 (a) illustrates that the ridge-top wind directions were primarily southwesterly or northeasterly. The ridge-top winds shift between northeasterly and southwesterly as the mountain-top winds pass through southwest and north. This observation is fairly consistent with Doran's hypothesis that wind direction within the Tennessee River Valley is at times determined by the component of the large-scale pressure gradient which is parallel to the valley axis. This observation was not as well defined for lower wind speeds

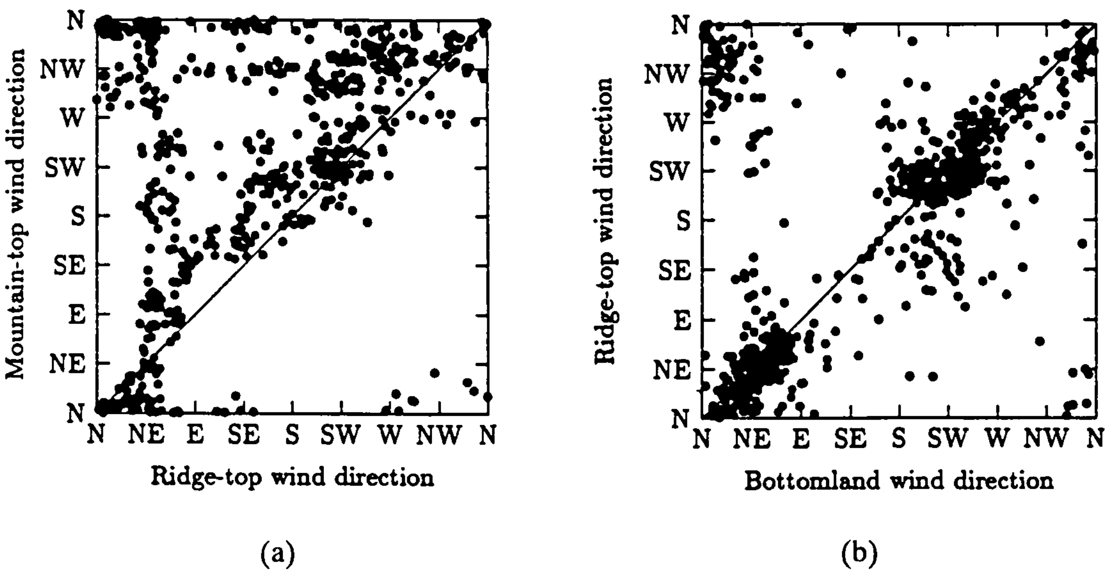

Figure 2-3: Scatterplots of Observed Wind Direction: (a) mountain-top versus ridge-top (b) ridge-top versus valley-bottom

Source: Eckman, R. M., Dobosy, R. J., Pendergrass, W. R., "Spatial Variability of the Wind Over Moderately Complex Terrain," Presented at the Tenth Symposium on Turbulence and Diffusion, September 29 - October 2, 1992, Portland, Oregon [22].

aloft. The overall conclusion was that ridge-top winds were strongly coupled with flow aloft when winds aloft were strong; however, at lower speeds, valley and ridge-top winds became decoupled from winds aloft.

Figure 2-3 (b) shows that ridge-top and valley wind directions align very closely along the axis of the valley (southwest and northeast). The majority of the data points show similar results between ridge-top and valley. However, some variations were noted when ridge-top winds were perpendicular to the ridge alignment. For example, northwesterly winds on the ridge-tops resulted in valley winds between north and east. Also, southeasterly ridge-top winds often resulted in valley winds from the southwest. Therefore, the valley winds were at times determined upon the component of the ridge-top wind that was parallel to the ridge alignment.

Important conclusions from this research project include the following: (1) when winds aloft were strong, pressure-driven channeling tended to dominate the valley flow, (2) in light winds, the valley winds were sometimes decoupled from those aloft, (3) meteorological towers located on ridge-tops were found to be representative over a larger area than towers located in valleys, (4) along-valley wind components were more easily estimated using few meteorological towers than cross-valley wind components, and (5) fewer towers are needed to characterize the wind field when upper-level winds are strong.

2.4.3 Mesoscale Flow Over Complex Terrain

Another study conducted by ATDD in 1977 evaluated mesoscale flow over the entire eastern Tennessee region [23]. This study used data extending from middle to eastern Tennessee, including surface and upper air data from Crossville, New Tazewell, Sevierville, Athens, and Oak Ridge. The primary purpose of this project was to study wind observations within the boundary layer during stable, unstable, and transition periods so that general conclusions regarding terrain-dominated flows could be made. In contrast, the two studies discussed in Sections 2.4.1 and 2.4.2 compared air flow significantly above the boundary layer to surface-level flows.

Vertical profiles of average wind speed and wind direction from all of the sites in Tennessee were compared to other studies conducted in flat terrain locations. Standard deviation of area-averaged (e.g. station-averaged) wind speed and wind direction were used for comparison purposes. Comparisons were conducted during stable, unstable, and transition periods. Stable conditions were assumed to occur from midnight until 6:00 a.m., unstable conditions between 10:00 a.m. and 4:00 p.m., and transition conditions between 6:00 p.m. and 10:00 p.m.. Observations were not conducted during other hours of the day.

Two specific conclusions from this research project are relevant to this study: (1) variations in wind direction among the stations (e.g., Crossville, New Tazewell, Sevierville, Athens, and Oak Ridge) increased with increasing stability, and (2) variations in wind speed between the stations decreased with increasing stability.

2.4.4 Accuracy of Dispersion Models in Complex Terrain

A number of research studies have evaluated the relative accuracy of Gaussian dispersion models when used in complex terrain. Start and Wendell [24] demonstrated that over mountainous terrain, predicted concentrations were two to four times less than would be expected over flat terrain. In addition, Start, Dickson, and Wendell [25] found that the ratio of estimated concentration (C_e) to observed concentration (C_o) depends upon stability category as follows: Class C, C_e/C_o = 1.4; Class D, C_e/C_o = 5.3; and Class F, C_e/C_o = 18.7. Hovind, Spandler, and Anderson [26] determined that the ratio of calculated to observed concentrations is a function of travel distance, decreasing from eight at 3 km to approximately one at 12 km. Dispersion modeling of radionuclides on the ORR also found that predicted concentrations using EPA's CAP-88 computer code are two to 10 times higher than actually measured [27]. Nappo [28] hypothesized that the decrease in plume concentration over complex terrain is in part due to increased pollutant spreading caused by horizontal variability of the wind.

CHAPTER 3

EVALUATION OF METEOROLOGICAL DATA

3.1 DESCRIPTION OF EXISTING METEOROLOGICAL MONITORING PROGRAM

The ORR maintains a number of on-site meteorological monitoring stations to support ongoing compliance, emergency response, and research related activities. The monitoring network, shown in Figure 3-1, consists of one 60-m tower at the K-25 Site; one 100-m tower at ORNL; and one 100-m tower and one 60-m tower at the east and west ends of the Y-12 Plant, respectively. These towers will be referred to hereafter as K-25, ORNL, Y-12 West and Y-12 East towers and abbreviated as K25, X10, YW, and YE, respectively.

Data are collected at various levels to determine the vertical structure of the atmosphere. At all towers, data is collected at the 10-m level and at the top of the tower. In addition, on the 100-m towers, intermediate level (e.g., 30- and 60- meters) data are also collected. At each measuring level, temperature, wind speed, and wind direction are measured; the standard deviation of the horizontal wind direction is monitored at the upper level of each tower and is used to determine atmospheric stability [29].

Each tower utilizes a dedicated control computer which stores data and performs necessary calculations and quality assurance checks. Fifteen-minute and hourly values are stored at each site for a running 24-hour period. Only hourly data are stored beyond 24

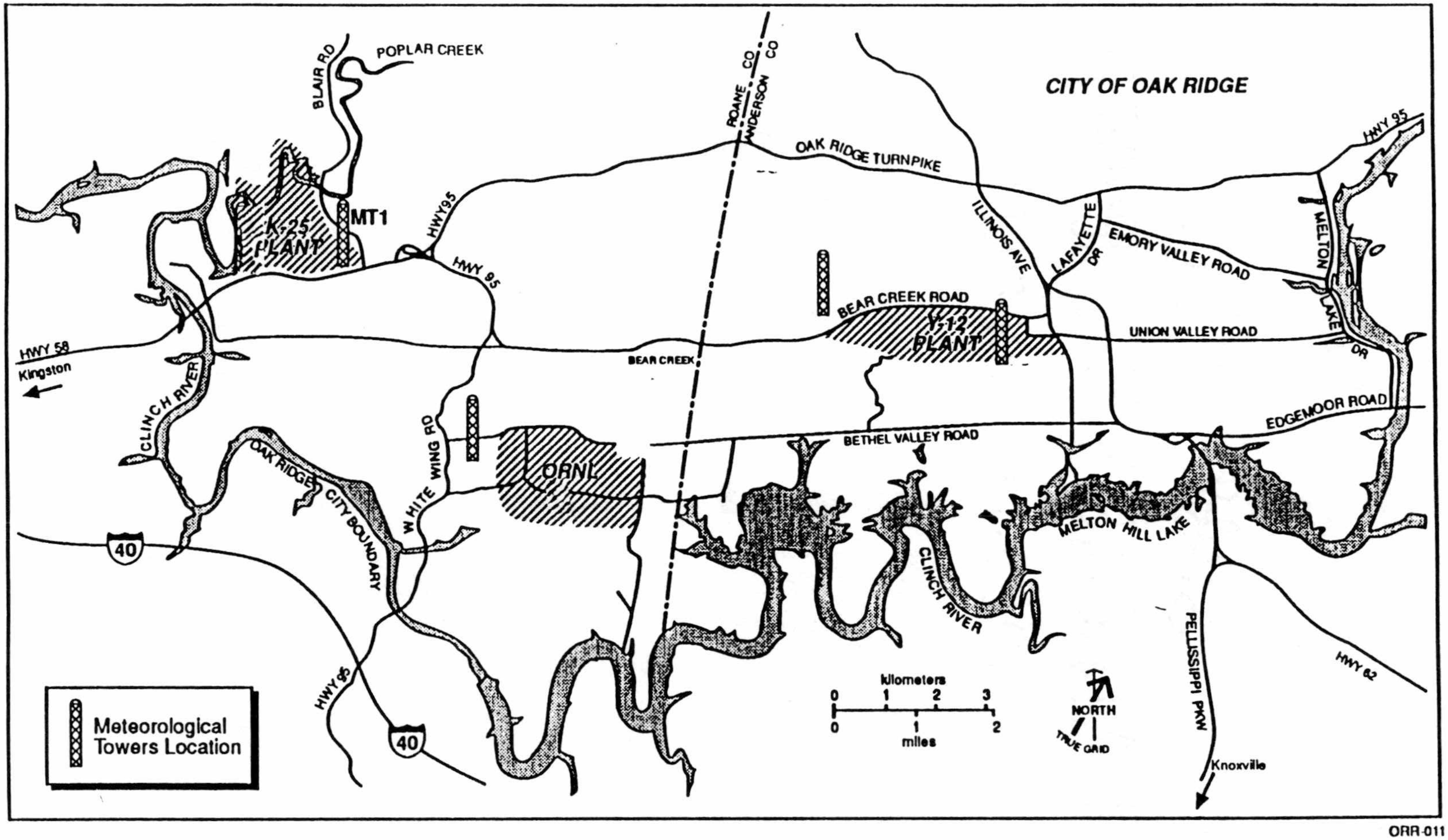

Figure 3-1: Locations of Meteorological Towers on the Oak Ridge Reservation

Source: Adapted from Martin Marietta Energy Systems, Inc., "Oak Ridge Reservation Surveillance Report for 1991," ES/ESH-22/V1, October 1992, Oak Ridge, Tennessee, p. 3-36.

hours. Quarterly calibration of the instruments is conducted at each tower. The meteorological data is processed using the ORNL Meteorological Data Retrieval and Analysis Program (OMDRAP). OMDRAP is a FORTRAN-77 computer program that analyzes meteorological data and places the data in an unformatted file for use by ISC [30].

3.2 SCOPE OF EVALUATION

For this study, data from the 10-m level is evaluated because it is the standard elevation used for most wind measurements and is available at all monitoring locations. In addition, other studies conducted on the ORR and described in Section 2.4 also used the 10-m elevation. The Y-12 West, ORNL, and K-25 towers were selected because they are all located in different valleys and are most commonly used in dispersion modeling studies on the ORR. The Y-12 Plant East tower was selected because it is located in the same valley as the Y-12 West tower. Therefore, this evaluation includes towers located in different valleys as well as one set of towers located in the same valley.

The three meteorological towers (YW, X10, and K25) located in different valleys will be compared to each other. In addition, the two Y-12 Plant towers will be compared to each other since they are located in the same valley. Therefore, the specific comparisons include: YE versus YW (YE/YW), YW versus X10 (YW/X10), YW versus K25 (YW/K25), and X10 versus K25 (X10/K25). The general approach is to compare one year (1991) of data less those hours where the data may be in question or missing. For example, wind direction cannot be accurately measured at wind speeds below 0.5 m/s; therefore, when evaluating wind direction, all hours where the wind speeds were less than 0.5 m/s will not be included in the analysis. This is consist with similar research studies. After a complete year of data is evaluated, subsets of the entire data set will be evaluated. For example, the data were compared under certain meteorological conditions only (e.g., low wind speeds, high wind speeds, stable condition, unstable conditions, etc.).

The following meteorological parameters are considered most important from a dispersion modeling standpoint and will be evaluated in this study: wind speed, wind direction, and stability class. The standard deviation of the horizontal wind direction, σ_A, is also measured at each tower but is of lesser importance since it is not directly used in the Gaussian equation. Differences in standard deviation of horizontal wind direction from one site to another is reflected in changes in stability category.

3.3 COMPARISON OF STABILITY ARRAY (STAR) METEOROLOGICAL DATA

As indicated in Section 2.3.4, the meteorological input file used to define the meteorological conditions for ISCLT is a joint frequency distribution. The joint frequency distribution data are commonly referred to as stability array (STAR) data. The frequency distribution defines the percentage of time during a given year that certain meteorological conditions exists. STAR data for each meteorological tower is provided in Appendix A. The parameters included in the stability array are 16 primary wind direction sectors, six wind speed categories, and six stability classes. Each of these parameters are evaluated below.

3.3.1 Wind Direction

Figures 3-2, 3-3, 3-4, and 3-5 are wind roses for YW, YE, X10, and K25, respectively. Qualitative review of the wind roses identify several noteworthy characteristics. Each of the wind roses illustrate the typical southwest to northeast and northeast to southwest flow which is typical of eastern Tennessee due to the predominant wind direction and alignment of the ridges and valleys characteristic of the southern appalachians.

Several differences between the meteorological towers are noted. The Y-12 West tower shows a more pronounced flow pattern from the southwest to northeast than the other three sites. Wind directions at YW were between south-southwest and west-southwest approximately 40 percent of the time. However, wind direction at the other three sites were from these directions from 21 to 30 percent of the time. This difference may be the result of the YW tower being located within Bear Creek Valley which is substantially more narrow than the other nearby valleys. As a result, channelization is increased with less opportunity for cross-valley winds. Table 3-1 provides a summary of the frequency of winds from the southwest and northeast at each of the towers.

Another notable feature of the data presented in Table 3-1 is that the Y-12 Plant East Tower has a significantly higher frequency of winds from the northeast than the other towers. The frequency of wind from the northeast at the other three towers ranges from 25 to 28 percent; while, the frequency at the Y-12 Plant East Tower is approximately 39 percent. Several possible factors may be causing YE to have a higher frequency of flow from the northeast. First, the Y-12 East Tower is located on the extreme eastern edge of Bear Creek

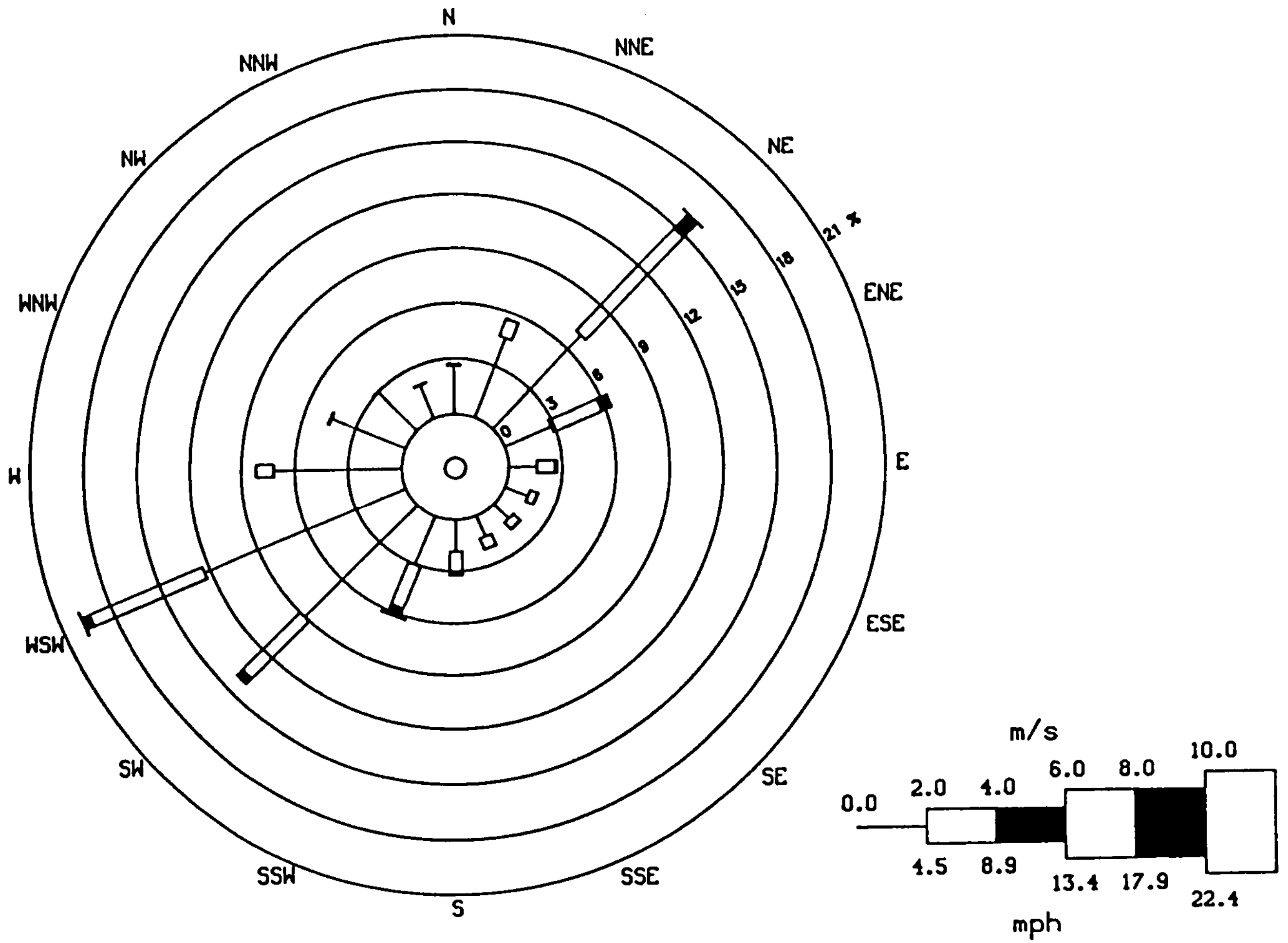

Figure 3-2: 1991 Wind Rose for Y-12 Plant West - 10 m level (99.3% data recovery)

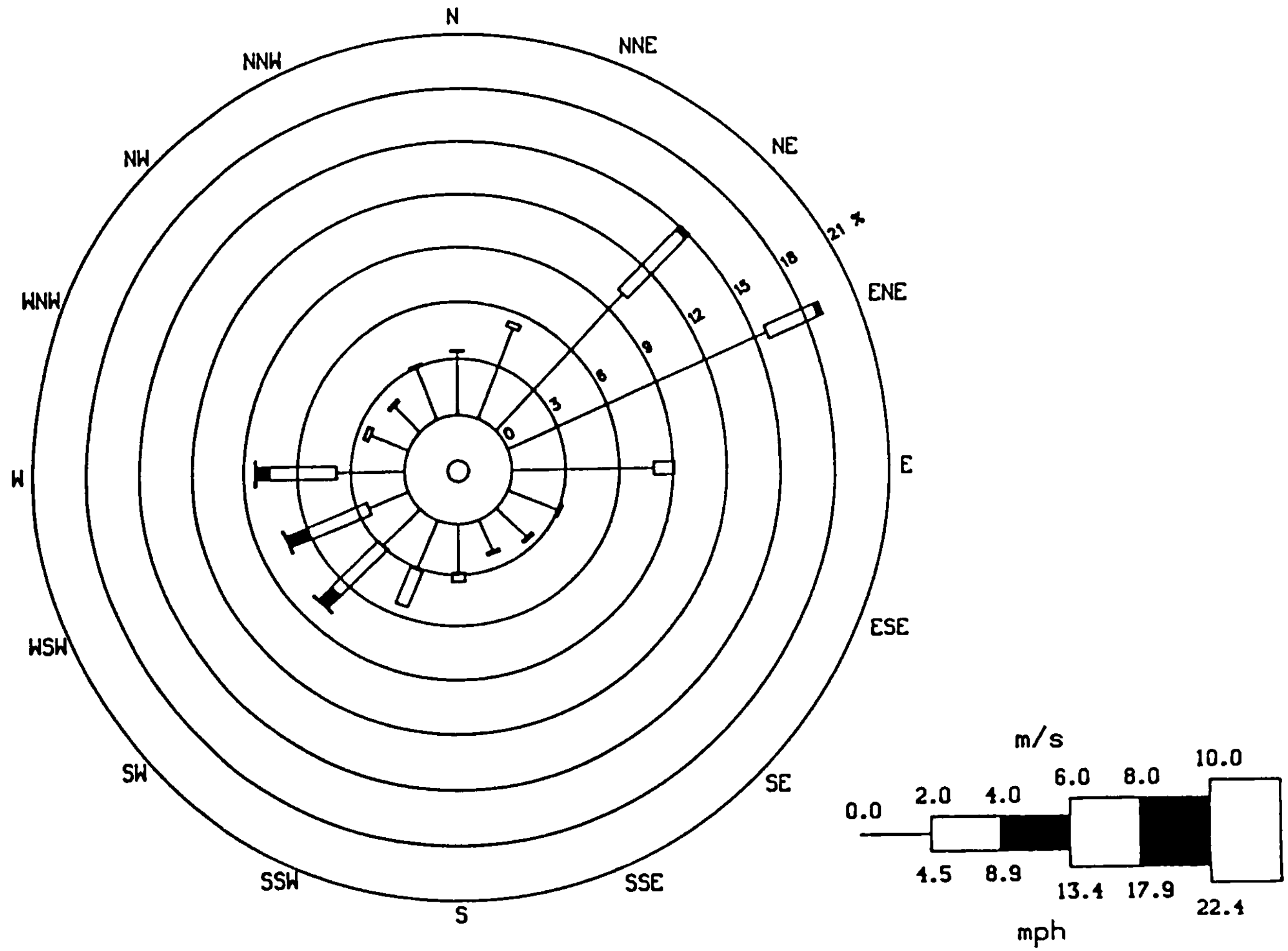

Figure 3-3: 1991 Wind Rose for Y-12 Plant East - 10 m level (99.3% data recovery)

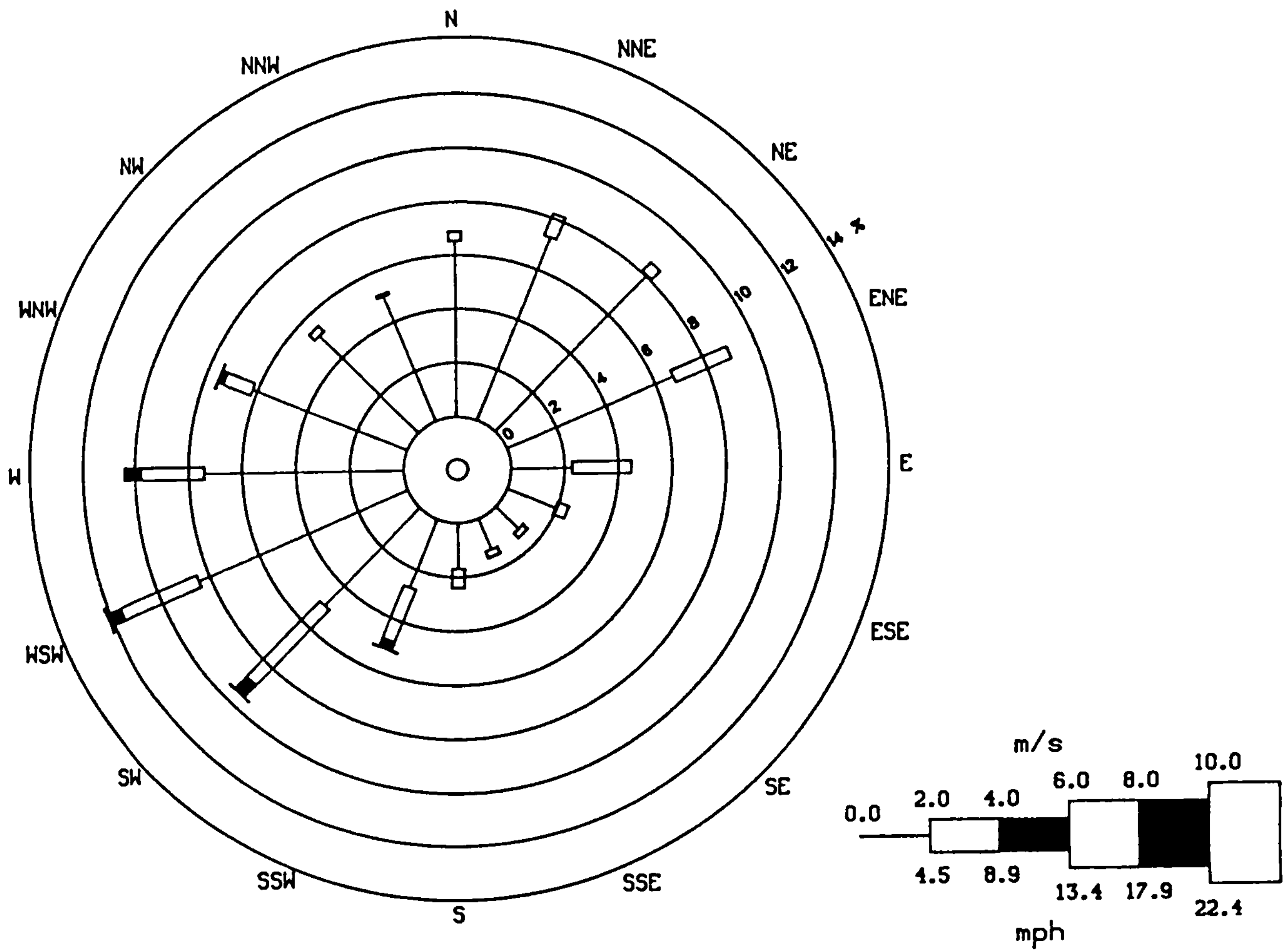

Figure 3-4: 1991 Wind Rose for ORNL - 10 m level (81.8% data recovery)

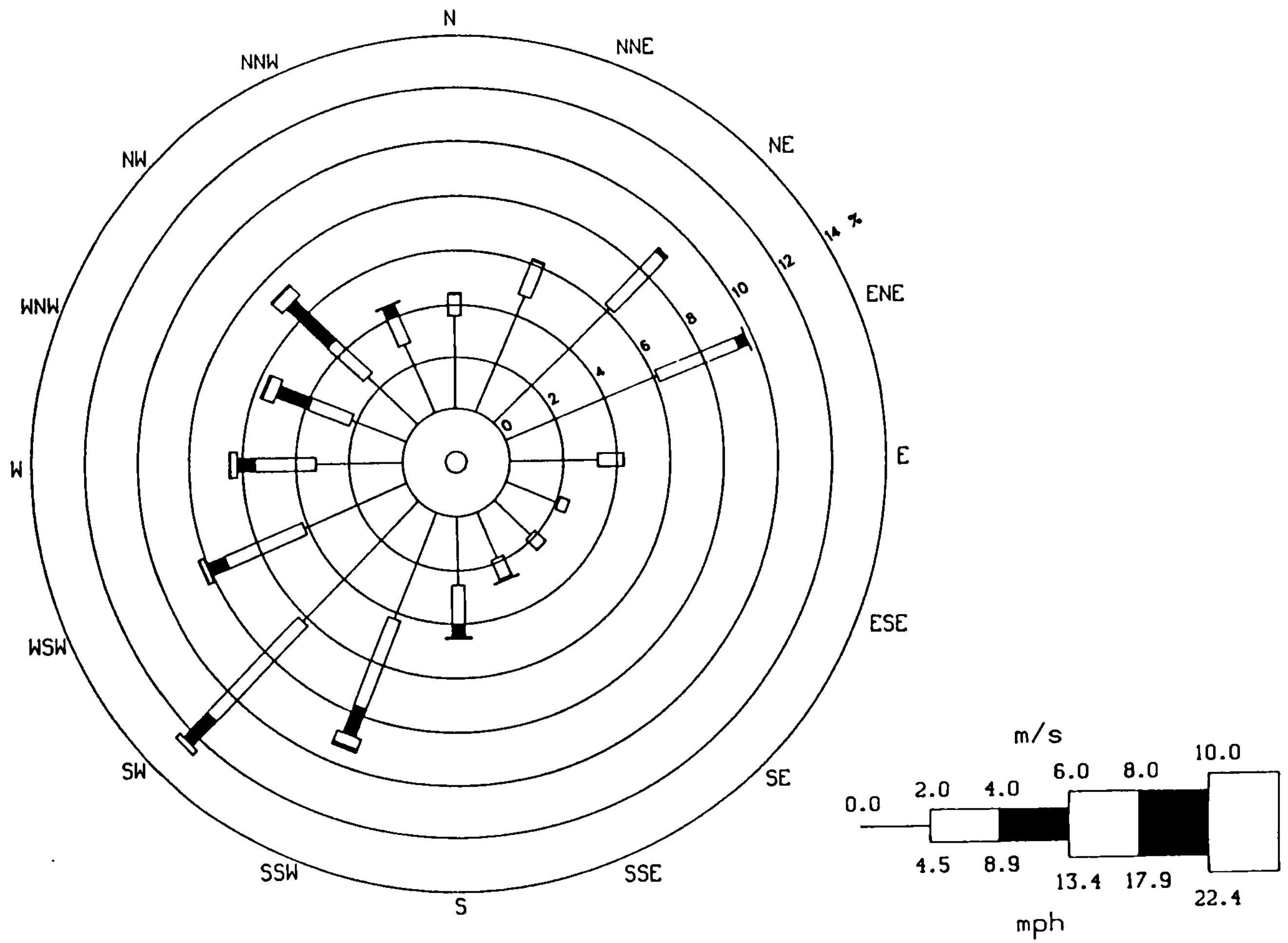

Figure 3-5: 1991 Wind Rose for K-25 Site - 10 m level (91.4% data recovery)

Table 3-1: Frequency of Winds Blowing from Southwest and Northeast

Meteorological Tower	Frequency (%) of Winds Blowing From Direction		
	Southwest[1]	Northeast[2]	Total
Y-12 Plant West	40	28	68
Y-12 Plant East	21	39	60
ORNL	27	26	53
K-25 Site	30	25	55

[1] Includes winds from SSW to WSW.
[2] Includes winds from NNE to ENE.

Valley. At this location, a small gap oriented from northwest to southeast is located along Scarborough Road. This small gap separates Bear Creek Valley from Union Valley and may cause variation in wind flow at the east tower. In addition, a 2.5 acre pond (Lake Reality) located approximately 50 feet southwest of the Y-12 Plant East Tower may also influence wind direction at the east tower. Lake Reality serves as a flow equalization pond for wastewater effluents from the Y-12 Plant. Effluents from the Y-12 Plant are often considerably warmer than the ambient air, especially in the early morning hours during the cold weather season. As a result, convective currents rising from the pond may influence wind direction around the pond. However, without further studies or analysis, the degree of influence from the valley cross-roads and adjacent pond cannot be determined.

Another notable difference between the wind direction frequency data is that the Y-12 Plant East Tower has a higher frequency of easterly winds. The frequency of easterly winds from the YE, YW, X10, and K25 is 9.0, 2.7, 4.5, and 4.2 percent, respectively. This difference may also be caused by the valley cross-roads near the east tower.

As another means of comparison, the correlation coefficient was calculated for the wind direction frequency data for each data set compared. The correlation coefficients for YE/YW, YW/X10, YW/K25, and X10/K25 were 0.51, 0.77, 0.71, and 0.72, respectively. The best correlation was found to occur when YW and X10 were compared (coefficient of 0.77). The poorest correlation occurred when YE and YW were compared (coefficient of 0.51). Correlation coefficients for YW/X10, YW/K25, and X10/K25 were all fairly close (within 8 percent).

Even though YE and X10 are located in separate valleys, they show more similar wind direction frequency data than the other sites compared. This may occur since YE and X10 are located in similar topographical settings. In contrast, YE and YW are located in the same valley but show less correlation than the other towers. As indicated above, the Y-12 Plant East Tower is located in a crossroads of two valleys and adjacent to a large pond and therefore may be highly influenced by these local effects. It is anticipated that differences in wind fields between these two site may be more pronounced during stable conditions. To further evaluate differences in wind direction data at the Y-12 Plant, Figures 3-6 and 3-7 provide wind roses for YW and YE, respectively, during F-stability. The two wind roses are considerably different. YE shows persistent wind flows from the northeast quadrant during F-stability; however, YW shows equally persistent flows from the west and southwest quadrants. The YE wind rose is more characteristic of down-valley thermal drainage commonly observed in eastern Tennessee. However, the YW wind rose only shows a relatively small fraction of winds from the northeast during F-stability. Review of the

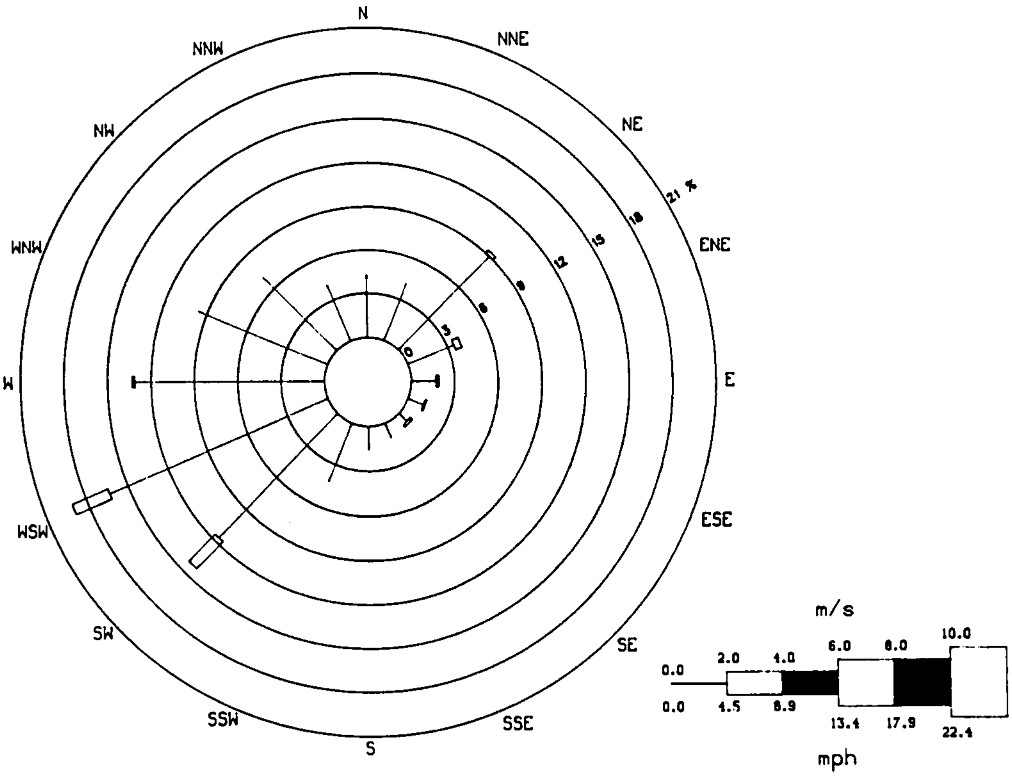

Figure 3-6: 1991 Wind Rose for Y-12 Plant West During F-Stability - 10 m level

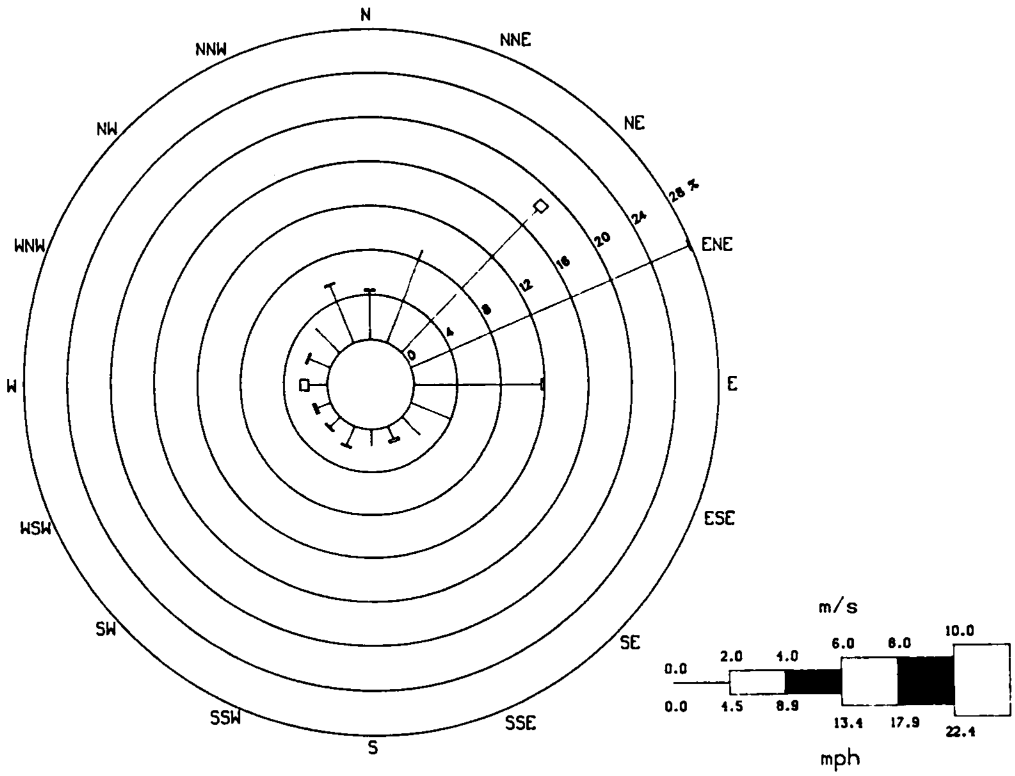

Figure 3-7: 1991 Wind Rose for Y-12 Plant East During F-Stability - 10m level

topography near YW identified nearby terrain features which may influence flow during stable conditions. YW is located on top of a small hill at the base of nearby ridges to the northwest and west. These terrain features may result in thermal drainage causing a higher frequency of westerly winds in comparison to YE. The differing wind directions observed at the Y-12 Plant are an interesting observation since the towers are located relatively close together and in the same valley.

3.3.2 Wind Speed

In addition to wind direction data, the stability array also includes wind velocity information. As previously indicated, the wind speeds are divided into six categories: 0-3, 3-6, 6-10, 10-16, and greater than 21 knots. Figure 3-8 provides a comparison of the frequency of each wind speed category for each set of meteorological data.

The most notable difference in the wind speed data is the significantly higher wind speeds observed at the K-25 Site. The percentage of time that winds exceed 6 knots (3.08 m/s) for the K-25 Site, Y-12 Plant East, Y-12 Plant West, and ORNL towers is 18.8, 10.2, 11.4, and 6.7 percent respectively. Using the ISCLT default mean wind speeds for each wind speed category, the weighted average wind speed for each of these towers is 2.5 (4.8), 2.1 (4.1), 2.3 (4.5), and 2.0 (3.9) m/s (knots), respectively. Higher wind speeds at the K-25 Site may result since the site is located in a wider valley with less obstructions from nearby terrain. The lightest wind speeds are noted at ORNL. Table 3-2 provides a summary of the wind speed data.

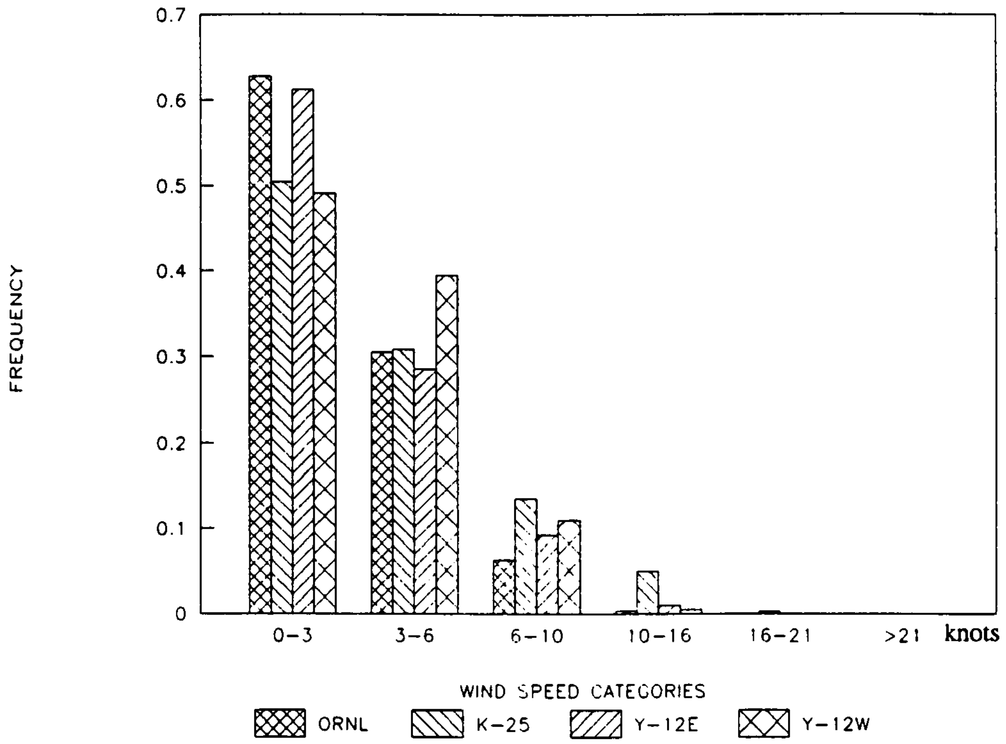

Figure 3-8: Comparison of Wind Speed Categories at Each Meteorological Tower (Wind Speed Categories in Knots)

Table 3-2: Comparison of Wind Speed Frequency Data

Meteorological Tower	Frequency Greater than 6 knots[1]	Average Wind Speed[2] m/s (knots)
Y-12 Plant East	10.2	2.1 (4.1)
Y-12 Plant West	11.4	2.3 (4.5)
ORNL	6.7	2.0 (3.9)
K-25 Site	18.8	2.5 (4.9)

[1] Expressed in percentage of time.
[2] Average wind speed as calculated using default ISCLT mean wind speed for each category.

3.3.3 Stability Class

The final parameter evaluated in the frequency distribution data was stability class. Figure 3-9 illustrates the frequency of each stability class at each of the meteorological towers. As readily visible, the ORNL tower has a significantly lower frequency of class A stability. To further evaluate differences in stability class, the frequency of occurrences was broken down into three broader stability categories: Unstable (A and B), Neutral (C and D), and Stable (E and F). In addition, the average stability category for each set of data was calculated. This was accomplished by assigning a numeric value to each of the stability categories (i.e., A=1, B=2, C=3, D=4, E=5, and F=6) and performing a weighted average calculation.

The frequency distribution data from both the Y-12 towers and the K-25 Site tower were very similar. However, the ORNL tower again showed a significantly less frequent occurrence of unstable conditions. Unstable and transition conditions at ORNL occurred more frequently than the other sites. Also, the weighted average numeric stability class at ORNL was 4.3. All other sites had a weighted average numeric stability class of 3.8. Results of this evaluation are summarized in Table 3-3. Actual differences in stability category from one site to another are unlikely; therefore, it is believed that some difference may exist between the instrumentation or data handling systems at the different sites. Further review and analysis is needed to determine the cause for this difference.

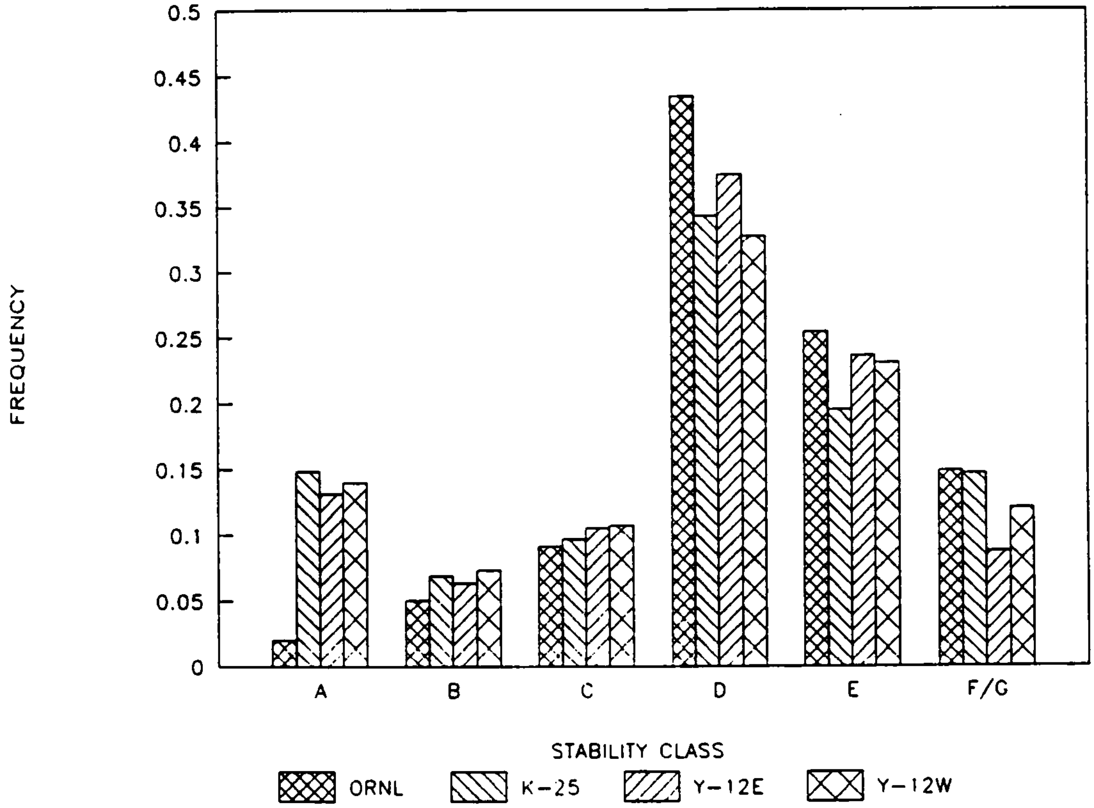

Figure 3-9: Comparison of Stability Class Frequency Data at Each Meteorological Tower

Table 3-3: Comparison of Stability Frequency Data

Meteorological Tower	Unstable[1]	Neutral[2]	Stable[3]	Average [4]
Y-12 Plant West	21	43	35	3.8
Y-12 Plant East	20	48	32	3.8
ORNL	7	53	40	4.3
K-25 Site	22	44	34	3.8

[1] Includes stability classes A and B.
[2] Includes stability classes C and D.
[3] Includes stability classes E and F.
[4] Weighted average stability class (A=1, B=2, C=3, D=4, E=5, and F=6)

3.4 COMPARISON OF HOURLY METEOROLOGICAL DATA

Hourly meteorological data is used by ISCST to calculate both short- and long-term average concentrations. This section will conduct a similar review as conducted for stability array data; however, a more thorough evaluation can be conducted since larger amounts of data are available. First, data will be compared using all hours of valid observations. Secondly, various subsets of the entire data set will be compared. For example, a comparison of wind direction data will be made under different observed wind speed ranges and stability classes. Details of these evaluations are presented below.

3.4.1 Wind Direction Data

The first step in reviewing the hourly wind data was to exclude all data where wind speeds were less than 0.5 m/s. This was necessary since wind speeds at these levels are below the threshold of the wind direction instruments, and the results are unreliable. In addition, all hours where one or both of the wind direction data were missing were also excluded from the analysis. After the data set was reduced as described above, the wind directions were compared on a hourly basis to determine the relative degree of similarity.

As a means of direct comparison, the angle between the two wind directions was calculated for each hour for each data set tested. The difference between the wind directions will be hereafter referred to as delta direction. From this evaluation, frequency distribution data were developed for each data set compared. The results of this evaluation indicate the percentage of time that the two wind directions are within 5, 10, 22.5, 45, 90, and 135 degrees. The results of this evaluation are shown in Table 3-4 and illustrated by a cumulative frequency plot in Figure 3-10. Also shown in the table are correlation coefficients for the wind direction data as calculated using a 540 degree compass. A description of the 540 degree compass is provided in the following pages.

As illustrated in Table 3-4 and Figure 3-10, wind direction data compare more closely for YW/YE and YW/X10; the poorest comparison occurs for X10/K25. Only 24 percent of the hourly wind direction data is within ten percent for the Y-12 East and Y-12 West towers. For all data sets compared, over 55 percent of the hourly data was greater than 22.5 degrees apart. This data indicate very poor comparison of wind direction between the sites on an hourly basis. Differences in wind direction at the Y-12 Plant towers are greater than 135 degrees approximately 12 percent of the time.

Table 3-4: Frequency (%) of Hourly Wind Direction Data Within 5, 10, 22.5, 45, 90, and 135 Degrees

	Meteorological Data Compared			
Delta Direction (degrees)	YW/YE	YW/X10	YW/K25	X10/K25
5	13.2	11.1	8.4	7.4
10	24.1	21.4	16.8	14.2
22.5	45.0	44.3	34.5	30.0
45	67.0	67.2	55.3	52.6
90	81.0	84.3	78.2	74.6
135	88.4	92.9	90.1	87.3
Correlation Coefficient	0.79	0.84	0.76	0.74

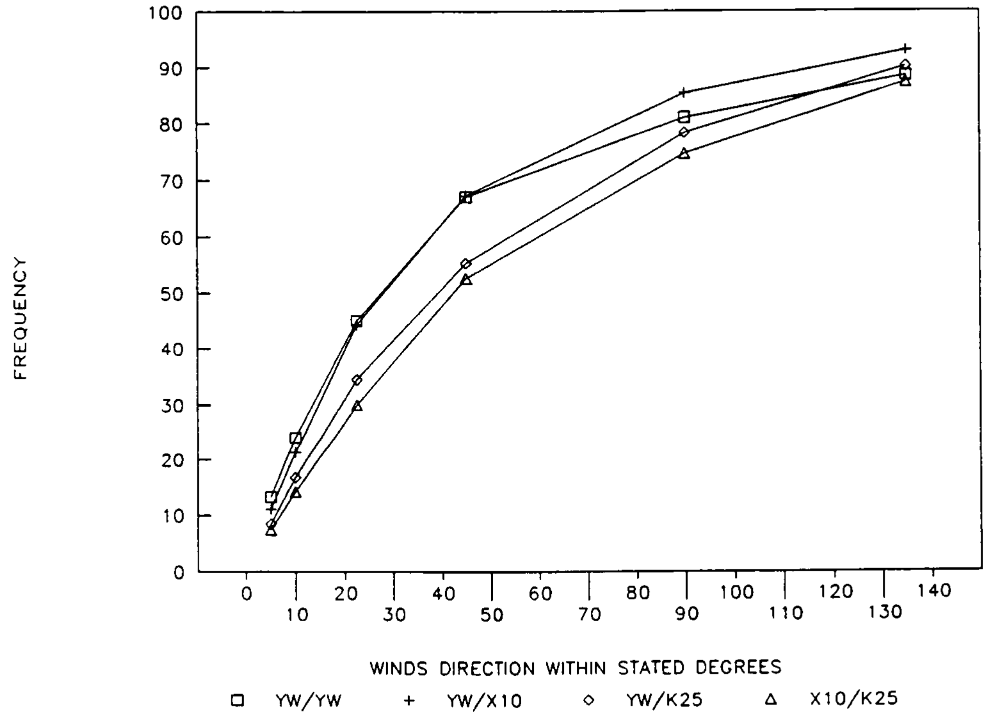

Figure 3-10: Cumulative Frequency Plot Showing Variations in Hourly Wind Direction for Each Meteorological Data Set Compared.

Figures 3-11, 3-12, 3-13, and 3-14 are scatterplots of hourly wind direction data for YE/YW, YW/X10, YW/K25, and X10/K25, respectively. The scatterplots are shown on a 540 degree compass. In plotting the wind direction data on a 540 degree compass, the following relationships are used:

$$\text{If } WD1 - WD2 > 180° \text{ and } WD1 < WD2, \text{ then } WD1 = WD1 + 360 \quad (3\text{-}1)$$

$$\text{If } WD1 - WD2 > 180° \text{ and } WD2 < WD1, \text{ then } WD2 = WD2 + 360 \quad (3\text{-}2)$$

where WD1 and WD2 are the two wind directions being plotted. The reader must recognize that wind directions from 360 to 540 degrees correspond to 0 to 180 degrees on the standard 360 degree compass. For example, 405 degrees equates to a northeasterly wind.

These plots show a significant amount of scatter of wind direction data for the various tower locations compared. Most notably, hourly wind direction data at Y-12 East and Y-12 West have three distinct patterns. Wind directions from the southwest and northeast appear to be well aligned as indicated by a large number of data points in those areas of the plot. This feature is common to all other scatterplots and is expected since these two directions represent the predominant wind directions in the Oak Ridge valley. However, for the YE/YW plot, another large number of data points are observed in the far left and right edges of the plot. In this area of the plot, winds at the east tower are from the northeast quadrant while winds from the west tower are from the southwest quadrant. Approximately 7 percent of the wind direction data for YW and YE were greater than 157.5 degrees apart. This is notable since the towers are relatively close together.

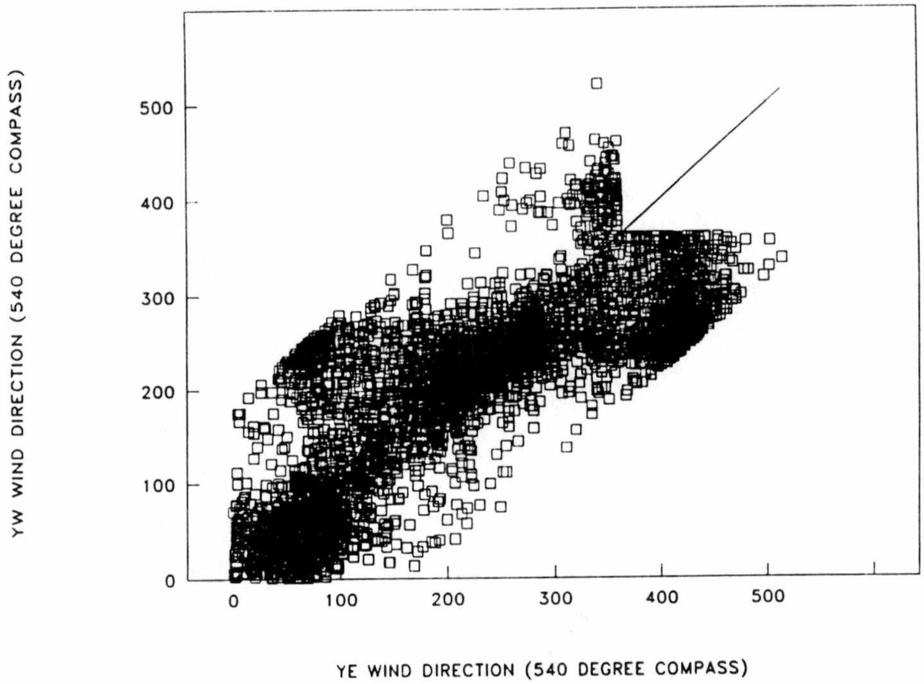

Figure 3-11: Scatterplot of Hourly Wind Direction (Degrees) for Winds Greater Than 0.5 m/s: YE versus YW

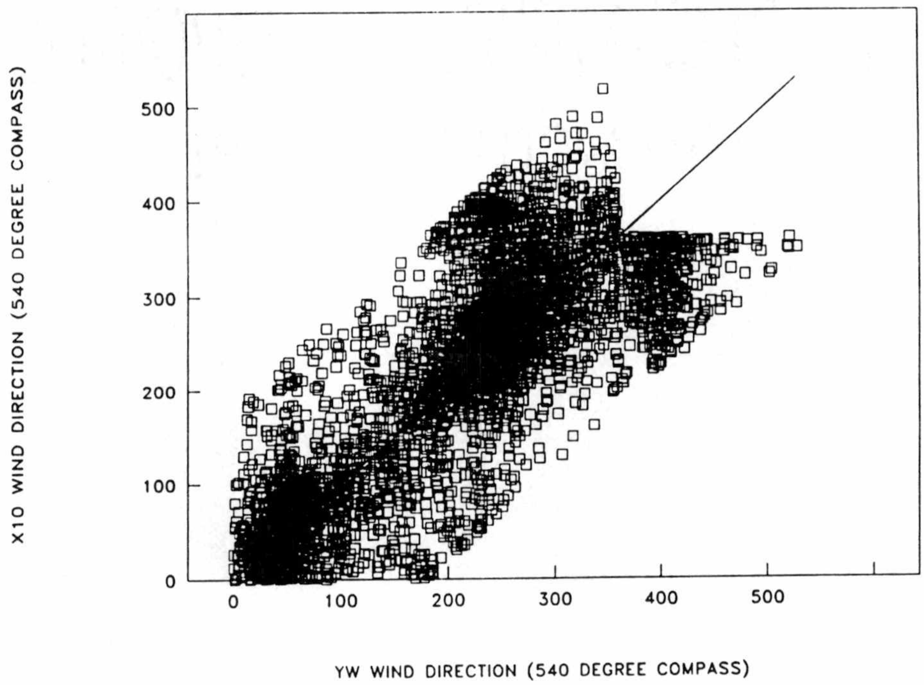

Figure 3-12: Scatterplot of Hourly Wind Direction (Degrees) for Winds Greater Than 0.5 m/s: YW versus X10

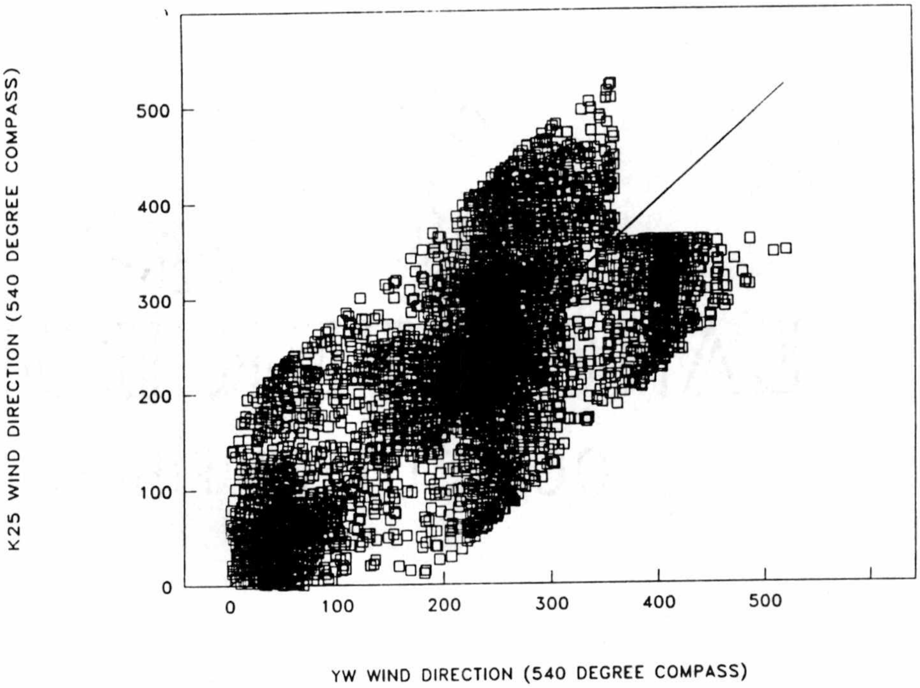

Figure 3-13: Scatterplot of Hourly Wind Direction (Degrees) for Winds Greater Than 0.5 m/s: YW versus K25

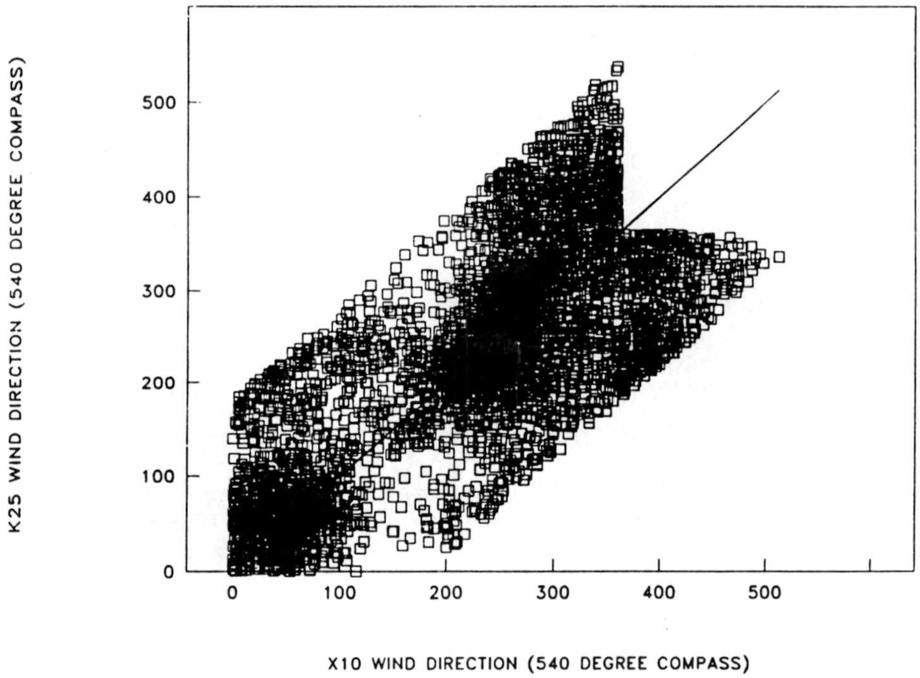

Figure 3-14: Scatterplot of Hourly Wind Direction (Degrees) for Winds Greater Than 0.5 m/s: X10 versus K25

To further compare hourly wind direction data, subsets of the entire hourly data set were compared. First, wind direction data were compared under various wind speed ranges: 0.5 to 1.5 m/s, 1.5 to 3.0 m/s, and greater than 3.0 m/s. Frequency distribution plots and scatterplots were developed under these various wind speed categories. This evaluation found that wind direction better correlates as wind speed increases. Under high wind speed conditions, the effects of terrain and micro-scale meteorology appear to be minimized. Figures 3-15 and 3-16 provide cumulative frequency plots for differences in hourly wind direction for YE/YW and YW/X10 under varying wind speeds. The other plots are not shown since they show the same basic pattern (better comparison at higher wind speeds). Wind direction at Y-12 West better compares with ORNL wind direction data than Y-12 East data during light wind conditions. However, during higher wind speeds, Y-12 East more closely compares with Y-12 West data than ORNL data.

Figures 3-17, 3-18, and 3-19 provide scatterplots for YE/YW during light wind speeds (0.5 to 1.5 m/s), light to moderate wind speeds (1.5 to 3.0 m/s), and moderate to high wind speeds (greater than 3.0 m/s). These three figures clearly illustrate that with increasing wind speed, hourly wind direction data becomes more closely related. The number of data points on the left and right edges which illustrate wind directions approximately 180 degrees apart decrease in frequency with increasing wind speed. The frequency of wind directions greater than 157.5 degrees apart decrease from 15 percent for low wind speeds to near zero percent for high wind speeds. Table 3-5 shows the frequency of hourly wind direction data which is greater than 90 degrees apart for the various data sets compared at each wind speed category.

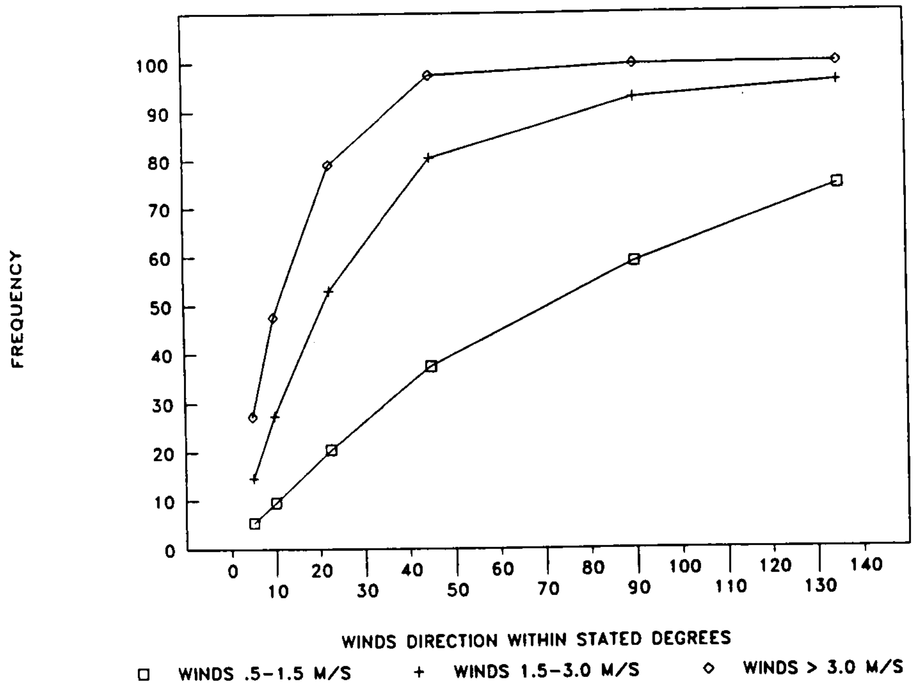

Figure 3-15: Cumulative Frequency Plot of Differences in Wind Direction (Degrees) at Various Wind Speeds: YE versus YW

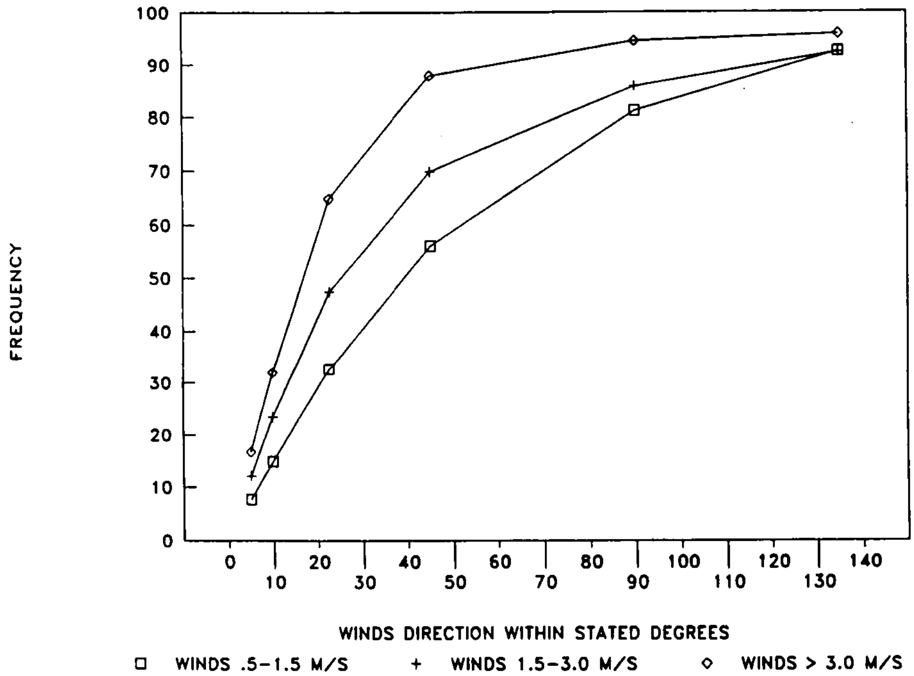

Figure 3-16: Cumulative Frequency Plot of Differences in Wind Direction (Degrees) at Various Wind Speeds: YW versus X10

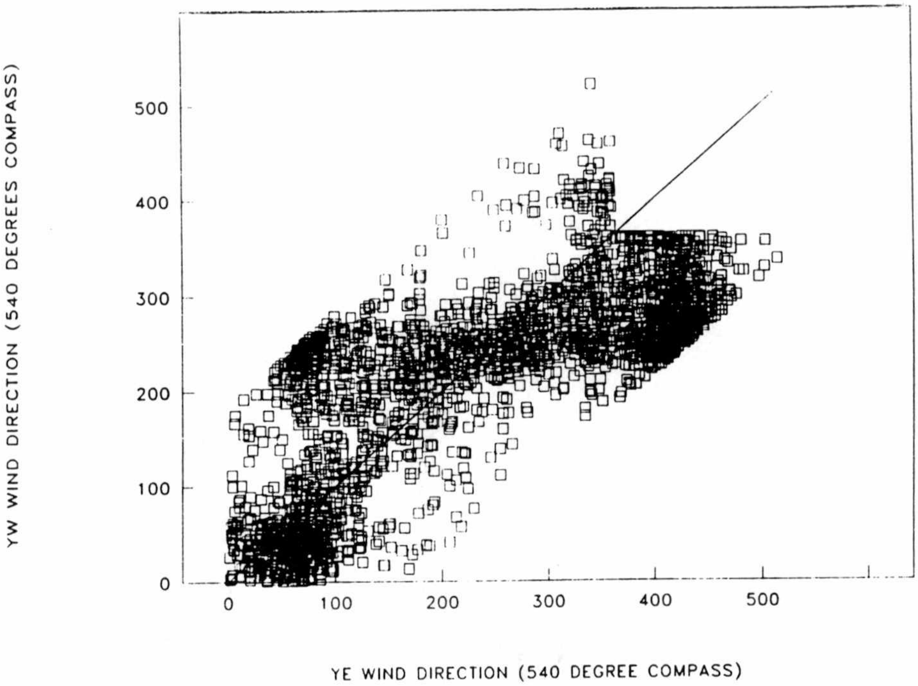

Figure 3-17: Scatterplot of Hourly Wind Direction (Degrees) at Wind Speeds Between 0.5 and 1.5 m/s: YE versus YW

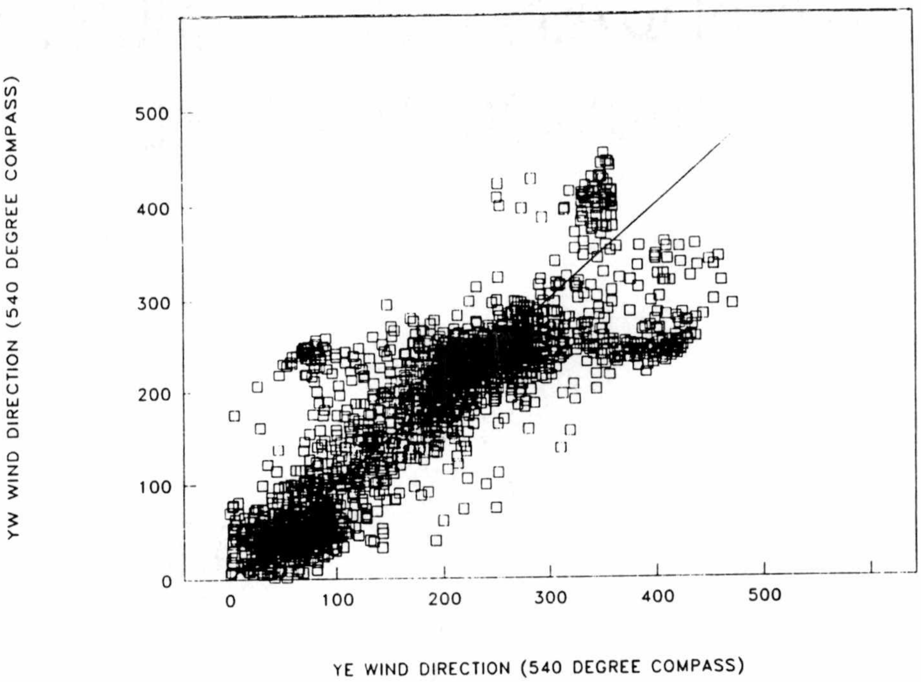

Figure 3-18: Scatterplot of Hourly Wind Direction (Degrees) at Wind Speeds Between 1.5 and 3.0 m/s: YE versus YW

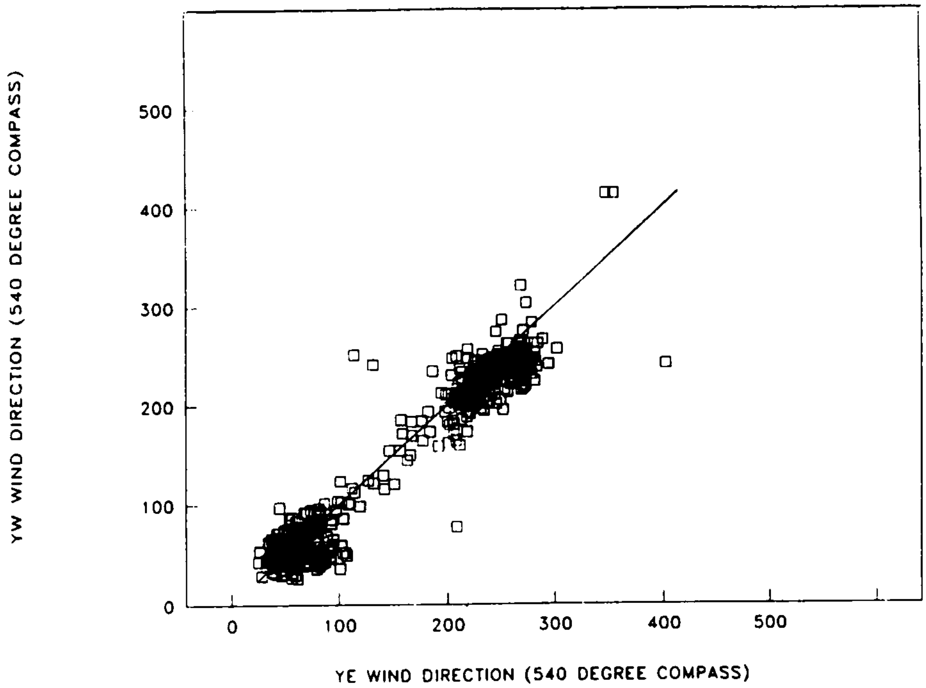

Figure 3-19: Scatterplot of Hourly Wind Direction (Degrees) at Wind Speeds Greater Than 3.0 m/s: YE versus YW

Table 3-5: Frequency (%) of Hourly Wind Direction Data Greater than 90 Degrees Apart During Light, Moderate, and High Winds.

	Frequency of Wind Directions Greater Than 90 Degrees Apart			
Wind Speed Range	YW/YE	YW/X10	YW/K25	X10/K25
0.5 - 1.5 m/s	41	19	39	36
1.5 - 3.0 m/s	7	14	17	22
> 3.0 m/s	<1	5	7	8

Another method used to further evaluate wind direction was to consider wind direction under the three different atmospheric stability conditions: Unstable (A and B), Neutral/Transition (C and D), and Stable (E and F). Again, cumulative frequency distribution plots and scatterplots are used to illustrate the results. Results of this evaluation indicate that hourly wind direction data compare best under neutral conditions; however, under stable and unstable conditions, correlation is poor. These results are consistent with those obtained when wind direction was evaluated under different wind speeds. For example, during high wind speeds, atmospheric stability is typically characterized as neutral; and low wind speeds typically occur during stable and unstable conditions. Figures 3-20 and 3-21 show a cumulative frequency plot of hourly wind direction data under the three basic stability classes for YE/YW and YW/K25. As illustrated in these plots, wind directions compare more favorably during neutral conditions.

To further illustrate the differences in wind direction as a function of stability class, Figures 3-22, 3-23, and 3-24 provide scatterplots for YE/YW during unstable, neutral, and stable conditions. During unstable conditions, significant scatter of data points is observed. During neutral conditions, the predominant wind direction is up- and down-valley with a noticeable amount of data points showing opposite wind directions (northeast versus southwest). However, during stable conditions, a considerable number of data points indicate winds in near opposite directions (as illustrated by the number of data points on the right and left edges of the plot). The percentage of time with winds greater than 157.5 degrees apart was approximately 14.1, 3.6, and 2.9 percent during stable, neutral, and unstable conditions, respectively.

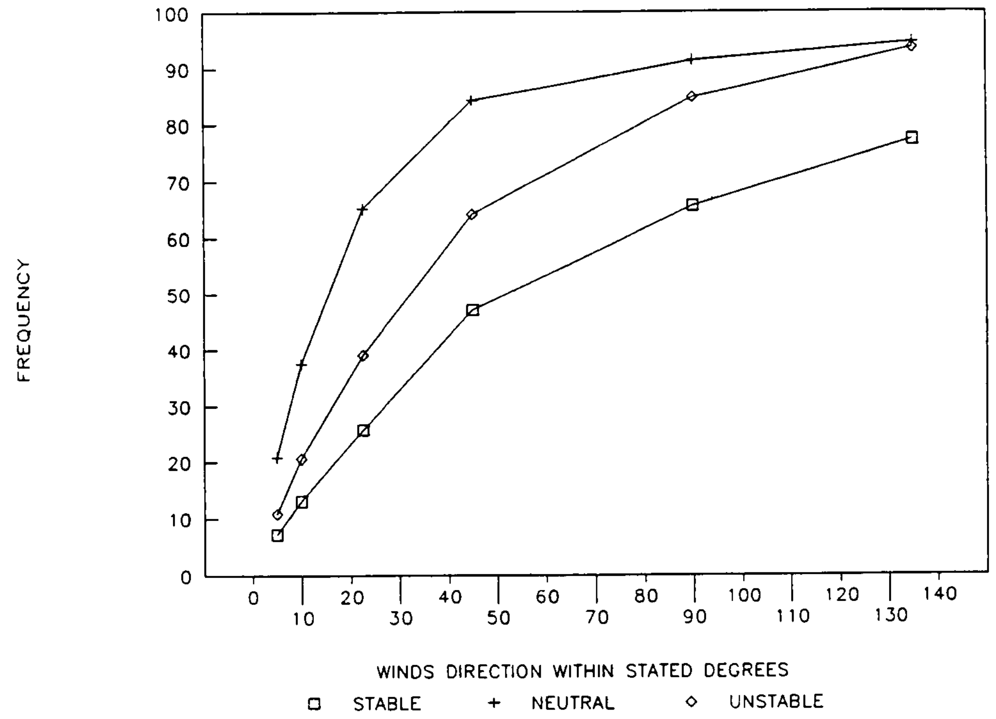

Figure 3-20: Cumulative Frequency Plot of Hourly Wind Direction (Degrees) During Stable, Neutral, and Unstable Conditions: YE versus YW

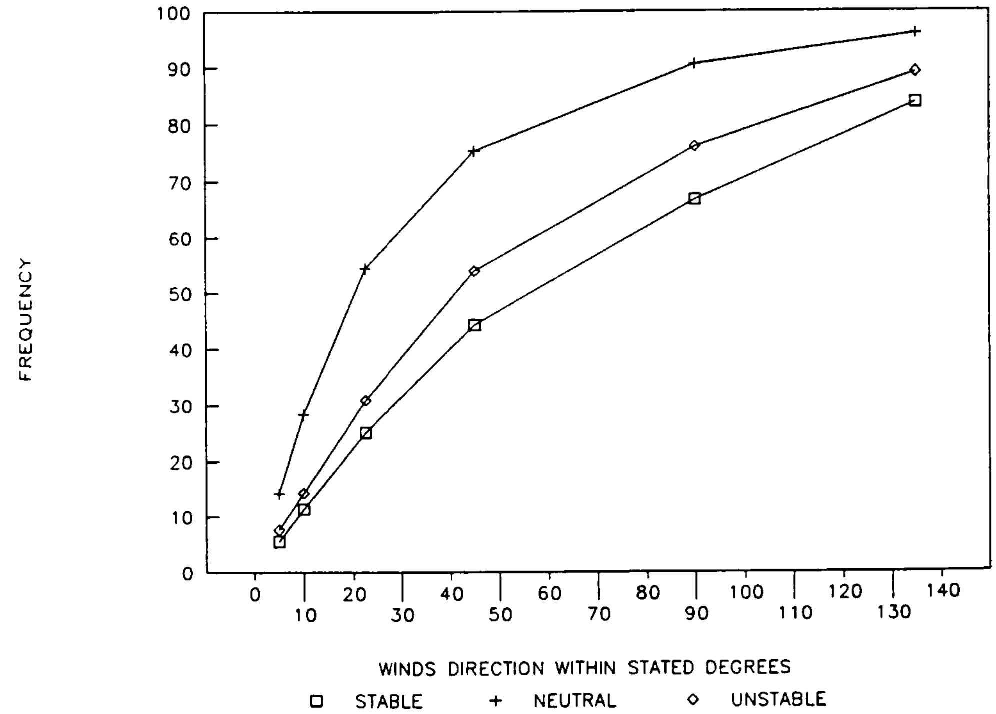

Figure 3-21: Cumulative Frequency Plot of Hourly Wind Direction (Degrees) During Stable, Neutral, and Unstable Conditions: YW versus K25

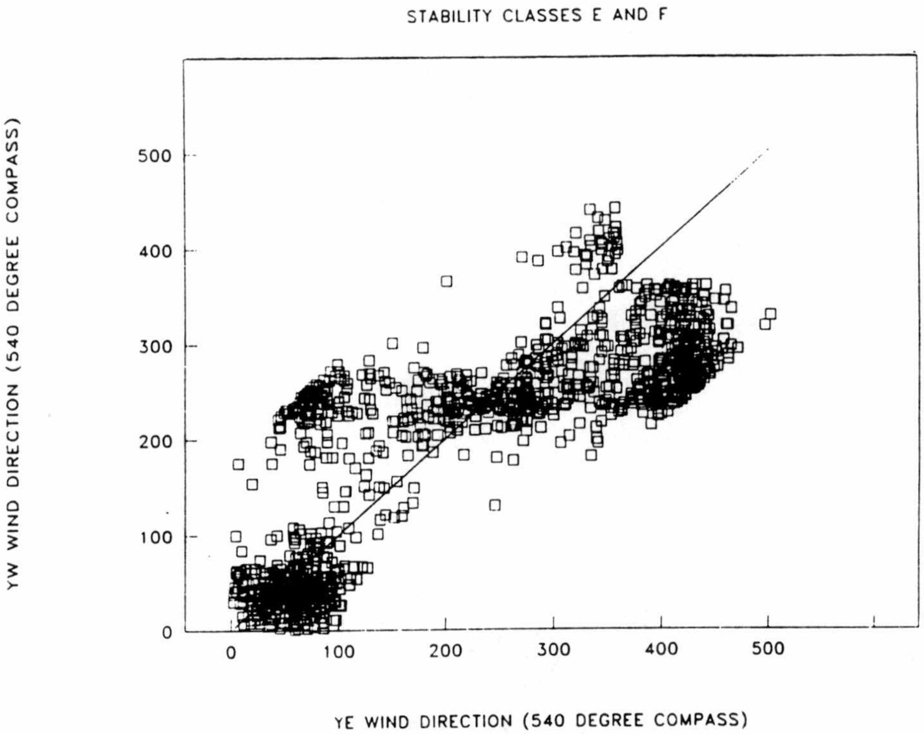

Figure 3-22: Scatterplot of Hourly Wind Direction (Degrees) During Stable Conditions: YE versus YW

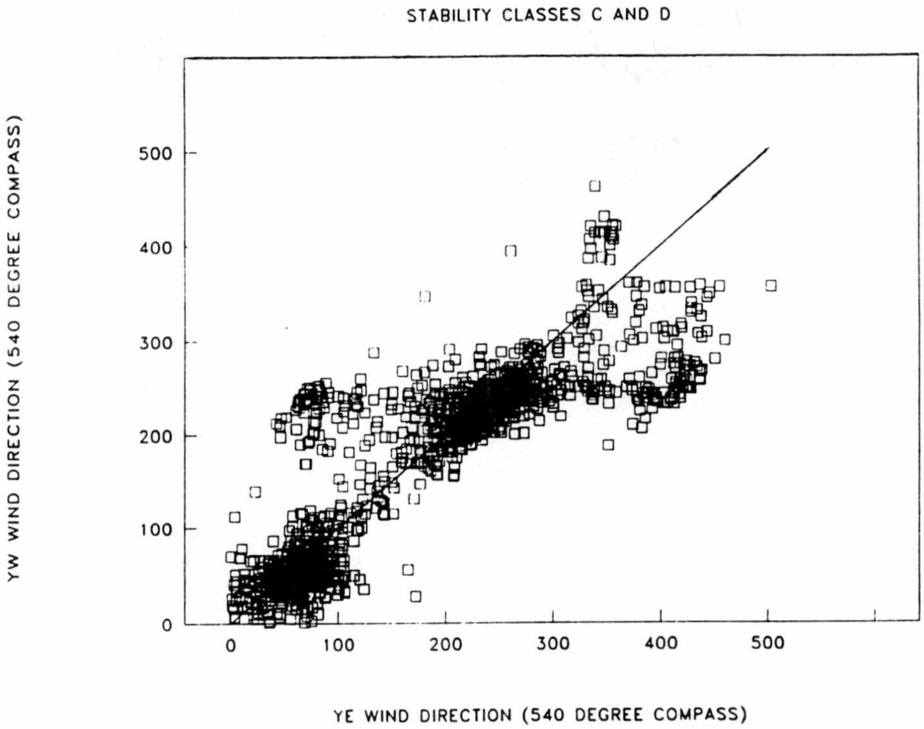

Figure 3-23: Scatterplot of Hourly Wind Direction (Degrees) During Neutral Conditions: YE versus YW

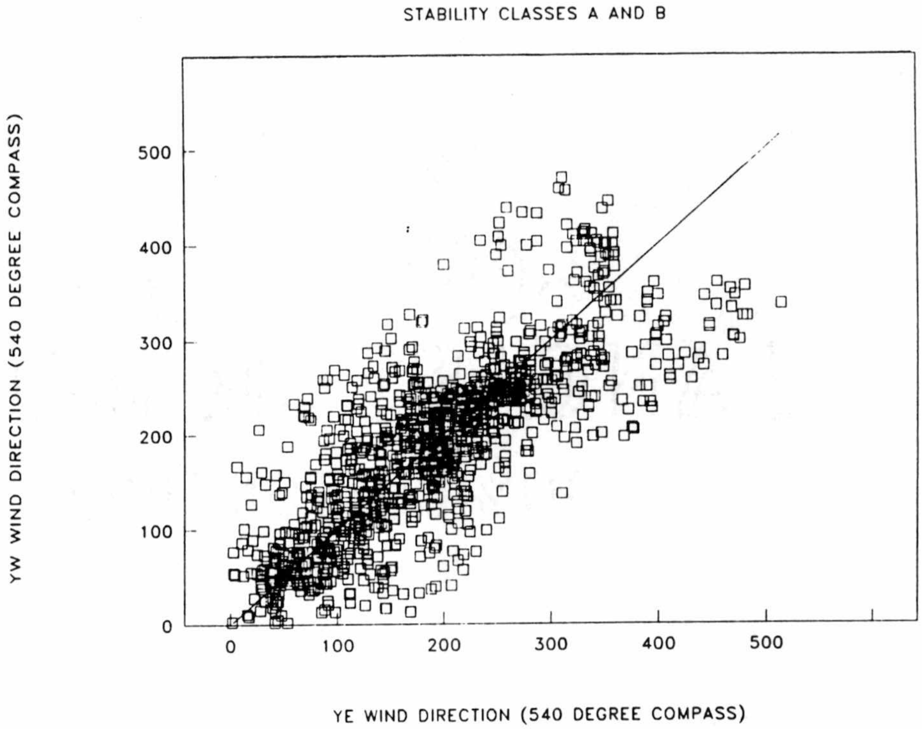

Figure 3-24: Scatterplot of Hourly Wind Direction (Degrees) During Unstable Conditions: YE versus YW

As another means of comparison, the differences in the wind directions at YE and YW were compared during cold weather. When ambient air temperatures were greater than 30 degrees F, wind directions were greater than 157.5 degrees apart approximately 6.6 percent of the time; however, when ambient temperatures were less than 30 degrees F, winds were greater than 157.5 degrees apart approximately 13.3 percent of the time. This data indicate that cold ambient temperatures may enhance differences between wind directions at the two towers. As previously indicated, convective currents from Lake Reality may cause northeasterly winds at YE and may partly explain these differences. Another potential explanation would be a heat island effect caused by the Y-12 Plant which would cause winds from opposite directions at the two towers. However, before definitive conclusions regarding the effect of cold ambient temperatures on wind directions at the two Y-12 Plant towers can be made, additional analysis and evaluation are needed.

3.4.2 Wind Speed

Hourly wind speed data was also compared for each set of meteorological data. As with wind direction, all hours where one or both of the wind speed observations were missing were omitted from the evaluation. Wind speeds were compared using two methods. First, hourly wind speed data were subtracted from each other. The absolute value of the difference in hourly wind speed will be referred to as delta wind speed. Cumulative frequency distribution data was calculated for delta wind speed for each data set compared. Secondly, correlation coefficients for each set of data were calculated. The results of this evaluation are presented in Table 3-6 and Figure 3-25.

This evaluation found that wind speed data correlate best when YE and YW were compared (correlation coefficient = 0.78); poorest correlation occurred when X10 was compared to K25 (correlation coefficient = 0.54). At least 20 percent of the time, each data set compared were within the accuracy level of the wind instruments (0.2 m/s). Eighty-four percent of the time YE and YW wind speeds were within 1 m/s; however, when YW and K25 were compared, 68 percent of the data were within 1 m/s. Overall, YE/YW compared the best and YW/K25 showed the poorest comparison.

Wind speeds were also compared during the three basic stability classes. From this evaluation, it was determined that wind speed varied more between the sites during neutral conditions than during stable and unstable conditions. This can be explained since during

Table 3-6: Frequency (%) of Hourly Wind Speed Data Within 0.2, 0.5, 1.0, 1.5, 2.0, 2.5, and 3.0 m/s and Correlation Coefficients for Each Data Set Compared

	Meteorological Data Compared			
Delta Wind Speed (m/s)	YW/YE	YW/X10	YW/K25	X10/K25
0.2	24.6	26.7	20.9	31.8
0.5	57.0	55.5	45.7	56.9
0.7	67.7	65.0	54.1	63.7
1.0	84.4	79.6	68.1	74.1
1.5	95.7	91.0	81.1	84.6
2.0	99.0	96.1	89.2	91.7
2.5	99.7	98.9	93.8	95.6
3.0	99.9	99.7	96.1	97.9
Correlation Coefficient	0.78	0.65	0.54	0.77

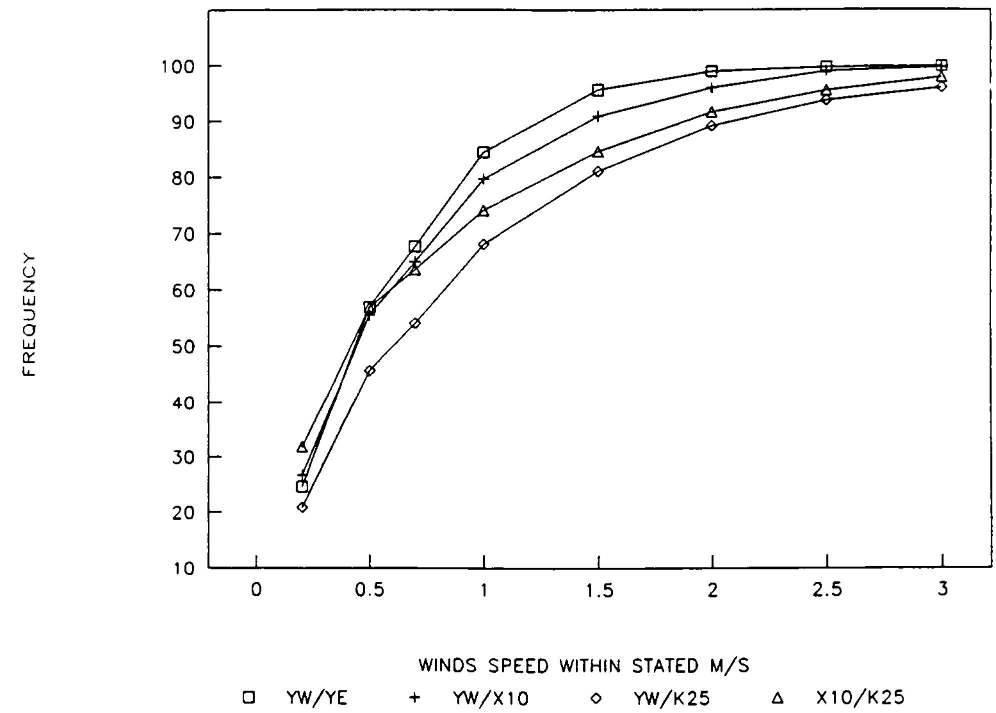

Figure 3-25: Cumulative Frequency Plot of Hourly Wind Speeds for Each Data Set Compared

neutral conditions, wind speeds are usually higher than occur during stable and unstable conditions. Therefore, variation of wind speed is more likely. Figure 3-26 provides a cumulative frequency diagram for wind speed data compared at X10 and K25. Cumulative frequency diagrams for other data sets compared are similar. Figures 3-27, 3-28, and 3-29 are scatterplots of X10/K25 wind speed data during unstable, neutral, and stable conditions, respectively. These scatterplots, and slopes of the best fit lines, clearly indicate that wind speed data at the K-25 Site is higher than observed at ORNL.

As another means of comparison, average wind speeds were calculated using hourly observations for each data set. The average wind speeds for Y-12 West, Y-12 East, ORNL, and K-25 were 1.8, 1.5, 1.5, and 2.0, m/s, respectively. These values are notably lower than calculated when using the default average wind speeds from the stability array data. The average wind speed calculated using stability array data ranged from 25 to 44 percent higher than when calculated using hourly data.

3.4.3 Stability Class

The hourly stability data were compared in a similar fashion as wind speed. The absolute value between the difference in the hourly stability classes was calculated.
This difference will be referred to as delta stability. Likewise, the correlation coefficient of the hourly data was calculated. Correlation coefficients of this data did not vary significantly from one set of data to another. The coefficients range from 0.77 to 0.66. Best correlation occurred when comparing Y-12 East and Y-12 West data. The poorest correlation occurred when comparing ORNL and K-25 data.

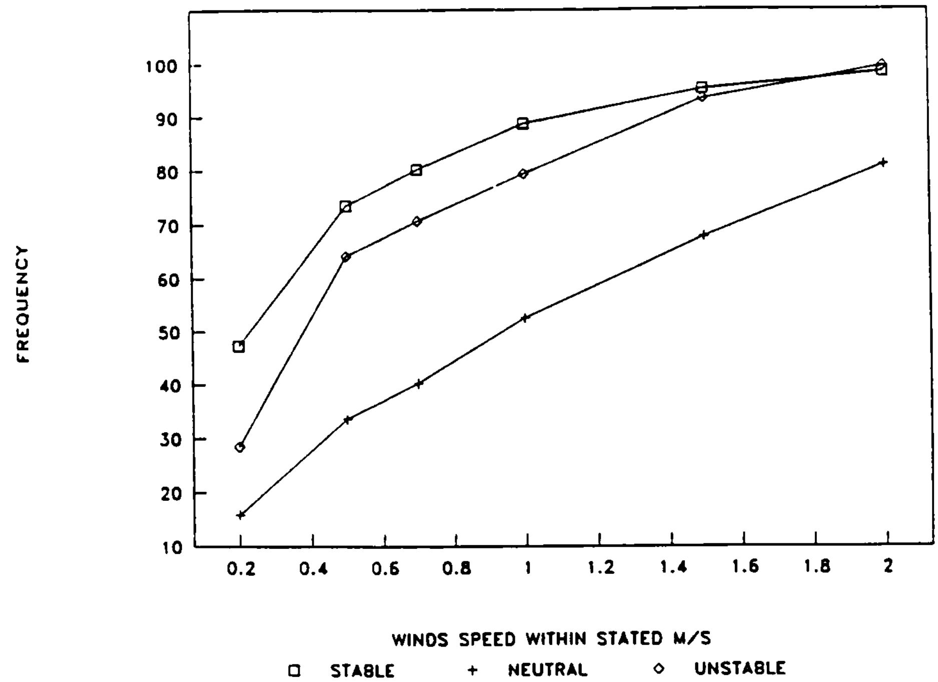

Figure 3-26: Cumulative Frequency Plot of Hourly Wind Speed (m/s) During Stable, Neutral and Unstable Conditions: X10 versus K25

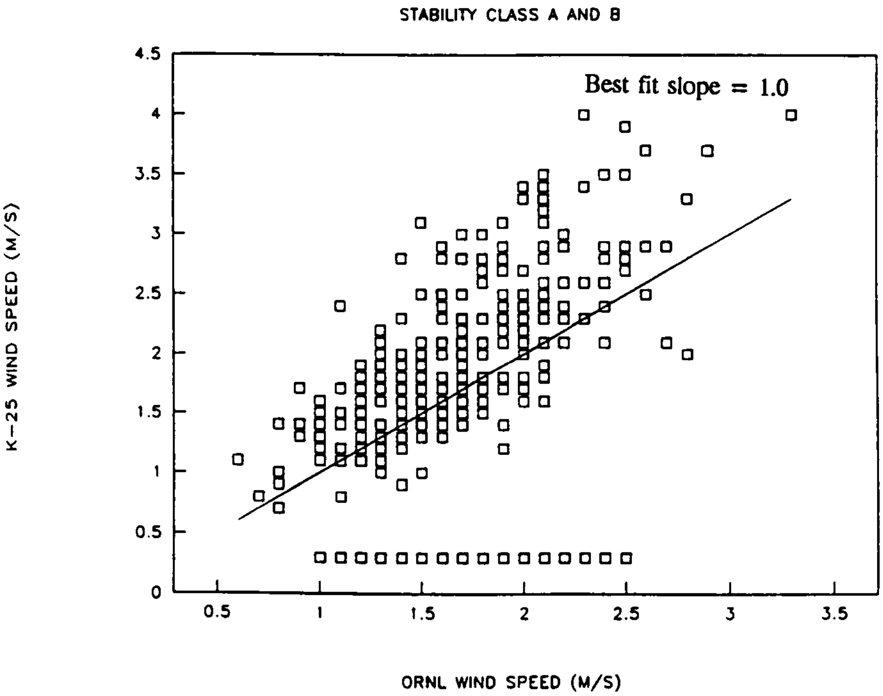

Figure 3-27: Scatterplot of Hourly Wind Speed (m/s) During Unstable Conditions: X10 versus K25

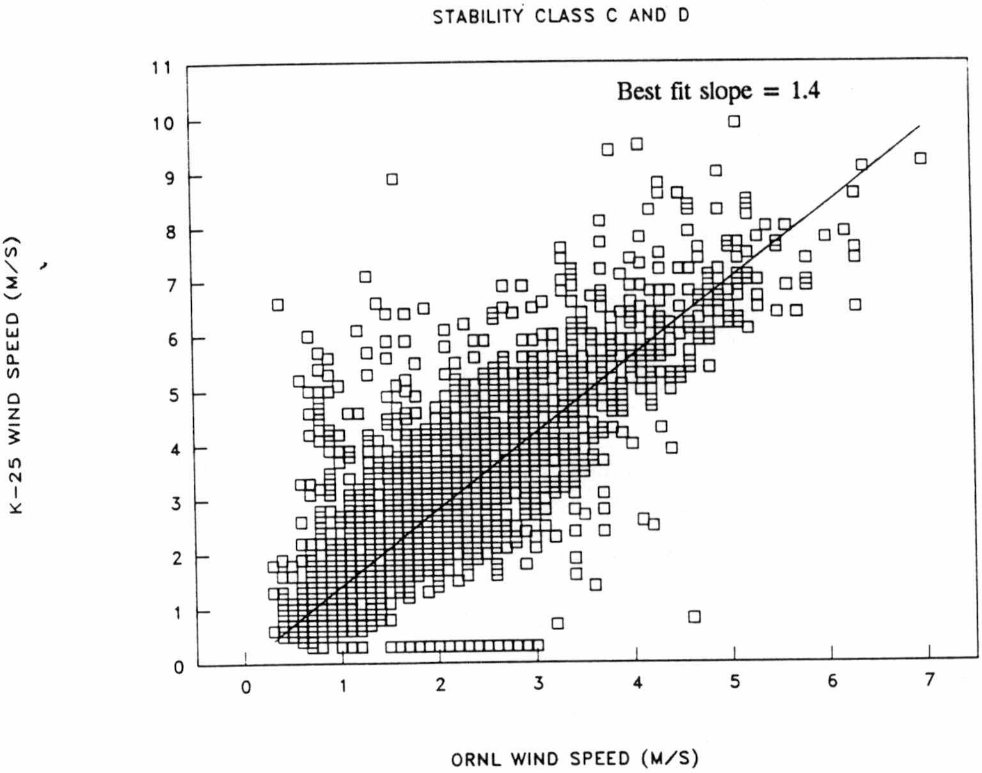

Figure 3-28: Scatterplot of Hourly Wind Speed (m/s) During Neutral Conditions: X10 versus K25

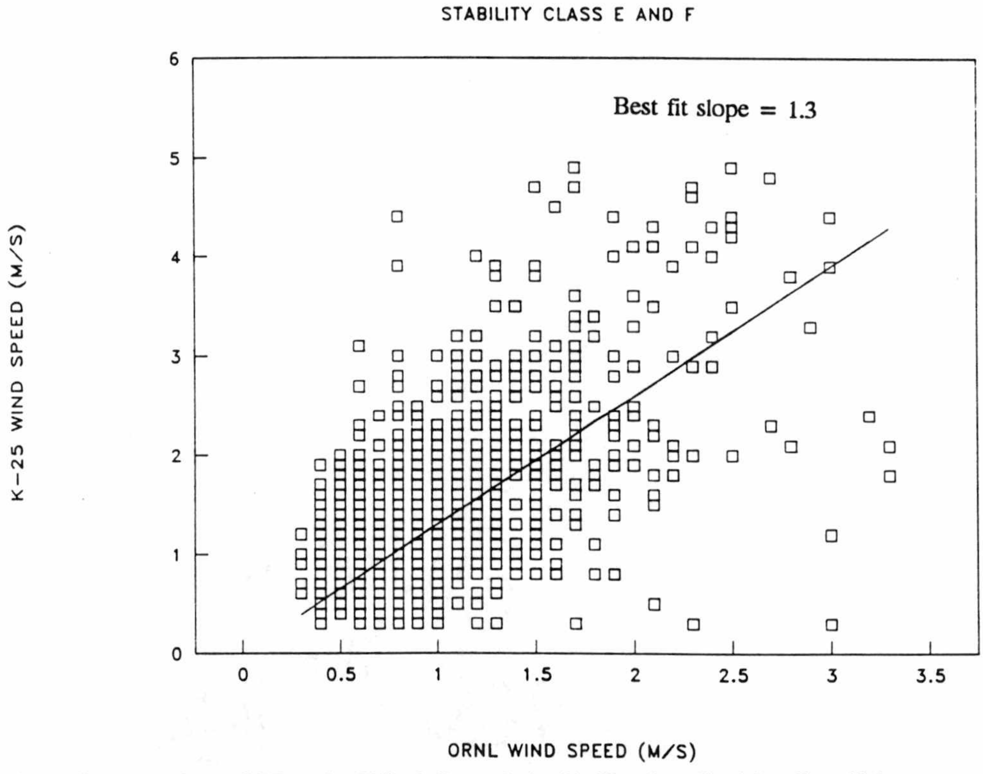

Figure 3-29: Scatterplot of Hourly Wind Speed (m/s) During Stable Conditions: X10 versus K25

Results of the cumulative frequency distribution of delta stability show similar results. The Y-12 Plant towers show the same stability class approximately 49 percent of the time. Among all data sets compared, the stability classes are within one category at least 78 percent of the time. All data sets compared were within 3 stability classes 100 percent of the time. Results of this evaluation are shown in Table 3-7. Overall, hourly variation in stability category between the sites is significantly less than wind direction.

Table 3-7: Frequency (%) of Hourly Stability Classes Within 0, 1, 2, and 3 Stability Categories.

	Meteorological Data Compared			
Delta Stability Category	YW/YE	YW/X10	YW/K25	X10/K25
0	49	37	40	37
1	87	79	79	78
2	98	95	95	94
3	100	100	100	100
Correlation Coefficient	0.77	0.68	0.68	0.66

3.5 COMPARISON OF UPPER- AND SURFACE-LEVEL WINDS

Although the purpose of this study was to evaluate variations in meteorological data within the boundary layer, this section briefly examines the relationship between observed upper-air flow and valley-flow. A significant amount of research has been conducted in this area as discussed in Section 2.4. Several of the hypotheses postulated by Doran and

Whiteman and Gross and Wippermann are discussed as they relate to data from this study.

Daily surface and 500 millibar (mb) upper-air weather maps for 1991 were reviewed in order to identify a period of time when upper air flows were strong and persistent from the southwest and northwest. The elevation of the 500 mb surface is approximately 16,000 to 18,000 feet above sea level. Although it is preferable to use upper-air data from lower elevations (i.e., 850 mb), only 500 mb data were available for this study. Two specific days were identified in which upper-air winds were relatively strong and consistently from the northwest and southwest. For these two days, hourly wind direction at each of the four meteorological towers was recorded and compared to the upper-air wind direction.

Figure 3-30 provides a graph illustrating the hourly wind directions at each of the four meteorological towers and the upper-air wind direction for November 20, 1991. The upper-level winds were from the southwest and are illustrated by the solid line on the graph; surface winds are illustrated by various data labels for each tower. The surface winds are very similar to upper-air winds until late afternoon when some deviation in the surface winds are noted. Through late afternoon, the surface winds are generally 10 to 30 degrees out of phase with the upper-air winds. This is consistent with the turning of the geostrophic wind toward the direction of lower pressure caused by friction at the earth's surface. Although southwesterly upper-level winds can produce southwesterly surface winds in each of the four mechanism described by Doran and Whiteman, the 10 to 30 degrees difference between the wind direction is most consistent with the downward momentum transport mechanism.

Figure 3-31 provides a graph illustrating the hourly 10 meter wind directions at each

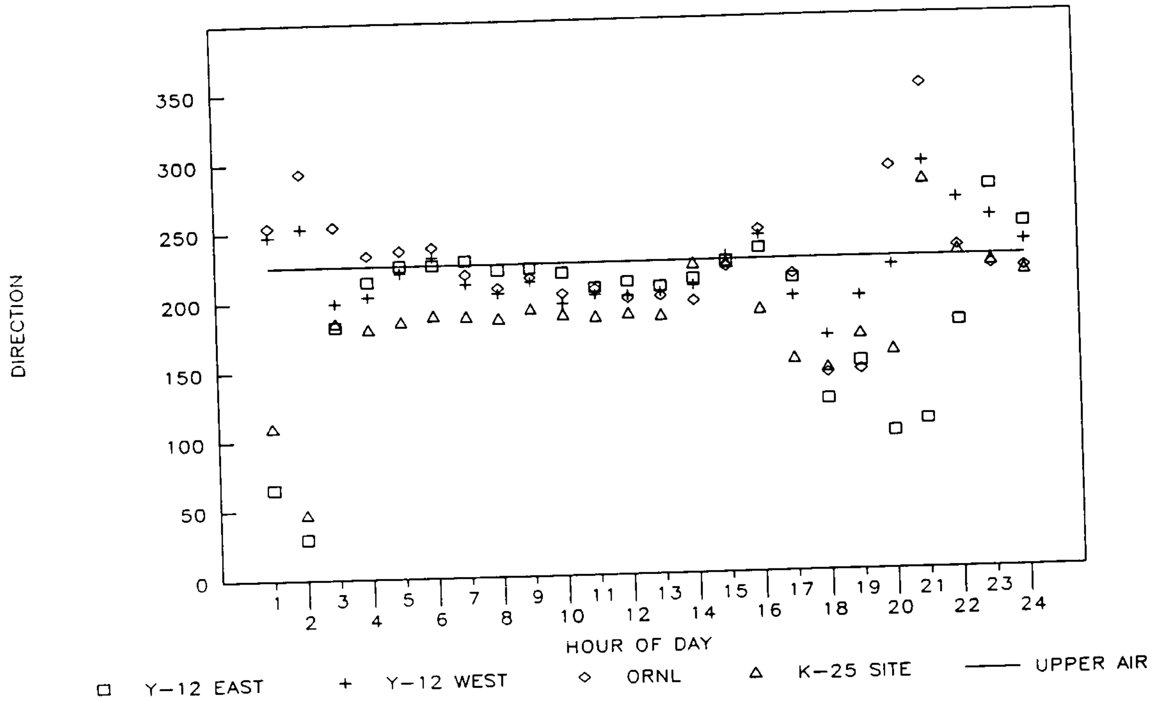

Figure 3-30: Comparison of Upper- and Surface-Level Wind Directions on November 20, 1991

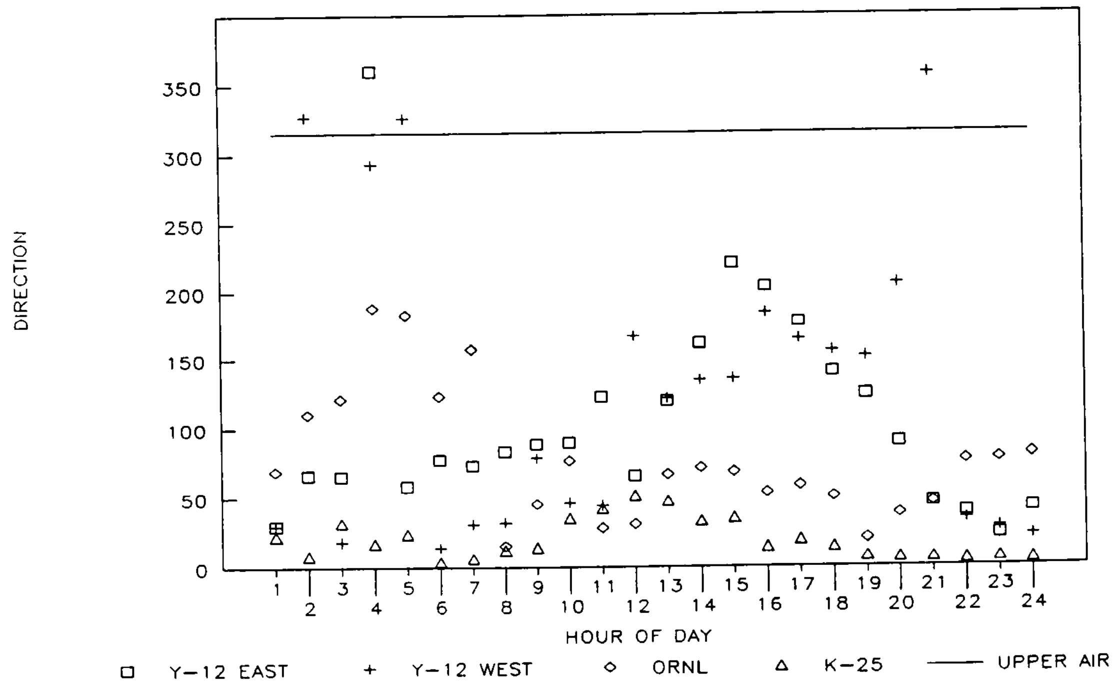

Figure 3-31: Comparison of Upper- and Surface-Level Wind Directions on March 11, 1991

of the four meteorological towers and the upper-air wind direction for March 11, 1991. In this case, the upper-level winds are from the northwest; however, most of the surface winds are from the northeasterly quadrant. The scenario may be the result of the forced channeling mechanism since the northwest upper-air direction marks the transition between southwesterly and northeasterly surface winds. For the forced channeling mechanism, slight variations in upper-air winds on either side of northwest can shift winds from southwest to northeast, depending upon the component of flow along the valley axis. A northeasterly surface flow with northwesterly upper-level winds is not consistent with the pressure driven channeling mechanism. It is also noted that winds at YE and YW shift from the northeast quadrant in the morning toward the south and southwest quadrant in mid-afternoon. This shift in wind direction may be caused by thermally driven up-valley currents. It is also noted that significantly more variation in wind direction is observed with northwesterly upper-air flow than with southwesterly upper-air flow. This may be caused by cross-valley flow resulting in enhanced turbulence and eddies as the air flows perpendicular to the ridges.

CHAPTER 4

COMPUTER DISPERSION MODELING

4.1 MODELING APPROACH AND METHODOLOGY

In Chapter 3, the important meteorological parameters which affect results of computer dispersion modeling were evaluated independently. These results showed significant variation in meteorological parameters, particularly for hourly wind direction data. Since the evaluation addressed only one parameter at a time, it did not consider the cumulative or aggregate effects due to differences in all three parameters. Therefore, computer dispersion modeling of a unit release (1 g/s) was conducted using each set of meteorological data. The modeling results are used as another tool in comparing differences in the meteorological data and in determining the effect of different meteorological data on predicted concentrations on the ORR. Annual average and 1-hour maximum concentrations were evaluated since they represent the most commonly used averaging periods for hazardous air pollutants.

Since unit releases were modeled, the predicted concentrations for each emission point represent concentration per unit release and are expressed in the units of micrograms per cubic meter per gram per second ($\mu g/m^3$ per g/s). This term is frequently referred to as normalized concentration, χ/Q, where χ equals concentration in $\mu g/m^3$ and Q equals emission rate in g/s. Therefore, once emissions are determined, the resulting concentration (χ_a) can be estimated by multiplying the actual emission rate (Q_a) in g/s times χ/Q as determined by computer dispersion modeling. This relationship is illustrated in the equation below:

$$\chi_a = Q_a \left(\frac{\chi}{Q}\right) \tag{4-1}$$

One emission point was modeled for each of the three major installations on the ORR. In addition, a fourth emission point was modeled to represent the TSCA Incinerator since the incinerator has significantly different effluent characteristics than other typical hazardous air pollutant emission sources at the ORR. Due to an extremely large number of emission points on the ORR, modeling of individual sources becomes impractical. The Y-12 Plant, for example, has over 700 different emission points. In addition, it is estimated that the ORR has over 1600 emission points associated with various research and development activities.

4.2 MODELING ASSUMPTIONS AND INPUT PARAMETERS

The ISC model was used for this study since it has historically been used by DOE and state regulatory agencies for dispersion modeling studies on the ORR. Both the short-term and long-term version of ISC were used since each model uses a different type of meteorological input file.

All modeling runs utilized the regulatory default option which included consideration of the following: final plume rise, stack-tip downwash, calm wind processing routines (ISCST only), default wind profile exponents, default potential temperature gradients, and default mean wind speeds for each wind speed category (ISCLT only). Building downwash was not addressed since the emission points were theoretical and detailed data on nearby buildings were not available. Rural dispersion coefficients were used since the installations are located in a predominantly rural area and the installations, although relatively large, do not contain numerous tall buildings or heat sources [31]. The simple terrain option was employed for all modeling. Therefore, any terrain elevations above stack elevation are assumed to be at the stack elevation (i.e., terrain chopping). ISC does not have the capability of estimating concentration on elevated terrain (terrain above stack height).

4.2.1 Source Identification and Location

The four point sources modeled included one at each of the installations and the TSCA Incinerator. The three theoretical emission points are identified as KPOINT, YPOINT, and XPOINT to represent emissions from the K-25 Site, Y-12 Plant, and ORNL, respectively. The TSCA Incinerator is represented by emission point KTSCA. Modeling all emissions from one release point at each installation is generally a conservative assumption as indicated in Appendix B of the *Draft New York Air Guide-1*. The conservatism is further pronounced when conservative effluent characteristics are utilized. In particular, short-term concentration estimates may be highly conservative if actual sources are located significant distances apart and have varying effluent characteristics [32].

The locations of emission points XPOINT, YPOINT, and KPOINT were selected to best represent locations within the respective installations where hazardous air pollutants are most likely to be centered. The locations of these emission points were determined by discussion with personnel familiar with hazardous air pollutant emissions from the respective installation.

At ORNL, the emission point is located in the approximate vicinity of the 4500-N and 4500-S laboratory complex. The majority of research and development operations and potential hazardous air pollutant emissions are associated with these two research buildings. The emission point for the Y-12 Plant was located slightly north of the approximate center of the installation. Thus, the emission point is located in the general area of the major production facilities within the Y-12 Plant (e.g., Buildings 9212, 9206, and 9215). Since most manufacturing operations (and associated emissions) at the K-25 Site have been discontinued, selection of the point source location required more consideration. After review, it was determined that the location most representative of current and future emissions would be slightly east of the center of the installation. The general area includes buildings K-1035, K-1501, and K-1037 and areas where waste management and remedial action projects (e.g., Pond Waste Management Project) are planned. The TSCA Incinerator emission point was located at its approximate location in the extreme eastern section of the K-25 Site.

Figures 4-1, 4-2, and 4-3 show the approximate locations of YPOINT, XPOINT, and KPOINT and KTSCA, respectively.

4.2.2 Source Effluent Characteristics

Since effluent characteristics of the TSCA Incinerator are well known and documented, actual values were utilized. However, with the three hypothetical emission points at each of the installations, it was necessary to select effluent characteristics which

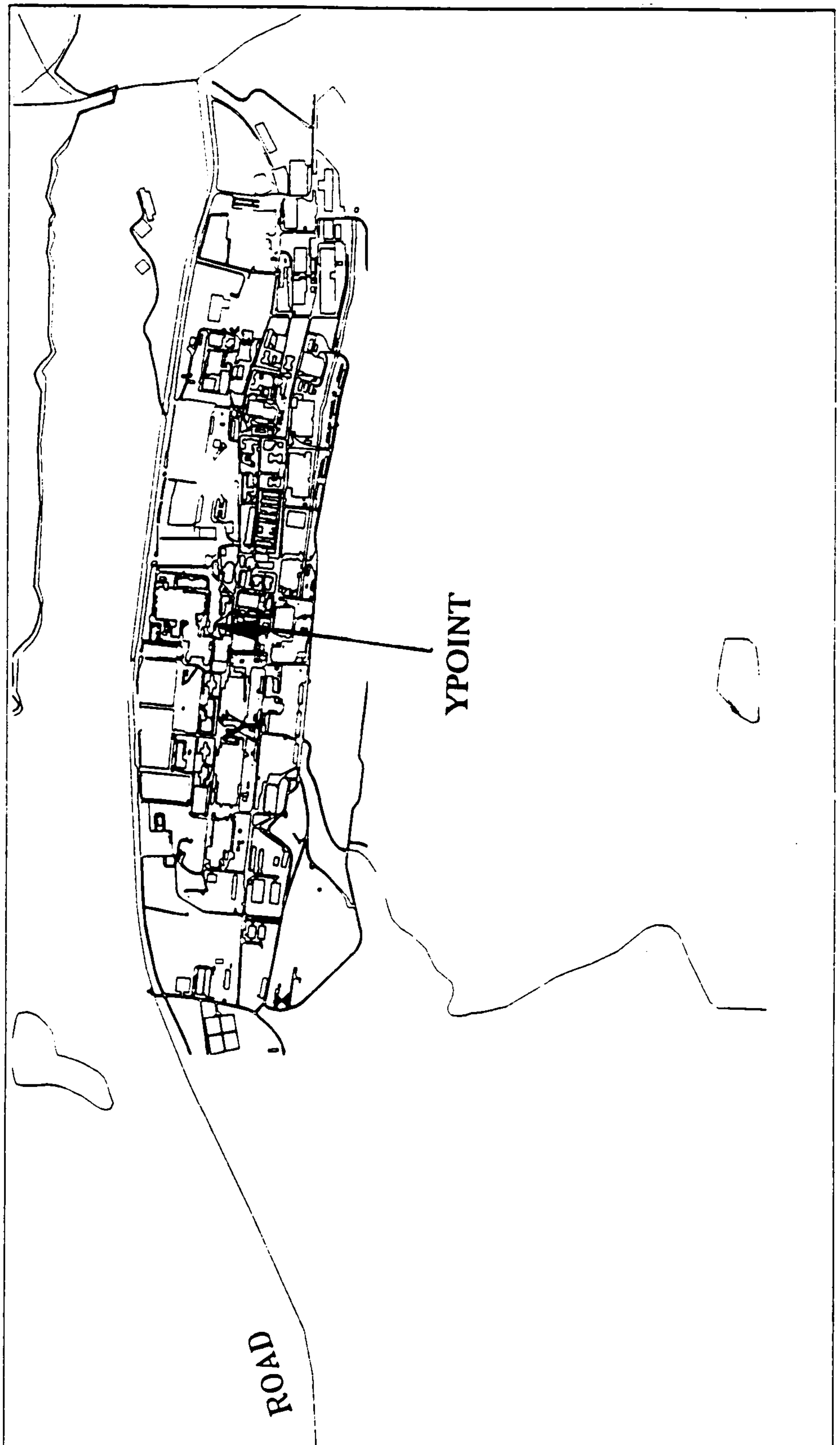

Figure 4-1: Approximate Location of YPOINT

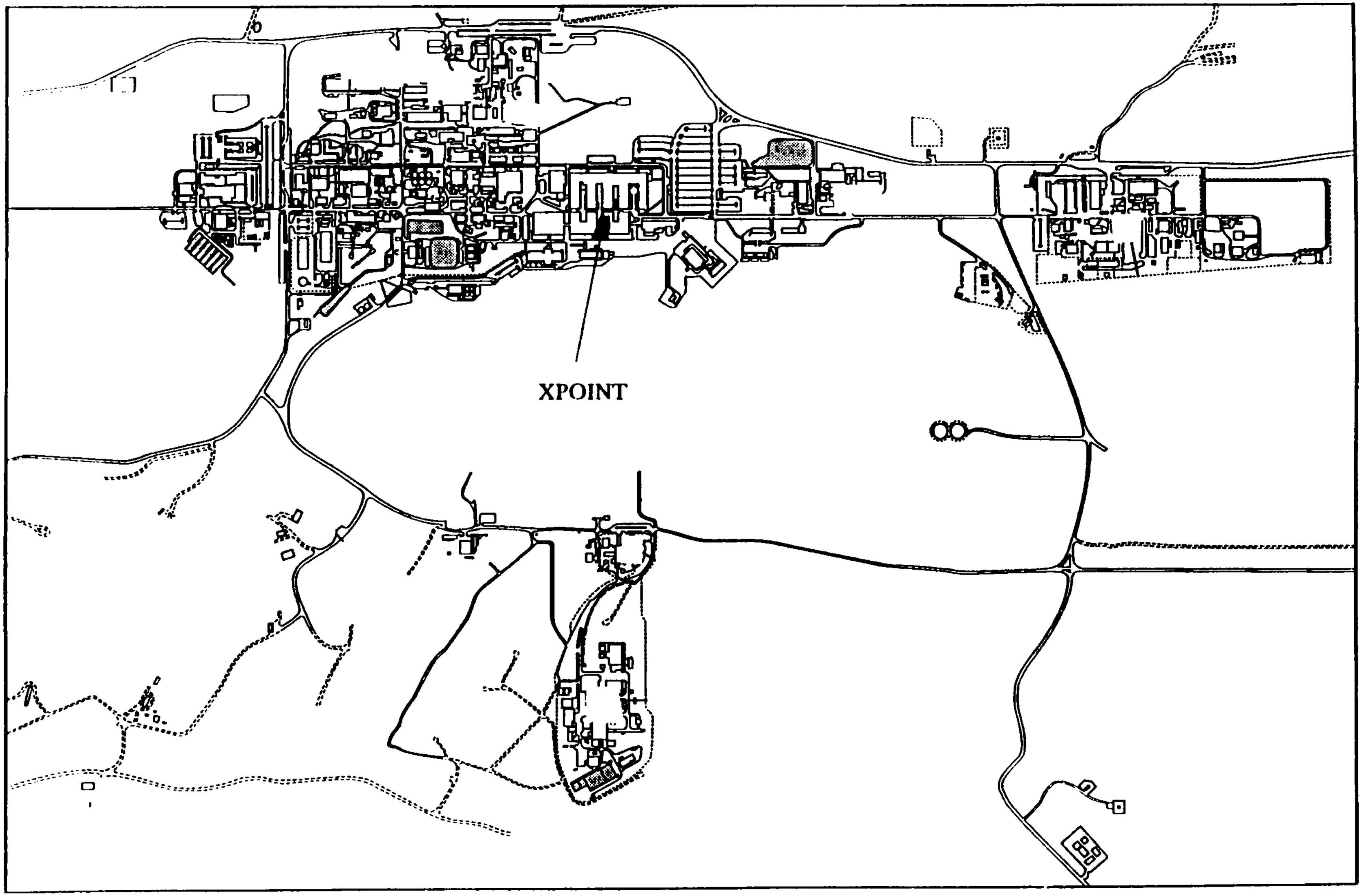

Figure 4-2: Approximate Location of XPOINT

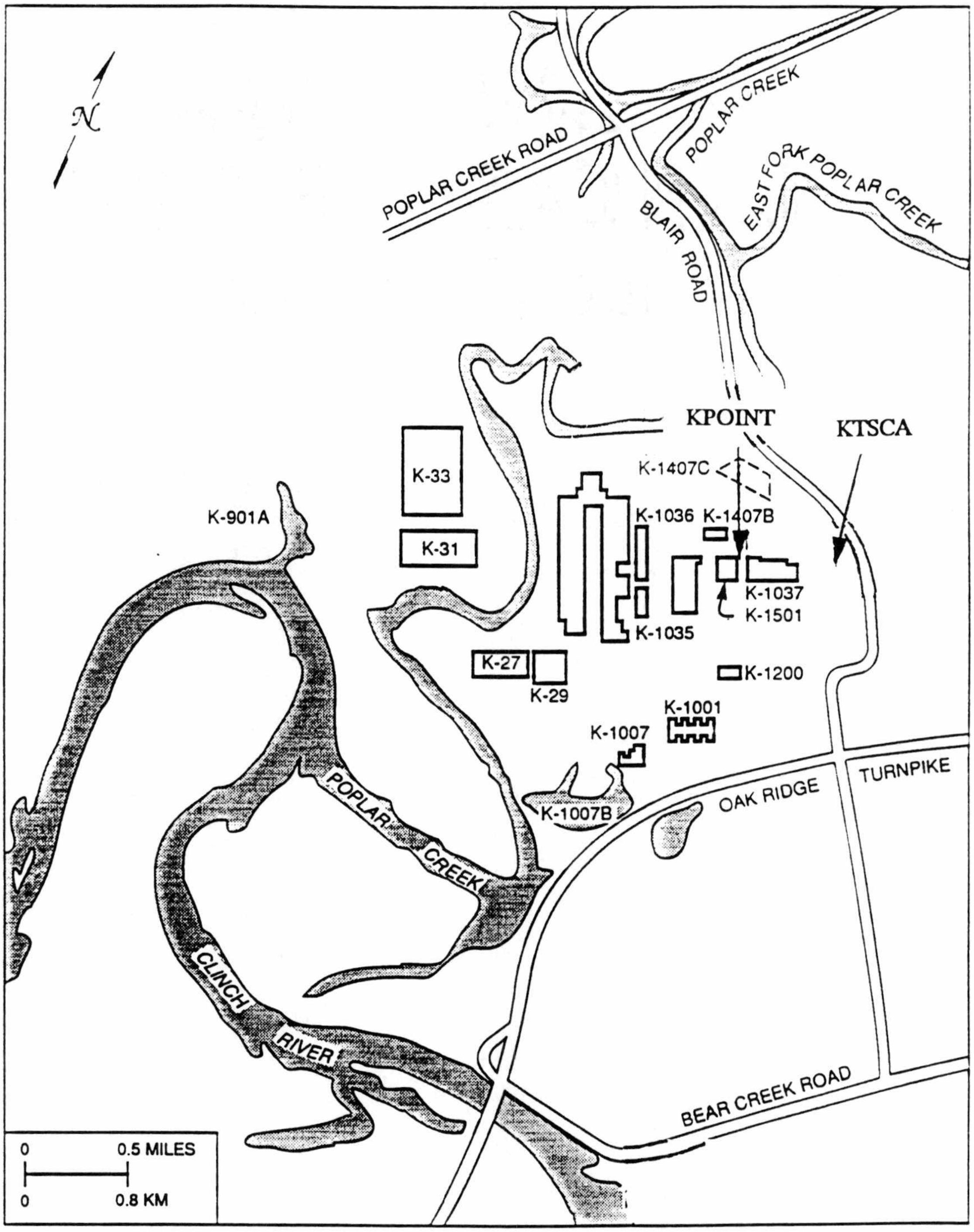

Figure 4-3: Approximate Location of KPOINT and KTSCA

would likely be representative.

Effluent characteristics for these three emission points are assumed to be identical. Ten meters was selected for the stack height since it is an estimate of typical building heights of production and research facilities where hazardous air pollutant emissions may arise. A stack diameter of 0.5 meters was selected since it was believed to be representative of many hazardous air pollutant stacks. The exit temperature of the three hypothetical emission points was assumed to be approximately the temperature in most production and research areas (20° Celsius). Overall, this is likely to be a minimum exit temperature since some emissions originate from heated processes. Exit velocity will vary widely from source to source; therefore, selection of a representative exit velocity is difficult. Due to these uncertainties, the exit velocity was assumed to be zero meters per second (m/s). A summary of effluent characteristics and coordinate locations for each emission point is provided in Table 4-1.

Table 4-1: Summary of Effluent Characteristics and Coordinate Locations for Emission Points

SOURCE PARAMETER	YPOINT	XPOINT	KPOINT	KTSCA
Stack Height (m)	10	10	10	30.5
Exit Temperature (°K)	293	293	293	350
Exit Velocity (m/s)	0.0	0.0	0.0	5.5
Stack Diameter (m)	0.5	0.5	0.5	1.37
X-Coordinate (m)	0.0	-4,700	-11,800	-11,400
Y-Coordinate (m)	0.0	-6,300	-5,400	-5,400
Z-Coordinate (m)	286	244	247	247
Stack Elevation (m)	296	254	257	277.5

4.2.3 Receptor Grid

The chosen receptor grid has historically been used by DOE in demonstrating compliance with Tennessee air pollution regulations and has been approved by the Tennessee Department of Health and Environment for evaluating hazardous air pollutant emissions [33]. Two-hundred sixty-five (265) discrete receptors were located on the boundary of the ORR. For each receptor, the corresponding X-Y coordinate was identified. In addition, the elevation (Z-coordinate) of each receptor was input into the model. A list of each receptor number and the corresponding coordinate location is found in Appendix B. Figure 4-4 shows the grid system, associated receptor numbers at increments of twenty, and the approximate location of each emission point.

4.3 MODELING RESULTS: ANNUAL AVERAGE CONCENTRATION

As previously indicated, the output of the computer dispersion modeling will be normalized concentrations ($\mu g/m^3$ per g/s) since unit emissions were modeled. These results will be analyzed to determine the maximum normalized concentration and location (receptor number) for each individual emission point when modeled with each set of meteorological data. Model runs were conducted using ISCST and ISCLT; sample input files for each model are provided in Appendix C. Results of the modeling are discussed below.

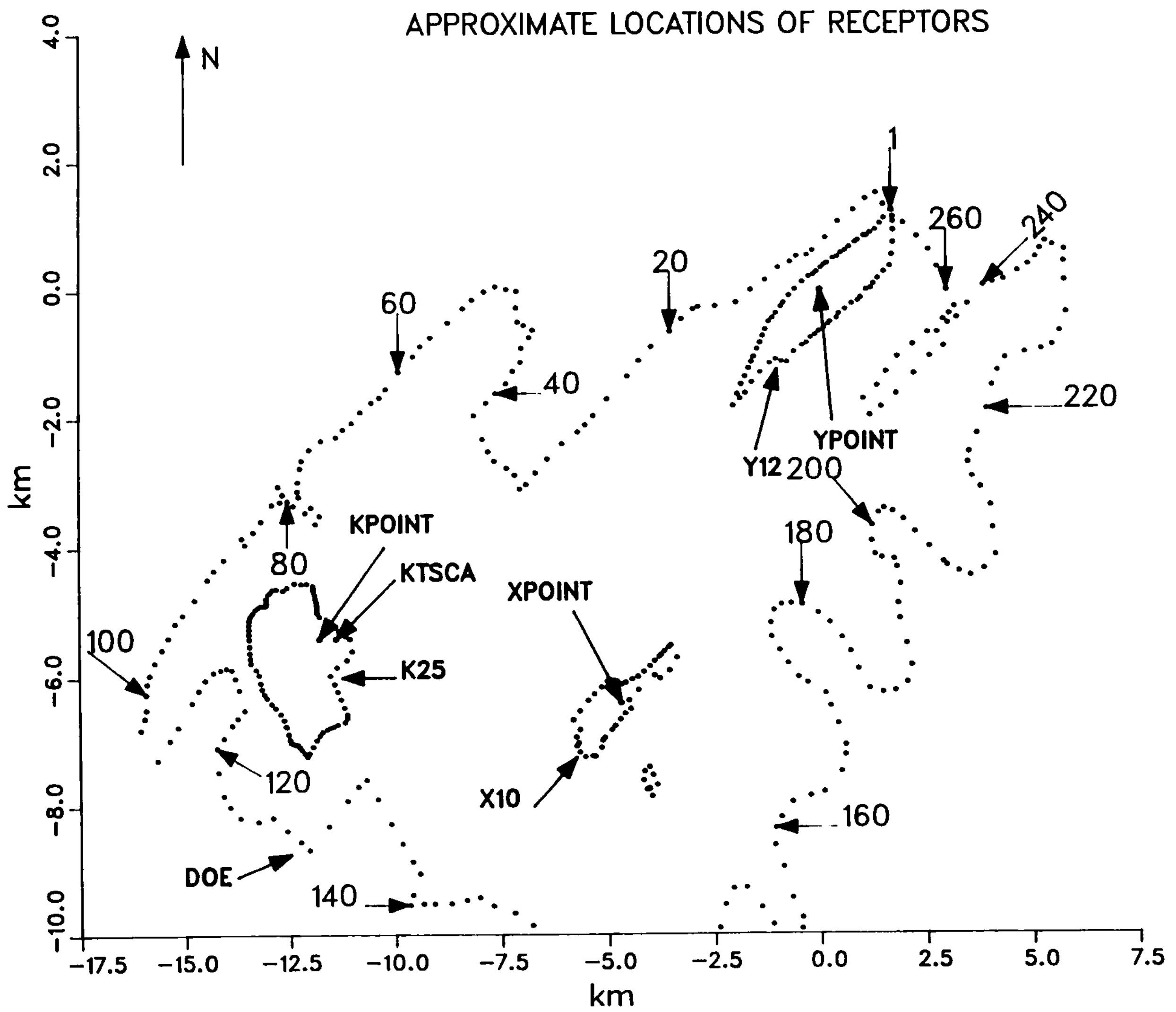

Figure 4-4: Receptor Grid Used in Dispersion Modeling

4.3.1 Industrial Source Complex Short-Term

Annual average, normalized concentrations were calculated at each of the 265 receptors using each set of meteorological data. Tables 4-2 and 4-3 provide summaries of the maximum concentration and location (receptor number) for each emission point when modeled with each meteorological data set. The magnitude of maximum concentration varied from a factor of 1.65 to 2.08, depending upon the emission point. KTSCA showed the greatest variation, and KPOINT showed the least variation.

For XPOINT, the maximum concentration was predicted using YW meteorological data and occurred northeast of the emission point. YE meteorological data resulted in the maximum concentration southwest of the emission point for KPOINT and KTSCA. As indicated in Table 3-1, YW meteorological data had a significant fraction (40 percent) of the winds from south-southwest to west-southwest. Likewise, YE data had a large fraction (39 percent) from north-northeast to east-northeast. These characteristics explain the relatively high concentrations and location of maximum concentrations to the southwest and northeast, respectively. However, the maximum concentration for YPOINT occurred north of the emission point when using K25 meteorological data. K25 meteorological data had a significantly higher frequency of southerly winds (SSE to SSW) than the other three sites. Approximately 16.6 percent of the winds at K25 were from SSE to SSW versus 8.9 to 11.5 percent at the other sites. The property boundary to the north is closer than any other direction at the Y-12 Plant.

The location of maximum concentration for each emission point showed some

Table 4-2: Comparison of Maximum Annual Average Concentration and Location for Each Set of Meteorological Data When Using ISCST

Meteorological Data	Maximum Concentration ($\mu g/m^3$ per g/s) and Location (Receptor Number) for Each Emission Point			
	YPOINT	XPOINT	KPOINT	KTSCA
Y-12 West	2.65 (265)	0.96 (176)	0.90 (121)	0.46 (34)
Y-12 East	2.39 (14)	0.91 (136)	1.49 (116)	0.52 (110)
ORNL	1.80 (265)	0.87 (176)	1.45 (116)	0.31 (131)
K-25 Site	3.46 (8)	0.47 (144)	1.43 (116)	0.25 (37)

Table 4-3: Comparison of Distance and Direction to Receptor of Maximum Annual Average Concentration For Each Set of Meteorological Data When Using ISCST

Meteorological Data	Distance (km) and Direction (in parenthesis) to Receptor of Maximum Concentration			
	YPOINT	XPOINT	KPOINT	KTSCA
Y-12 West	2.5 (NE)	4.1 (NE)	4.2 (SW)	6.1 (NE)
Y-12 East	1.7 (W)	6.1 (WSW)	2.5 (SW)	3.1 (WSW)
ORNL	2.5 (NE)	4.1 (NE)	2.5 (SW)	0.9 (S)
K-25 Site	0.9 (N)	6.1 (SW)	2.5 (SW)	5.8 (NE)

variations when using different meteorological data sets. Differences in locations of maximum concentration are a function of meteorology (primarily wind direction), source characteristics (e.g., stack height, plume rise), geometry of property boundary with respect to location of the emission point, and the elevation of receptors relative to the release height. Table 4-3 provides a summary of the distance and direction to maximum concentration for each emission point when modeled with each set of data.

For YPOINT, the maximum concentration occurred northeast of the plant at receptor 265 when using YW and X10 meteorological data; however, when using YE and K25 meteorological data, the maximum concentration occurred north and west of the plant at receptors 14 and 8, respectively. These results are likely caused by more pronounced channelized flow observed in the wind rose data for YW and X10. Wind roses for K25 and YE show a higher frequency of winds from the southerly and easterly quadrants, respectively, than the other wind roses. As a result, maximum concentrations occur to the north and west of the emission point instead of to the northeast. The distance to the boundary is closer toward the north and west of the emission point than toward the northeast.

A similar pattern was observed for the location of maximum concentration for emissions from XPOINT as was observed for YPOINT. The location of maximum concentration for XPOINT when using YW and X10 meteorological data was northeast of the plant at receptor 176; however, the location of maximum concentration for YE and K25 meteorological data was west-southwest and southwest of the plant at receptors 136 and 144, respectively. Unlike YPOINT, the distance to the property boundary to the north and west is much farther than to the southwest; therefore maximum concentration when using YE and

K25 data was in the southwesterly direction.

The location of maximum concentration for KPOINT was southwest of the plant for all meteorological data sets modeled because the distance to the property boundary in this direction is significantly closer than other directions. The location of maximum concentration for KTSCA when using YW and K25 meteorological data was northeast of the plant at receptors 34 and 37, respectively; however, the location of maximum concentration for YE and X10 data was west-southwest and south of the plant at receptors 110 and 131, respectively.

As another means of comparing the results of modeling, predicted concentrations obtained from the different meteorological data at each of the 265 receptors were compared to each other with the correlation coefficient. In this hypothetical situation, the total concentration at each receptor was calculated when each emission point was releasing 1 g/s. The correlation coefficients for YW/YE, YW/X10, YW/K25, and X10/K25 were 0.09, 0.78, 0.47, and 0.46, respectively. Concentrations obtained when using Y-12 East and West meteorological data resulted in the poorest correlation (correlation coefficient = 0.09). This low correlation coefficient indicates essentially no relationship between concentrations obtained when using YE and YW meteorological data. The best correlation occurred when comparing concentrations obtained from X10 and YW meteorological data (correlation coefficient = 0.78). These results are consistent with the correlation coefficients calculated for wind direction frequency data in Section 3.3.1 (i.e., poorest correlation for YE/YW and best correlation for YW/X10). Figures 4-5 and 4-6 provide scatterplots of concentration at all 265 receptors to graphically illustrate the degree of correlation for YW/YE and YW/X10.

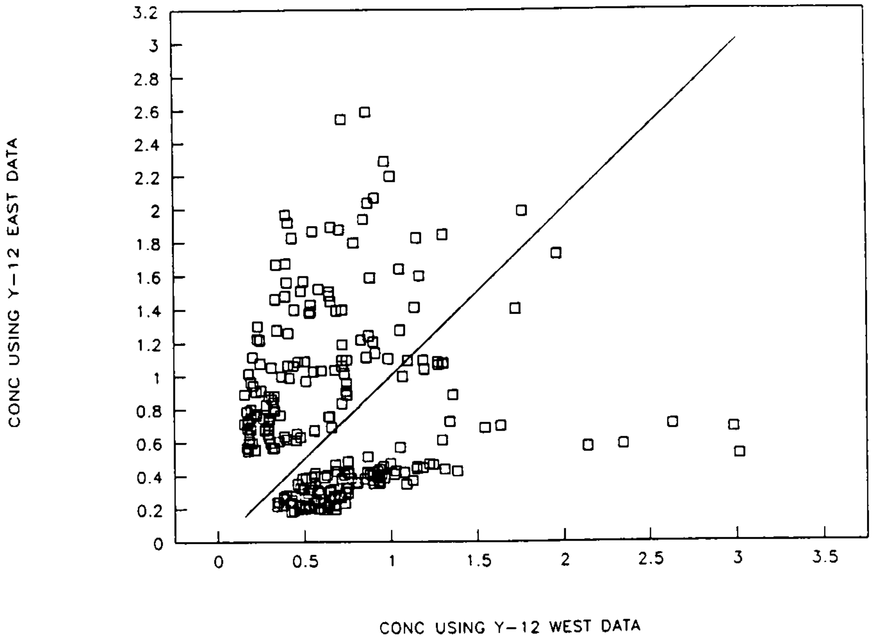

Figure 4-5: Scatterplot of Annual Average Concentrations ($\mu g/m^3$ per g/s) at 265 Receptors Along ORR Boundary When Using YW and YE Meteorological Data (Emissions = 1 g/s at Each Emission Point)

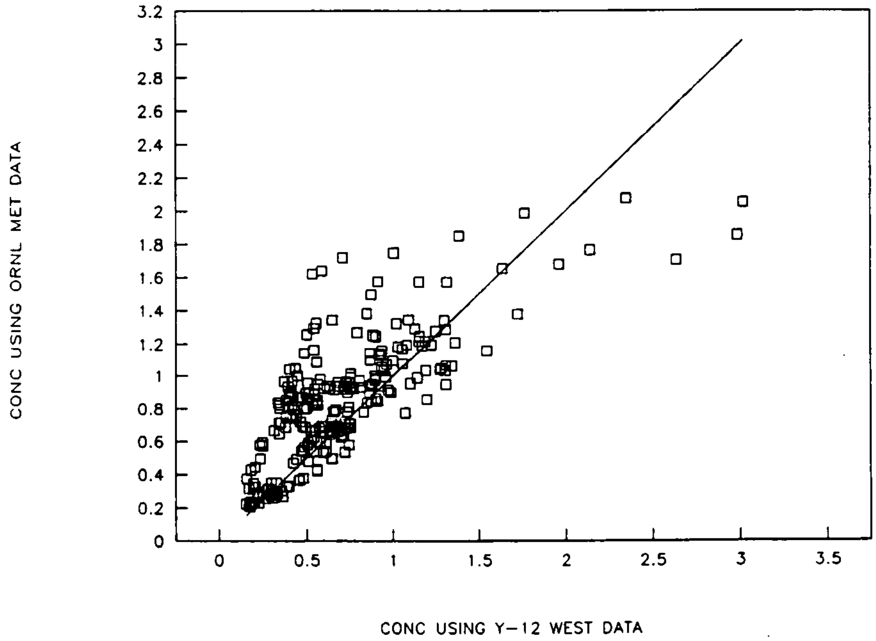

Figure 4-6: Scatterplot of Annual Average Concentrations ($\mu g/m^3$ per g/s) at 265 Receptors Along ORR Boundary When Using YW and X10 Meteorological Data (Emissions = 1 g/s at Each Emission Point)

4.3.2 Industrial Source Complex Long-Term

A similar analysis conducted for ISCST was also conducted for ISCLT. As anticipated, the location of maximum concentration for each emission point as determined using ISCLT was at or near that obtained when using ISCST. Minor differences in location of maximum concentration between ISCST and ISCLT can be expected since ISCLT breaks down the wind direction into the 16 primary meteorological directions, and ISCST uses actual hourly wind direction data. The same basic pattern observed when comparing results from ISCST also occurred with results from ISCLT. The general tendency was for YW and X10 meteorological data to have maximum concentrations occurring northeast of the installation due to predominate southwesterly winds. Table 4-4 provides a summary of the maximum concentration and location for each emission point when using each meteorological data set and ISCLT.

The correlation coefficient of concentrations at each of the 265 receptors was calculated for each meteorological data set compared. The correlation coefficients for YW/YE, YW/X10, YW/K25, and X10/K25 were 0.15, 0.82, 0.53, and 0.57. Consistent with the result of ISCST, the best correlation occurred when concentrations obtained from YW meteorological data were compared to that obtained using X10 meteorological data. Likewise, poorest correlation occurred when concentrations obtained using YW and YE meteorological data were compared. In all cases, the correlation coefficients obtained from ISCLT concentration data were higher than that obtained from ISCST concentration data. This is most likely the result of using annual joint frequency distribution data (STAR) instead of hourly data.

Table 4-4: Comparison of Maximum Annual Average Concentration and Location for Each Set of Meteorological Data When Using ISCLT

Meteorological Data	Maximum Concentration ($\mu g/m^3$ per g/s) and Location (Receptor Number) for Each Emission Point			
	YPOINT	XPOINT	KPOINT	KTSCA
Y-12 West	1.74 (265)	0.71 (176)	0.75 (116)	0.29 (32)
Y-12 East	1.94 (13)	0.56 (136)	2.24 (115)	0.39 (110)
ORNL	1.30 (265)	0.59 (176)	1.00 (116)	0.26 (131)
K-25 Site	2.78 (7)	0.31 (147)	0.92 (115)	0.16 (37)

4.3.3 Comparison of ISCST and ISCLT Concentrations

As indicated in Section 4.3.2, the location of maximum concentration for each emission point when using ISCST and ISCLT were essentially the same. However, one significant difference noted between the results when using ISCST and ISCLT was the magnitude of maximum concentration. In all cases except one, the maximum concentration obtained when using ISCST was greater than when using ISCLT. On average, the maximum concentration obtained when using ISCST was 37 percent greater than when using ISCLT. Some differences between ISCST and ISCLT results are expected since each model uses different meteorological input data (hourly versus STAR). In addition, the long-term model assumes a uniform lateral distribution across the sector width and does not use the standard deviation of the lateral dispersion (σ_y). However, the significant differences in predicted concentration could not be explained solely by these model differences.

To further evaluate differences in calculated concentration between ISCST and ISCLT for a given meteorological data set, the predicted concentrations at all 265 receptors were compared (assuming 1 g/s release from all four emission points). For each meteorological data set and all 265 receptors, the correlation coefficient and slope of the best fit line was calculated. In addition, the average, maximum, and minimum ratios of concentrations obtained while using ISCLT and ISCST were calculated. Results of this evaluation are shown in Table 4-5.

Table 4-5: Comparison of Annual Average Concentrations at 265 Receptors as Obtained from ISCLT and ISCST (Emission = 1 g/s at Each Emission Point)

	Meteorological Data Used			
Parameter	Y-12 West	Y-12 East	ORNL	K-25 Site
Correlation Coefficient	0.98	0.91	0.98	0.99
Slope of Best Fit Line	0.70	0.90	0.70	0.75
ISCLT/ISCST Concentration Ratio				
average	0.75	0.67	0.75	0.72
minimum	0.59	0.41	0.55	0.57
maximum	1.01	1.46	1.04	0.93

As anticipated, the correlation coefficient when using ISCST and ISCLT was very good (correlation coefficient = 0.91 to 0.99); however, as noted by the slopes of the best fit lines and the ISCLT/ISCST concentration ratios, the concentrations obtained when using ISCLT were significantly lower than when using ISCST. To graphically illustrate this point, a scatterplot of concentration obtained when using ISCLT and ISCST is provided in Figure 4-7 for meteorological data from YW.

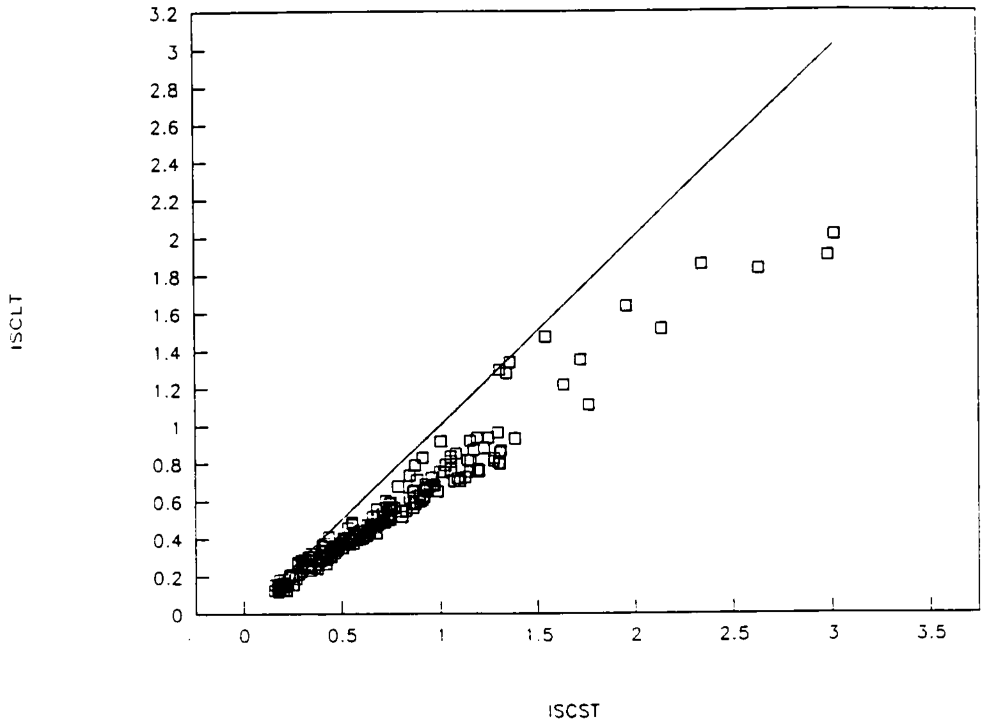

Figure 4-7: Scatterplot of Annual Average Concentration ($\mu g/m^3$ per g/s) When Using ISCST and ISCLT at 265 Receptors Along ORR: YW Meteorological Data (Emissions = 1 g/s at Each Emission Point)

It is expected that differences between results obtained from ISCST and ISCLT are partially due to error introduced in ISCLT by using the default mean wind speeds for each wind speed category. As indicated in Section 3.3.2, ISCLT assumes a mean wind speed for each wind speed category. For example, for the first category (0 - 1.54 m/s), ISCLT assumes a mean wind speed of 1.50 m/s. In Chapter 3, the mean wind speed as calculated from the STAR data and hourly wind speed data was presented. However, ISCST does not use wind speeds less than 1.0 m/s; instead, ISCST assumes a wind speed of 1.0 m/s when the hourly wind speed is less than 1.0 m/s. In addition, with the calm wind process routine, ISCST ignores all hours of calm wind data. Therefore, the average wind speed was recalculated by assigning a value of 1.0 m/s for all hours less than 1.0 m/s and ignoring all hours of calm winds.

Table 4-6 shows the average wind speed of each set of meteorological data as calculated from hourly and stability array data using the same assumptions used by the respective model (i.e., default mean wind speeds for ISCLT and calm wind processing routine for ISCST). In addition, the table shows the ratio of wind speeds from each data set and the ratio of average concentration obtained when using ISCLT and ISCST. It should be noted that the speed ratios are expressed in terms of ISCST to ISCLT while the concentration ratios are expressed in terms of ISCLT to ISCST. This is necessary since concentration is inversely proportional to wind speed.

Table 4-6: Comparison of Average Wind Speeds (m/s) as Calculated from Hourly Data and Stability Array Data

Meteorological Data	ISCST Wind Speed [1]	ISCLT Wind Speed [2]	Speed Ratio ISCST/ISCLT	Conc. Ratio ISCLT/ISCST
Y-12 West	1.9	2.3	0.82	0.75
Y-12 East	1.7	2.1	0.81	0.67
ORNL	1.6	2.0	0.80	0.75
K-25 Site	2.1	2.5	0.84	0.72

[1] Average wind speed calculated using same assumptions used by ISCST (e.g., values less than 1.0 m/s were assigned a value of 1.0 m/s, and calm winds were not included in the calculation).

[2] Average wind speed calculated using default ISCLT mean wind speed for each category.

The actual mean wind speed for the first wind speed category was calculated to be 1.1 m/s for all four data sets; therefore, an assumed mean value of 1.54 m/s used by ISCLT will overestimate average wind speed. Higher wind speeds assumed by ISCLT result in lower modeled concentrations. Further, since the wind speed ratios of ISCST to ISCLT are similar to the concentration ratios of ISCLT to ISCST, it appears that differences in wind speed used by the two models may account for a portion of the difference in predicted concentration. Therefore, before additional modeling using ISCLT is performed, an evaluation of actual average wind speed in each wind speed category should be conducted and the default mean wind speed values adjusted as necessary.

4.4 MODELING RESULTS: 1-HOUR MAXIMUM CONCENTRATION

In addition to annual average concentrations, 1-hour maximum concentrations are also frequently used to evaluate ambient impacts of air toxics. In order to evaluate the differences in the four sets of meteorological data, the magnitude and location of maximum 1-hour concentrations were calculated for each emission point using each set of meteorological data. The results of this evaluation are presented in Tables 4-7 and 4-8.

The magnitude of maximum concentrations was very similar for all meteorological data used on each emission point. The most significant difference was noted when YPOINT was modeled with YE meteorological data. In this case, the maximum concentration was

Table 4-7: Comparison of Maximum 1-Hour Average Concentration and Location for Each Emission Point When Modeled With Each Set of Meteorological Data

Meteorological Data	Maximum Concentration ($\mu g/m^3$ per g/s) and Location (Receptor Number) for Each Emission Point			
	YPOINT	XPOINT	KPOINT	KTSCA
Y-12 West	1,384 (9)	88 (31)	174 (87)	43 (67)
Y-12 East	986 (9)	86 (32)	188 (87)	41 (66)
ORNL	1390 (9)	86 (151)	186 (87)	39 (93)
K-25 Site	1354 (8)	87 (151)	186 (87)	43 (89)

Table 4-8: Comparison of Distance and Direction to Receptor of Maximum 1-Hour Average Concentration For Each Emission Point When Modeled with Each Set of Meteorological Data

Meteorological Data	Distance (km) and Direction (in parenthesis) to Receptor of Maximum Concentration			
	YPOINT	XPOINT	KPOINT	KTSCA
Y-12 West	0.9 (N)	5.8 (NNW)	2.8 (NW)	5.3 (N)
Y-12 East	0.9 (N)	5.8 (NNW)	2.8 (NW)	5.3 (N)
ORNL	0.9 (N)	5.3 (SE)	2.8 (NW)	3.9 (WNW)
K-25 Site	0.9 (N)	5.3 (SE)	2.8 (NW)	3.3 (NW)

approximately 30 percent less than when modeled with the other three sets of meteorological data. All other maximum concentrations were within 10 percent for any given emission point. This is an important observation considering the significant differences noted between hourly meteorological data. It is likely that the maximum 1-hour concentrations are similar for all data sets modeled since, during any given year, a large number of meteorological conditions exists. The meteorological conditions (i.e., wind speed/direction and stability category) that result in the maximum concentration likely occur for each of the four data sets at some time during the year. Therefore, the maximum concentration values are similar.

With regard to location of maximum concentration, the results when using the various meteorological data were similar but showed more variation than concentration. When modeling in flat terrain, maximum 1-hour concentration many times occurs at the closest receptors for sources with low release heights. However, of all the combinations of modeling runs conducted for this study, only one emission scenario resulted in maximum concentration at the nearest receptor. Due to the complex topography on the ORR, the locations of maximum 1-hour concentrations were affected by the elevation of receptors in addition to their relative proximity to the source. For example, even though a receptor is located relatively close to an emission point, if the receptor elevation is low compared to the release height, the plume may remain aloft and not significantly impact the receptor. However, another receptor, perhaps located at a farther distance, may be at an elevation similar to the release height. In this case, the plume centerline may impact the receptor resulting in higher concentrations than the receptor located closer to the emission point. As indicated in Chapter 2, ISC uses "terrain chopping" for receptors with elevations above the physical stack height. Therefore, receptors located above the release height are assumed to be at the release height.

For YPOINT, the location of maximum concentration was essentially the same for each set of meteorological data modeled. The maximum concentration for all data sets modeled occurred north of YPOINT at receptors 8 and 9. Receptors 8 and 9 are adjacent and represent the closest receptors to the Y-12 Plant; therefore, it is not unexpected that the maximum 1-hour concentration occurs at these locations. Receptors 8 and 9 are located on elevated terrain (approximately 15 meters above stack height).

For KPOINT, the location of maximum concentration for all data sets was 2.8 km northwest of the emission point at receptor 87. Unlike YPOINT, this receptor is not the closest receptor to the emission point. Receptor 115 and other receptors to the southwest of the plant are approximately 2.2 km from the emission point; however, the elevation of this receptor is approximately 23 meters below the stack height. Therefore, the plume remains quite some distance above the receptors to the southwest of the plant. On the contrary, plumes moving toward the north and northwest may impact elevated terrain.

For XPOINT, the location of maximum concentration when using YE and YW meteorological data was north-northwest of the plant at receptors 31 and 30, respectively. Both of these receptors are located on elevated terrain. However, when using X10 and K25 meteorological data, the location of maximum concentration was southeast of the plant at receptor 151. The elevation of receptor 151 is located approximately 3 meters below the stack height; therefore, it is located near the centerline of the plume. The closest receptor to XPOINT is receptor 176 which is approximately 4.2 km from the emission point; however, the elevation of this receptor is approximately 19 meters below the stack height.

For KTSCA, the locations of maximum concentrations when using YE and YW data were in the northerly direction at receptors 63 and 67, respectively. When using X10 and K25 meteorological data, the maximum concentrations occurred north-northwest and northwest of the incinerator at receptors 93 and 89, respectively. Each of the receptors of maximum concentration are located on elevated terrain. Like KPOINT, receptors to the southwest of the site are closer; however, these receptors are significantly below the effective plume height.

Each of the maximum 1-hour concentrations calculated above occurred during F-stability with wind speeds less than 1 m/s. Therefore, the primary meteorological variable affecting location and magnitude of maximum 1-hour concentration is wind direction. Due to the large number of receptors (265) and number of hours in a year (8,760), an hourly comparison of concentration using each set of meteorological data for each emission point and receptor is not practical. Instead, differences in hourly wind direction between two meteorological towers and its theoretical effect on concentration is evaluated below.

The equation used by ISCST to calculate concentration (χ) was provided in Section 2.2 in Equation (2-9) and is repeated below:

$$\chi = \frac{QKVD}{2\pi u_s \sigma_y \sigma_z} \exp[-0.5 \left(\frac{Y}{\sigma_y}\right)^2] \qquad (2\text{-}9)$$

Consider two theoretical meteorological towers which measure hourly wind direction: let each wind direction be referred to as WD_1 and WD_2. The difference between the wind direction (WD_1 -WD_2) is referred to as theta (θ). The receptor, R, is the location where concentration is to be estimated using both sets of meteorological data with emissions from a fixed emission point, EP. The downwind distances of plume centerline will be X_1 and X_2 for each set of meteorological data. The cross-wind distance for the second meteorological data set is Y. Since it is assumed that the receptor is directly downwind for WD1, the cross-wind distance for WD1 is zero. This hypothetical scenario is illustrated in Figure 4-8.

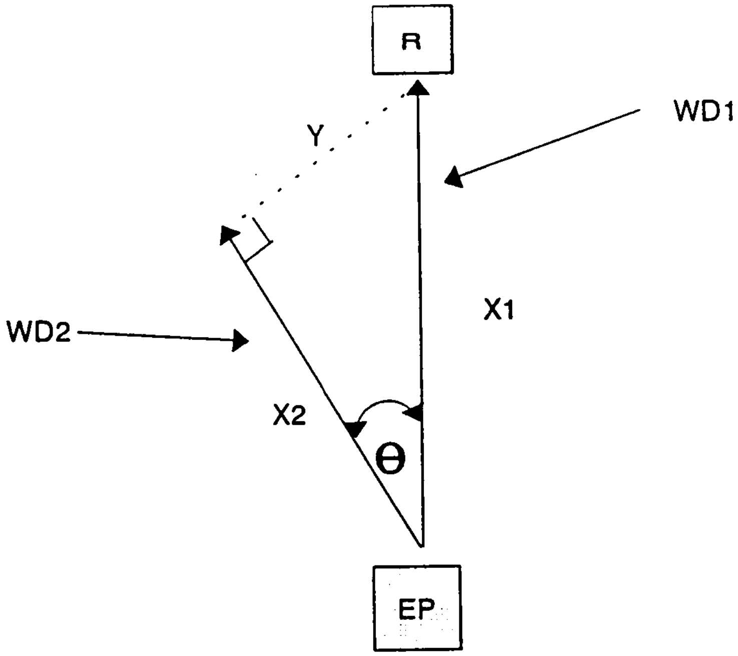

X2 = X1 COS (THETA)

Y = X1 SIN (THETA)

Figure 4-8: Schematic Showing Two Hypothetical Wind Vectors Used to Calculate Concentration at Receptor

X_2 and Y can be calculated using standard trigonometric functions for given values of X_1 as follows:

$$X_2 = X_1 \cos(\theta) \tag{4-2}$$

$$Y = X_1 \sin(\theta) \tag{4-3}$$

With given values of θ, X_2 and Y can be calculated for a receptor located at various distances from the source. From these values, σ_y can be calculated for F-stability using equations which approximate the Pasquill-Gifford curves [34].

The ratio of concentration (concentration from WD1 divided by concentration from WD2) can be calculated as follows:

$$\text{Conc Ratio} = \left[\frac{\sigma_{y_1}}{\sigma_{y_2}}\right] \exp\left[-0.5 \left[\frac{Y}{\sigma_{y_2}}\right]^2\right] \tag{4-4}$$

Since the term QKVD / $2\pi u\sigma_z$ in Equation 2-9 is assumed the same for both wind directions, it equals one and factors out to result in Equation 4-4. The actual distance from the emission point to the location of maximum concentration ranges from approximately 1 km at YPOINT to 7.5 km for XPOINT. To illustrate the sensitivity of concentration with variations in wind direction, the concentration ratio was calculated when the difference between the wind directions (θ) varied from 0 to 10 degrees. Results of this evaluation, presented in Table 4-9 and Figure 4-9, illustrate the sensitivity of wind direction on maximum 1-hour concentration. Even when the receptor is very close to the emission point (100 m), only a 5 degree difference in wind direction can have a major impact (90 percent difference) on estimated concentration. The effect is more pronounced when the distance to the receptor is increased.

To consider the potential differences on 1-hour average concentrations for the four sets of meteorological data, hourly wind direction data were compared during F-stability. The percentage of time that winds for each set of data were within specific angles was calculated. The results of this evaluation are presented in Table 4-10. As illustrated, during F-stability, wind directions varied significantly from one location to another. Even at the Y-12 Plant where the towers are relatively close together, over 96 percent of time, the wind direction difference was greater than 5 degrees. Over 40 percent of the time, wind direction varied by more than 90 degrees. Recognizing the sensitivity of 1-hour concentration to wind direction as demonstrated above, these results indicate that 1-hour concentration predicted using the various meteorological data sets would result in significant variations. Therefore, it is unnecessary to perform hour-by-hour comparisons of 1-hour concentrations using the various meteorological data to demonstrate the lack of correlation.

Table 4-9: Theoretical Concentration Ratios When Wind Direction Varies from Zero to Ten Degrees at Different Distances to Receptor (F-Stability)

	Concentration Ratio		
Difference in Wind Direction (θ)	Distance to Receptor = 0.1 km	Distance to Receptor = 1 km	Distance to Receptor = 10 km
0	1.0	1.0	1.0
1	0.91	0.88	0.81
2	0.69	0.59	0.44
3	0.44	0.30	0.15
4	0.23	0.12	0.036
5	0.10	0.036	0.0055
6	0.036	0.0082	0.0005
7	0.011	0.0014	0.0000
8	0.0026	0.0002	0.0000
9	0.0005	0.0000	0.0000
10	0.0001	0.0000	0.0000

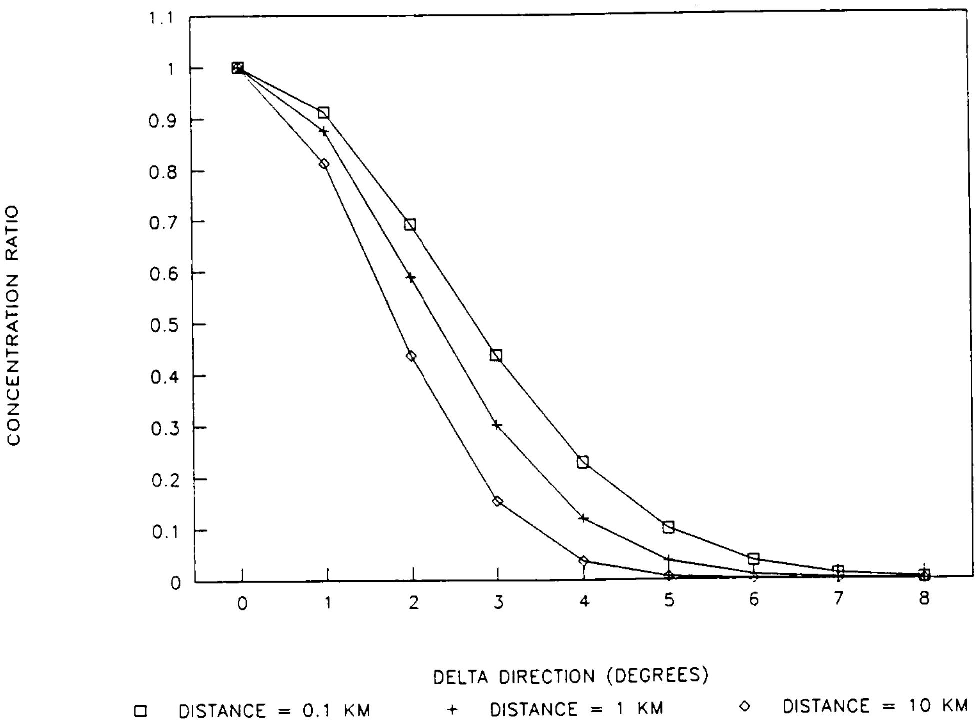

Figure 4-9: Ratio of Maximum Concentration Calculated for Two Wind Directions Separated by Angle Theta (F-Stability)

Table 4-10: Percentage of Time that Wind Directions Were Less Than 5, 10, 22.5, 45, 90, and 135 Degrees Apart During F-Stability.

	Meteorological Data Compared			
Delta Wind Direction (Θ)	YE/YW	YW/X10	YW/K25	X10/K25
5	3.3	8.2	3.4	4.7
10	10.5	20.4	7.1	8.5
22.5	20.6	38.7	16.0	19.4
45	39.8	66.9	30.2	43.0
90	59.4	92.8	53.3	65.1
135	74.0	96.1	80.0	81.4

CHAPTER 5

CONCLUSION

5.1 SUMMARY

This study included three major components: (1) literature review, (2) evaluation of hourly and stability array meteorological data, and (3) evaluation of modeling results when using different meteorological data. Data from this study can be used by those responsible for computer dispersion modeling on the ORR to better understand the effects of complex terrain on local meteorology and pollutant dispersion modeling.

The literature review identified common statistical techniques used to evaluate meteorological data and defined important meteorological parameters and their associated use in computer dispersion modeling. In addition, related research projects were reviewed and discussed. Previous research has identified a number of mechanisms which control wind fields in complex terrain. Some of these studies also evaluated the vertical and lateral variability of wind fields in complex terrain. In addition, other research projects have found that predicted concentrations of air pollutants in complex terrain are usually significantly higher than actually measured in the environment. Overall, the literature review indicated that wind flow in complex terrain is extremely complicated and not fully understood at this time.

Meteorological data (wind direction, wind speed, and stability class) from four meteorological towers on the ORR were compared using a variety of techniques. The towers evaluated include: Y-12 Plant West (YW), Y-12 Plant East (YE), ORNL (X10), and K-25 Site (K25). The first part of this evaluation used annual joint frequency distribution (e.g., STAR) data. Listed below are the some of the most important conclusions from this part of the study:

(1) The Y-12 Plant towers (YW and YE) show more pronounced channeling due to their location in a narrow valley. As a result, these two towers show a higher frequency of winds from the southwest and northeast than the other towers.

(2) YE appears to be significantly influenced by its proximity to a large flow-equalization pond and valley crossroads. The lateral area affected by these influences could not be determined; therefore, these influence may render the 10 - meter level of this tower unreliable for dispersion modeling applications.

(3) The best correlation of wind direction frequency data occurred when YW and X10 were compared. Poorest correlation occurred when YE and YW were compared. This result is surprising since YE and YW are located in the same valley and fairly close together. The poor correlation may be explained due to the local influences affecting YE as described above.

(4) Stability frequency data were very similar for YE, YW, and K25; however, X10 showed a significantly lower frequency of unstable conditions (seven percent versus approximately 21 percent at the other sites). The reason for

this difference is not readily apparent. It is recommended that a detailed review of the data acquisition system and meteorological instruments be conducted to determine the large difference.

The second part of the meteorological data review compared hourly data for calendar year 1991. Listed below are important conclusions regarding this portion of the study:

(1) Overall, hourly wind direction data compared very poorly between all the sites. For all data sets compared, over 55 percent of the hourly wind direction data were greater than 22.5 degrees apart.

(2) A review of hourly wind direction data indicates that approximately seven percent of the time, wind directions at YE and YW were from near opposite directions (e.g., northeast versus southwest). The observation was most commonly noted during light winds and stable conditions. Approximately 15 percent of the time, winds were greater than 157.5 degrees apart during stable conditions and light winds.

(3) Hourly wind direction data compares more favorably as wind speed increases. For example, when winds were less than 1.5 m/s, 41 percent of the hourly observations at YE and YW were greater than 90 degrees apart. However, with winds greater than 3.0 m/s, less than 1 percent of the winds were greater than 90 degrees apart. During high winds, it is likely that the pressure driven and forced channeling mechanisms described by Doran and Whiteman are

dominate. However, during light wind conditions, effects of micro-meteorology, local topography, and thermal driven currents cause significant wind flow variations between the sites.

(4) Consistent with the observation and reasoning above, wind direction compared more favorably during neutral conditions than during stable and unstable conditions. Wind speeds are typically higher during neutral conditions than during stable and unstable conditions.

(5) Wind speed data showed significantly less variation than wind direction. The correlation coefficient ranged from 0.78 when YE and YW were compared to 0.54 when YW and K25 were compared. Wind speed were within 1 m/s 84 percent of the time for YE and YW and 68 percent of the time for YW and K25.

(6) Hourly stability data also compared very favorable in contrast to wind direction data. The correlation coefficient ranged from 0.77 when YE and YW were compared to 0.68 when X10 and K25 were compared. Of all data sets compared, hourly stability categories were within one stability category at least 78 percent of the time.

The final part of this study evaluated the effects of the various meteorological data on dispersion modeling results. Each emission point was modeled using each set of meteorological data. Annual average normalized concentrations ($\mu g/m^3$ per g/s) were calculated using both ISCST and ISCLT for 265 receptors along the ORR boundary. In addition, maximum one-hour normalized concentrations were also calculated using ISCST. Listed below are the most important conclusions regarding this part of the study:

(1) Maximum annual average concentrations varied by approximately a factor of two for any given emission point, depending upon the meteorological data used. Maximum 1-hour concentrations varied from 10 to 30 percent. Given the large differences identified in meteorological data and the relative accuracy of dispersion modeling, these differences are not considered significant.

(2) The locations of maximum concentrations were more sensitive to differences in meteorological data than the actual concentration values themselves. The locations of maximum 1-hour concentrations were greatly affected by receptor height, even more so than proximity to the source. In only one case did maximum concentration occur at the nearest receptor for the 1-hour averaging period.

(3) Maximum annual concentrations were estimated at 265 receptors along the ORR using each set of meteorological data. This evaluation found that YW and X10 meteorological data resulted in predicted concentrations most similar. Poorest correlation occurred when concentrations predicted by YE and YW were compared. These results are consistent with correlation conducted on the wind direction frequency data.

(4) Modeling results from ISCLT correlated very well with ISCST; however, concentration values estimated by ISCLT were approximately 30 percent lower than ISCST. A large portion of this difference can be attributed to the use of default mean wind speeds in the ISCLT model. Due to low average wind speeds on the ORR, use of the default wind speeds in ISCLT results in overestimation of average wind speed by at least 20 percent. For any future modeling on the ORR using ISCLT, actual mean wind speeds should be calculated and input into the model.

(5) Maximum 1-hour concentration occurred during F-stability and with winds less than 1 m/s. During these condition, a five degree difference in wind direction can result in over 95 percent difference in predicted concentration for a receptor located 1 km from the source. During F-stability, over 90 percent of the hourly wind direction data were greater than 5 degrees apart for all data sets compared. Therefore, hourly correlation of predicted concentrations at any give receptor would be expected to be very poor.

5.2 RECOMMENDATIONS

Comparison of the meteorological data on the ORR indicate that wind direction varies significantly from one site to another. Although wind speed and stability class data also show some variations, they are not as significant identified for wind direction. The assumption of a uniform wind field over the entire reservation for modeling purposes is clearly not valid. The farther the receptor is located from the emission point, the more uncertain estimated concentrations become due to complicated wind fields. Unfortunately, the regulatory model historically used on the ORR (ISC) assumes straight-line Guassian dispersion and assumes an uniform wind field. In addition, the most commonly used model on the ORR, ISC does not have the capability to estimate concentration on elevated terrain. It was demonstrated that maximum 1-hour concentrations occurred most frequently on elevated terrain. As a result, significant uncertainties exists with these estimates.

Although research has indicated that most Gaussian models generally overestimate concentration in complex terrain, such conservatism may not be acceptable as risk-based standards are developed over the next five years pursuant to the Clean Air Act Amendments of 1990. In addition, under certain circumstances (e.g., elevated terrain, stagnant conditions), these models may not be conservative. The following recommendations are made:

(1) Results of modeling using straight-line Gaussian models on the ORR should be used with care. Special consideration is necessary for receptors located on elevated terrain and significant distances from the source.

(2) Consideration should be given to use of ambient air monitoring stations in conjunction with computer dispersion modeling to access potential impacts of hazardous air pollutants on off-site receptors.

(3) Models which have algorithms to estimate concentration on elevated terrain

(e.g., EPA's COMPLEX and Rough Terrain Dispersion Model) should be evaluated for use on the ORR. These models could be used in conjunction with ISC to ensure that concentrations are not being underestimated on elevated terrain.

(4) Since one set of meteorological data cannot be used to characterize the wind field over the entire ORR, simplifying or conservative assumptions must be made until refined models are available. A simplifying assumption would be to estimate concentrations at each receptor using the meteorological data for the closest tower. A conservative assumption would be to estimate concentrations at each receptor using each set of meteorological data, and use the highest predicted concentration for planning purposes.

(5) Additional research is needed to identify models which can accommodate complex terrain and/or non-uniform wind fields such as that found on the ORR. One model to evaluate may include EPA's Complex Terrain Dispersion Model (CTDM). Although CTDM assumes a uniform wind field, terrain features are directly incorporated into the model. In addition, other models are available which can use data from multiple meteorological sites to extrapolate a wind field. These models are typically used in emergency response applications.

LIST OF REFERENCES

LIST OF REFERENCES

1. Eckman, R. M., Dobosy, R. J., Pendergrass, W. R., "Preliminary Analysis of Wind Data from the Oak Ridge Site Survey," NOAA Technical Memorandum ERL ARL-193, February 1992, Atmospheric Turbulence and Diffusion Division, National Oceanic And Atmospheric Administration, Oak Ridge, Tennessee, p. 3 to 5 (hereinafter cited as "Preliminary Analysis").

2. Eckman, R. M., Dobosy, R. J., Shankar Rao, K., "Spatial Variability of the Wind Over Complex Terrain," Atmospheric Turbulence and Diffusion Division, National Oceanic And Atmospheric Administration, Oak Ridge, Tennessee, Presented at the Tenth Symposium on Turbulence and Diffusion, September 29 - October 2, 1992, Portland, Oregon, pp. (J4)84 to (J4)87 (hereinafter cited as "Spatial Variability").

3. Martin Marietta Energy Systems, Inc., "Oak Ridge Reservation Environmental Surveillance Report for 1991," ES/ESH-22/V1, October 1992, Oak Ridge, Tennessee, p. 1-9 (hereinafter cited as "Surveillance Report").

4. Neter, J., Wasserman, W., Whitmore, M., "Applied Statistics," 1978, Allyn and Bacon, Inc., Boston, Massachusetts, p. 26 (hereinafter cited as "Applied Statistics").

5. "Applied Statistics," p. 28.

6. "Applied Statistics," p. 30.

7. Mardia, K. V., "Statistics of Directional Data," 1972, Academic Press, New York, New York, pp. 20 and 21 (hereinafter cited as "Directional Data").

8. "Directional Data," p. 24.

9. U.S. EPA, "On Site Meteorological Program Guidance for Regulatory Modeling Applications," EPA-450/4-87-013, June 1987, Office of Air Quality Planning and Standards, U.S. EPA, Research Triangle Park, North Carolina, p. 6-5 (hereinafter cited as "On Site").

10. U.S. EPA, "User's Guide for the Industrial Source Complex (ISC2) Dispersion Models: Volume 2 - Description of Model Algorithms," EPA-450/4-92-008a, March 1992, Office of Air Quality Planning and Standards, U.S. EPA, Research Triangle Park, North Carolina, p. 1-3 (hereinafter cited as "ISC2 Volume 2").

11. U.S. EPA, "User's Guide for the Industrial Source Complex (ISC2) Dispersion Models: Volume 1 -User Instructions," EPA-450/4-92-008a, March 1992, Office of Air Quality Planning and Standards, U.S. EPA, Research Triangle Park, North Carolina, p. 1-1.

12. "On Site," p. 5-2 to 5-6.

13. U.S. EPA, "Guideline for Air Quality Models (Revised)," EPA-450/2-78-027R, July 1986, Office of Air Quality Planning and Standards, U.S. EPA, Research Triangle Park, North Carolina, p. 9-23 (hereinafter cited as "Air Quality Models").

14. "On Site," pp. 5-2 and 5-20.

15. U.S. EPA, "Industrial Source Complex (ISC) Dispersion Model User's Guide - Second Edition: Volume 1," EPA-450/4-86-005a, June 1986, Office of Air Quality Planning and Standards, U.S. EPA, Research Triangle Park, North Carolina, p. 2-3 (hereinafter cited as "ISC").

16. U.S. DOE, "Atmospheric Science and Power Production," DOE/TIC-27601, 1984, Office of Energy Research, Office of Health and Environmental Research, U.S. DOE, Washington D.C., pp. 43 and 44.

17. "ISC2 Volume 2", pp. 1-14 to 1-17.

18. "On Site," p. 6-43.

19. Doran, J. C., Whiteman, C. D., "The Coupling of Synoptic and Valley Winds in the Tennessee Valley," Pacific Northwest Laboratory; Richland, Washington, Presented at the Tenth Symposium on Turbulence and Diffusion, September 29 - October 2, 1992, Portland, Oregon.

20. Gross, G., Wipperman, F., "Channeling and Countercurrent in the Upper Rhine Valley: Numerical Simulations," 1987, Journal of Climate and Applied Meteorology, Vol. 26, pp. 1293-1304.

21. "Preliminary Analysis," pp. 1 to 45.

22. "Spatial Variability," pp. (J4)84 to (J4)87.

23. Nappo, C. J., "Mesoscale Flow Over Complex Terrain During Eastern Tennessee Trajectory Experiment (ETTEX)," 1977, Journal of Applied Meteorology, Vol. 16, pp. 1186 to 1196 (hereinafter cited as "Mesoscale").

24. Start, G. E., Wendell, L. L., "Regional Effluent Dispersion Calculations Considering Spatial and Temporal Meteorological Variations," 1974, NOAA Technical Memorandum ERL-ARL-44.

25. Start, G. E., Dickson, C. R., Wendell, L. L., "Diffusion in a Canyon Within Rough Mountainous Terrain," 1975, Journal of Applied Meteorology, Vol. 14, pp. 333 to 346.

26. Hovind, E. L., Spangler, T. C., Anderson, A. J., "The Influence of Rough Mountainous Terrain upon Plume Dispersion from an Elevated Source," 1974, Symposium on Atmospheric Diffusion and Air Pollution, September 9-13, 1974, Santa Barbara, California, pp. 214 to 217.

27. U.S. DOE, "Calendar Year 1991 Annual Emissions Report: Radionuclide National Emissions Standard for Hazardous Air Pollutants," unpublished report, June 1992.

28. "Mesoscale," p. 1186.

29. "Surveillance Report," p. 3-25.

30. Kornegay, F.C., Sharp, R.D., "Oak Ridge National Laboratory Meteorological Data Retrieval and Analysis Program (OMDRAP)," Unpublished report and personal interviews with authors, ORNL, Martin Marietta Energy Systems, Inc., Oak Ridge, Tennessee.

31. "ISC," p. 2-4.

32. New York State Department of Environmental Conservation, "Draft New York State Air Guide - 1: Guidelines for the Control of Toxic Ambient Air Contaminants," 1991 Edition, Division of Air Resources, New York State Department of Environmental Conservation, Albany, New York, pp. B-7, B-12 to B-13.

33. Letter from Mr. David G. Carson, Tennessee Department of Environment and Conservation, to Mr. Peter J. Gross, U.S. Department of Energy, dated May 17, 1991.

34. "ISC2 Volume 2," p. 1-14.

APPENDICES

APPENDIX A

STABILITY ARRAY (STAR) DATA

.000691	.000553	.000000	.000000	.000000	.000000
.000415	.000277	.000000	.000000	.000000	.000000
.000277	.000277	.000000	.000000	.000000	.000000
.000553	.000553	.000000	.000000	.000000	.000000
.000968	.001383	.000000	.000000	.000000	.000000
.000691	.000830	.000000	.000000	.000000	.000000
.000553	.001798	.000000	.000000	.000000	.000000
.000553	.000691	.000000	.000000	.000000	.000000
.001106	.001521	.000000	.000000	.000000	.000000
.000691	.000968	.000000	.000000	.000000	.000000
.000691	.000830	.000000	.000000	.000000	.000000
.000138	.001106	.000000	.000000	.000000	.000000
.000000	.000000	.000000	.000000	.000000	.000000
.000138	.000553	.000000	.000000	.000000	.000000
.000277	.000415	.000000	.000000	.000000	.000000
.000415	.000138	.000000	.000000	.000000	.000000
.001798	.001936	.000000	.000000	.000000	.000000
.001245	.001798	.000000	.000000	.000000	.000000
.001521	.000968	.000000	.000000	.000000	.000000
.000830	.000830	.000000	.000000	.000000	.000000
.000691	.002628	.000000	.000000	.000000	.000000
.001936	.001936	.000000	.000000	.000000	.000000
.001383	.001660	.000000	.000000	.000000	.000000
.000830	.002904	.000138	.000000	.000000	.000000
.001245	.004011	.000138	.000000	.000000	.000000
.001521	.004425	.000000	.000000	.000000	.000000
.001245	.003872	.000138	.000000	.000000	.000000
.001245	.000830	.000138	.000000	.000000	.000000
.000968	.001660	.000000	.000000	.000000	.000000
.000691	.001521	.000000	.000000	.000000	.000000
.000691	.000277	.000138	.000000	.000000	.000000
.000138	.000553	.000000	.000000	.000000	.000000
.003181	.002213	.000000	.000000	.000000	.000000
.002351	.001936	.000000	.000000	.000000	.000000
.002904	.001798	.000000	.000000	.000000	.000000
.002213	.004564	.000000	.000000	.000000	.000000
.002213	.006085	.000138	.000000	.000000	.000000
.002628	.002628	.000000	.000000	.000000	.000000
.000968	.002351	.000000	.000000	.000000	.000000
.001106	.001660	.000138	.000000	.000000	.000000
.002628	.002213	.000415	.000000	.000000	.000000
.003042	.008712	.000691	.000000	.000000	.000000
.001798	.009681	.000691	.000000	.000000	.000000
.001106	.004840	.001383	.000000	.000000	.000000
.001245	.004011	.000968	.000000	.000000	.000000
.000277	.001936	.001660	.000138	.000000	.000000

.000277	.000968	.000553	.000000	.000000	.000000
.000415	.000830	.000000	.000000	.000000	.000000
.015074	.004840	.000277	.000000	.000000	.000000
.021850	.014521	.001245	.000000	.000000	.000000
.022680	.008989	.000691	.000000	.000000	.000000
.022957	.026414	.003181	.000000	.000000	.000000
.006085	.016457	.004287	.000000	.000000	.000000
.006915	.003596	.000415	.000000	.000000	.000000
.002904	.001106	.000138	.000000	.000000	.000000
.003457	.000968	.000000	.000000	.000000	.000000
.004840	.002628	.000138	.000000	.000000	.000000
.009542	.010372	.004979	.000830	.000000	.000000
.016734	.022542	.013691	.000830	.000000	.000000
.025169	.024616	.009819	.001106	.000000	.000000
.018531	.014383	.010649	.000691	.000000	.000000
.013968	.006361	.002904	.000415	.000000	.000000
.012861	.001936	.000000	.000000	.000000	.000000
.013138	.001660	.000000	.000000	.000000	.000000
.022680	.000138	.000000	.000000	.000000	.000000
.020053	.004287	.000138	.000000	.000000	.000000
.022404	.002628	.000000	.000000	.000000	.000000
.009957	.006223	.000138	.000000	.000000	.000000
.001660	.000691	.000000	.000000	.000000	.000000
.001106	.000415	.000000	.000000	.000000	.000000
.000968	.000000	.000000	.000000	.000000	.000000
.000968	.000415	.000000	.000000	.000000	.000000
.001245	.000415	.000000	.000000	.000000	.000000
.002489	.001245	.000138	.000000	.000000	.000000
.010372	.004979	.001106	.000000	.000000	.000000
.022818	.008298	.000830	.000000	.000000	.000000
.025308	.006915	.000830	.000000	.000000	.000000
.025584	.001106	.000000	.000000	.000000	.000000
.022542	.000553	.000000	.000000	.000000	.000000
.022680	.000138	.000000	.000000	.000000	.000000
.015351	.000277	.000000	.000000	.000000	.000000
.014797	.000553	.000000	.000000	.000000	.000000
.021159	.000138	.000000	.000000	.000000	.000000
.010648	.000277	.000000	.000000	.000000	.000000
.001383	.000138	.000000	.000000	.000000	.000000
.000277	.000138	.000000	.000000	.000000	.000000
.000138	.000138	.000000	.000000	.000000	.000000
.000553	.000277	.000000	.000000	.000000	.000000
.000830	.000277	.000000	.000000	.000000	.000000
.000691	.000553	.000000	.000000	.000000	.000000
.004425	.000968	.000000	.000000	.000000	.000000
.016043	.001106	.000000	.000000	.000000	.000000

Stability Array Data (STAR) - Oak Ridge National Laboratory

.017010	.000277	.000000	.000000	.000000	.000000
.016734	.000415	.000000	.000000	.000000	.000000
.012723	.000000	.000000	.000000	.000000	.000000
.010787	.000000	.000000	.000000	.000000	.000000

.004884	.002004	.000000	.000000	.000000	.000000
.004758	.003631	.000000	.000000	.000000	.000000
.004884	.004132	.000000	.000000	.000000	.000000
.004633	.004257	.000000	.000000	.000000	.000000
.004508	.002630	.000000	.000000	.000000	.000000
.002379	.001252	.000000	.000000	.000000	.000000
.002755	.001127	.000000	.000000	.000000	.000000
.003130	.003381	.000000	.000000	.000000	.000000
.003256	.003882	.000000	.000000	.000000	.000000
.006011	.008891	.000000	.000000	.000000	.000000
.008515	.012021	.000000	.000000	.000000	.000000
.007388	.011019	.000000	.000000	.000000	.000000
.005510	.006762	.000000	.000000	.000000	.000000
.003631	.003256	.000000	.000000	.000000	.000000
.005510	.001878	.000000	.000000	.000000	.000000
.004633	.002129	.000000	.000000	.000000	.000000
.001127	.000626	.000000	.000000	.000000	.000000
.001503	.001127	.000000	.000000	.000000	.000000
.001503	.001753	.000877	.000000	.000000	.000000
.003130	.002755	.001252	.000000	.000000	.000000
.001252	.000877	.000125	.000000	.000000	.000000
.000626	.000501	.000000	.000000	.000000	.000000
.001127	.000877	.000125	.000000	.000000	.000000
.000626	.001127	.000250	.000000	.000000	.000000
.001127	.001503	.001628	.000000	.000000	.000000
.002129	.004383	.002129	.000000	.000000	.000000
.002004	.007513	.001878	.000000	.000000	.000000
.001377	.005009	.002379	.000000	.000000	.000000
.000751	.002254	.001127	.000000	.000000	.000000
.000376	.000877	.001503	.000000	.000000	.000000
.002129	.001127	.000501	.000000	.000000	.000000
.001127	.000751	.000250	.000000	.000000	.000000
.002254	.001377	.000250	.000125	.000000	.000000
.001628	.001002	.000250	.000000	.000000	.000000
.003256	.002880	.001377	.000000	.000000	.000000
.003256	.004633	.003130	.000125	.000000	.000000
.001503	.001503	.000501	.000000	.000000	.000000
.000501	.000125	.000125	.000000	.000000	.000000
.000626	.001002	.000125	.000125	.000000	.000000
.001127	.001503	.000376	.000000	.000000	.000000
.000501	.002254	.001628	.000626	.000000	.000000
.003005	.003256	.004257	.000376	.000000	.000000
.002004	.006637	.006386	.000751	.000000	.000000
.002129	.003882	.002004	.000250	.000000	.000000
.001377	.003381	.001252	.001127	.000000	.000000
.000626	.001628	.002630	.000877	.000000	.000000

.000751	.001377	.002755	.000877	.000000	.000000
.001127	.001002	.001002	.000751	.000000	.000000
.006511	.002254	.000877	.000000	.000000	.000000
.010769	.004758	.001878	.000000	.000000	.000000
.014150	.010393	.004132	.000376	.000000	.000000
.012522	.013023	.005635	.000125	.000125	.000000
.006637	.002504	.000501	.000000	.000000	.000000
.004758	.001377	.000125	.000000	.000000	.000000
.003882	.002004	.000376	.000000	.000000	.000000
.002504	.002504	.000376	.000376	.000000	.000000
.006637	.004257	.002880	.001628	.000125	.000000
.008891	.010143	.006887	.007889	.000751	.000000
.013524	.016905	.010518	.005259	.000000	.000000
.006887	.007388	.008264	.003130	.000376	.000000
.006011	.006511	.005134	.004758	.000376	.000000
.002880	.004758	.010644	.008139	.000626	.000000
.004383	.004508	.018282	.011270	.000250	.000000
.006637	.004383	.004508	.000877	.000000	.000000
.009391	.001753	.000125	.000000	.000000	.000000
.012397	.001628	.000501	.000000	.000000	.000000
.017656	.005259	.001127	.000000	.000000	.000000
.016404	.006511	.001252	.000000	.000000	.000000
.007263	.002504	.000250	.000000	.000000	.000000
.004508	.001377	.000000	.000000	.000000	.000000
.004132	.001628	.000000	.000000	.000000	.000000
.004132	.001377	.000000	.000000	.000000	.000000
.006011	.001377	.000250	.000000	.000000	.000000
.008765	.004758	.001252	.000000	.000000	.000000
.011395	.008891	.001878	.000000	.000000	.000000
.008765	.003381	.001252	.000000	.000000	.000000
.005760	.003256	.001002	.000000	.000000	.000000
.005009	.001878	.000877	.000000	.000000	.000000
.005510	.002504	.001377	.000000	.000000	.000000
.005635	.002880	.000626	.000000	.000000	.000000
.010017	.001002	.000000	.000000	.000000	.000000
.014651	.001252	.000000	.000000	.000000	.000000
.015152	.001377	.000000	.000000	.000000	.000000
.013022	.001753	.000000	.000000	.000000	.000000
.008765	.001127	.000000	.000000	.000000	.000000
.005384	.001377	.000000	.000000	.000000	.000000
.003381	.000751	.000000	.000000	.000000	.000000
.004007	.000626	.000000	.000000	.000000	.000000
.004508	.001252	.000000	.000000	.000000	.000000
.008264	.001628	.000000	.000000	.000000	.000000
.009016	.001252	.000000	.000000	.000000	.000000
.007262	.000376	.000000	.000000	.000000	.000000

Stability Array (STAR) Data - K-25 Site

.007638	.000877	.000000	.000000	.000000	.000000
.005384	.001377	.000000	.000000	.000000	.000000
.006887	.000626	.000000	.000000	.000000	.000000
.006637	.000376	.000000	.000000	.000000	.000000

Stability Array (STAR) Data - Y-12 Plant West

.002188	.000461	.000000	.000000	.000000	.000000
.003800	.000461	.000000	.000000	.000000	.000000
.006103	.004261	.000000	.000000	.000000	.000000
.004606	.003915	.000000	.000000	.000000	.000000
.003915	.002879	.000000	.000000	.000000	.000000
.003915	.002418	.000000	.000000	.000000	.000000
.004261	.003339	.000000	.000000	.000000	.000000
.004606	.003800	.000000	.000000	.000000	.000000
.005873	.004376	.000000	.000000	.000000	.000000
.006564	.005988	.000000	.000000	.000000	.000000
.007600	.010940	.000000	.000000	.000000	.000000
.007715	.012552	.000000	.000000	.000000	.000000
.006679	.002303	.000000	.000000	.000000	.000000
.005182	.000691	.000000	.000000	.000000	.000000
.005412	.000345	.000000	.000000	.000000	.000000
.002533	.000230	.000000	.000000	.000000	.000000
.000691	.000000	.000000	.000000	.000000	.000000
.000921	.000345	.000000	.000000	.000000	.000000
.001036	.004952	.000691	.000000	.000000	.000000
.000806	.002303	.002533	.000000	.000000	.000000
.000576	.002188	.000230	.000000	.000000	.000000
.000691	.001152	.000345	.000000	.000000	.000000
.000461	.002188	.000000	.000000	.000000	.000000
.000806	.002418	.000230	.000000	.000000	.000000
.001152	.003915	.000230	.000000	.000000	.000000
.001267	.005988	.000921	.000000	.000000	.000000
.002533	.007600	.002188	.000000	.000000	.000000
.001497	.008406	.005873	.000000	.000000	.000000
.001842	.001612	.000115	.000000	.000000	.000000
.000921	.000461	.000000	.000000	.000000	.000000
.001152	.000115	.000000	.000000	.000000	.000000
.000461	.000000	.000000	.000000	.000000	.000000
.000576	.000230	.000000	.000000	.000000	.000000
.000576	.000921	.000345	.000000	.000000	.000000
.002879	.006103	.003109	.000000	.000000	.000000
.001497	.003800	.004030	.000000	.000000	.000000
.000576	.001152	.001036	.000000	.000000	.000000
.001036	.001382	.000230	.000000	.000000	.000000
.000461	.001958	.000000	.000000	.000000	.000000
.000921	.002418	.000345	.000000	.000000	.000000
.001152	.004030	.000691	.000000	.000000	.000000
.001497	.009443	.003570	.000691	.000000	.000000
.004606	.011285	.007140	.000461	.000000	.000000
.002879	.011976	.005873	.000345	.000000	.000000
.000691	.001612	.000115	.000000	.000000	.000000
.001497	.000115	.000000	.000000	.000000	.000000

Stability Array (STAR) Data - Y-12 Plant West

.001036	.000000	.000000	.000000	.000000	.000000
.001152	.000230	.000000	.000000	.000000	.000000
.007485	.001036	.000000	.000000	.000000	.000000
.010018	.006333	.000576	.000000	.000000	.000000
.010479	.034777	.028558	.000921	.000000	.000000
.004261	.011631	.010479	.000345	.000000	.000000
.001842	.005067	.002418	.000115	.000000	.000000
.001842	.002073	.000230	.000000	.000000	.000000
.000576	.001267	.000230	.000115	.000000	.000000
.000576	.001727	.000230	.000000	.000000	.000000
.001497	.004836	.000461	.000115	.000000	.000000
.004146	.006794	.004952	.000921	.000000	.000000
.018885	.019576	.003915	.000230	.000000	.000000
.028443	.034201	.007370	.000461	.000000	.000000
.016352	.007715	.000230	.000000	.000000	.000000
.008521	.001612	.000000	.000000	.000000	.000000
.005412	.000691	.000000	.000000	.000000	.000000
.004721	.000000	.000000	.000000	.000000	.000000
.007830	.001152	.000000	.000000	.000000	.000000
.016813	.010018	.000000	.000000	.000000	.000000
.016813	.020728	.007946	.000000	.000000	.000000
.003800	.003800	.001036	.000000	.000000	.000000
.001497	.000806	.000115	.000000	.000000	.000000
.000921	.000345	.000115	.000000	.000000	.000000
.000921	.000461	.000000	.000000	.000000	.000000
.000806	.000230	.000000	.000000	.000000	.000000
.001382	.000921	.000000	.000000	.000000	.000000
.003109	.001267	.000115	.000000	.000000	.000000
.018194	.008291	.000345	.000000	.000000	.000000
.029595	.017734	.000461	.000000	.000000	.000000
.021764	.004376	.000115	.000000	.000000	.000000
.013934	.000691	.000000	.000000	.000000	.000000
.007024	.000461	.000000	.000000	.000000	.000000
.004836	.000230	.000000	.000000	.000000	.000000
.004837	.000345	.000000	.000000	.000000	.000000
.004721	.000345	.000000	.000000	.000000	.000000
.008176	.002994	.000000	.000000	.000000	.000000
.003339	.001382	.000000	.000000	.000000	.000000
.001958	.000345	.000000	.000000	.000000	.000000
.001382	.000115	.000000	.000000	.000000	.000000
.000806	.000345	.000000	.000000	.000000	.000000
.001152	.000115	.000000	.000000	.000000	.000000
.001842	.000000	.000000	.000000	.000000	.000000
.004376	.000691	.000000	.000000	.000000	.000000
.008982	.008176	.000000	.000000	.000000	.000000
.015086	.007838	.000000	.000000	.000000	.000000

Stability Array (STAR) Data - Y-12 Plant West

.015546	.000460	.000000	.000000	.000000	.000000
.011170	.000345	.000000	.000000	.000000	.000000
.008176	.000345	.000000	.000000	.000000	.000000
.004607	.000345	.000000	.000000	.000000	.000000

Stability Array (STAR) Data - Y-12 Plant East

.003680	.000690	.000000	.000000	.000000	.000000
.003220	.001725	.000000	.000000	.000000	.000000
.005060	.002875	.000000	.000000	.000000	.000000
.006325	.002185	.000000	.000000	.000000	.000000
.008165	.001265	.000000	.000000	.000000	.000000
.009315	.001265	.000000	.000000	.000000	.000000
.010005	.001840	.000000	.000000	.000000	.000000
.008165	.001495	.000000	.000000	.000000	.000000
.010120	.003335	.000000	.000000	.000000	.000000
.007015	.004945	.000000	.000000	.000000	.000000
.007130	.004370	.000000	.000000	.000000	.000000
.004830	.003450	.000000	.000000	.000000	.000000
.004025	.001840	.000000	.000000	.000000	.000000
.002530	.000805	.000000	.000000	.000000	.000000
.003105	.001265	.000000	.000000	.000000	.000000
.004715	.001035	.000000	.000000	.000000	.000000
.000805	.000230	.000000	.000000	.000000	.000000
.001610	.000920	.000000	.000000	.000000	.000000
.001840	.004255	.001035	.000000	.000000	.000000
.002530	.003220	.000460	.000000	.000000	.000000
.002530	.002300	.000115	.000000	.000000	.000000
.001840	.000345	.000000	.000000	.000000	.000000
.001265	.001495	.000000	.000000	.000000	.000000
.000805	.001380	.000000	.000000	.000000	.000000
.001265	.003450	.000000	.000000	.000000	.000000
.001610	.007015	.000345	.000000	.000000	.000000
.000805	.006670	.000575	.000000	.000000	.000000
.000690	.003335	.000920	.000000	.000000	.000000
.001265	.001610	.000690	.000000	.000000	.000000
.001150	.000805	.000000	.000000	.000000	.000000
.000460	.000345	.000000	.000000	.000000	.000000
.001035	.000690	.000000	.000000	.000000	.000000
.000920	.000345	.000000	.000000	.000000	.000000
.001265	.000920	.000115	.000000	.000000	.000000
.001725	.005290	.003910	.000000	.000000	.000000
.003910	.006095	.003680	.000115	.000000	.000000
.003680	.002990	.000805	.000000	.000000	.000000
.002070	.000575	.000115	.000000	.000000	.000000
.001840	.001265	.000000	.000000	.000000	.000000
.001265	.001265	.000000	.000000	.000000	.000000
.002070	.002875	.000230	.000000	.000000	.000000
.001380	.006670	.002070	.000000	.000000	.000000
.001380	.010005	.007245	.000575	.000000	.000000
.000805	.006210	.003795	.000460	.000000	.000000
.002070	.003795	.004140	.000230	.000000	.000000
.000805	.000920	.000230	.000000	.000000	.000000

Stability Array (STAR) Data - Y-12 Plant East

.000575	.000805	.000000	.000000	.000000	.000000
.001725	.000345	.000000	.000000	.000000	.000000
.010810	.000460	.000000	.000000	.000000	.000000
.016444	.001265	.000000	.000000	.000000	.000000
.029899	.020009	.013569	.000115	.000000	.000000
.049103	.018169	.004830	.000000	.000000	.000000
.023804	.008970	.001265	.000000	.000000	.000000
.006555	.001150	.000000	.000000	.000000	.000000
.002300	.000690	.000000	.000000	.000000	.000000
.002415	.000345	.000115	.000000	.000000	.000000
.003565	.001725	.000000	.000000	.000000	.000000
.004715	.008855	.000690	.000000	.000000	.000000
.004830	.014029	.008625	.003680	.000000	.000000
.005750	.015984	.015294	.003220	.000000	.000000
.008280	.023114	.013109	.001150	.000000	.000000
.007475	.002415	.000115	.000115	.000000	.000000
.005290	.000575	.000000	.000000	.000000	.000000
.008855	.000575	.000115	.000000	.000000	.000000
.012075	.000690	.000000	.000000	.000000	.000000
.017824	.001265	.000115	.000000	.000000	.000000
.037718	.005405	.001380	.000000	.000000	.000000
.059223	.004945	.000345	.000000	.000000	.000000
.021159	.003335	.000000	.000000	.000000	.000000
.004140	.000575	.000000	.000000	.000000	.000000
.002530	.000230	.000000	.000000	.000000	.000000
.002760	.000345	.000000	.000000	.000000	.000000
.003220	.000805	.000000	.000000	.000000	.000000
.003220	.003335	.000000	.000000	.000000	.000000
.003220	.003220	.000690	.000000	.000000	.000000
.003450	.003335	.000920	.000000	.000000	.000000
.006785	.008855	.000690	.000000	.000000	.000000
.004715	.001150	.000115	.000000	.000000	.000000
.005980	.000000	.000000	.000000	.000000	.000000
.006900	.000230	.000000	.000000	.000000	.000000
.003680	.000230	.000000	.000000	.000000	.000000
.007360	.000460	.000000	.000000	.000000	.000000
.015064	.001495	.000000	.000000	.000000	.000000
.023689	.000805	.000000	.000000	.000000	.000000
.010005	.000460	.000000	.000000	.000000	.000000
.003335	.000000	.000000	.000000	.000000	.000000
.002070	.000000	.000000	.000000	.000000	.000000
.001035	.000345	.000000	.000000	.000000	.000000
.001380	.000000	.000000	.000000	.000000	.000000
.001265	.000575	.000000	.000000	.000000	.000000
.000920	.000345	.000000	.000000	.000000	.000000
.000805	.000575	.000000	.000000	.000000	.000000

Stability Array (STAR) Data - Y-12 Plant East

.001380	.000805	.000000	.000000	.000000	.000000
.001840	.000115	.000000	.000000	.000000	.000000
.002645	.000000	.000000	.000000	.000000	.000000
.004600	.000345	.000000	.000000	.000000	.000000

APPENDIX B

RECEPTOR LOCATIONS (X, Y, Z COORDINATES)

Receptor Number	Coordinate Locations (m) of Receptors X-Coordinate	Y-Coordinate	Z-Coordinate
1	1674	1251	298
2	1481	1334	303
3	1308	1511	286
4	1064	1422	273
5	785	1246	273
6	421	1068	291
7	122	819	311
8	-184	619	311
9	-321	550	311
10	-558	532	294
11	-703	445	294
12	-988	355	290
13	-1294	160	311
14	-1638	6	311
15	-1984	-192	311
16	-2474	-249	311
17	-2877	-259	303
18	-2999	-294	303
19	-3274	-448	301
20	-3540	-646	311
21	-3979	-886	293
22	-4273	-1107	280
23	-4544	-1353	270
24	-5018	-1709	283
25	-5341	-1967	288
26	-5532	-2109	282
27	-5709	-2218	274
28	-6070	-2396	280

	Coordinate Locations (m) of Receptors		
Receptor Number	X-Coordinate	Y-Coordinate	Z-Coordinate
29	-6418	-2632	303
30	-6691	-2843	311
31	-6910	-3030	310
32	-7056	-3097	303
33	-7179	-2876	308
34	-7370	-2767	298
35	-7656	-2660	289
36	-7798	-2514	277
37	-7931	-2323	274
38	-8131	-1958	262
39	-7839	-1767	252
40	-7624	-1618	241
41	-7371	-1462	242
42	-7214	-1265	235
43	-7037	-1127	239
44	-7015	-903	238
45	-6833	-736	238
46	-6751	-618	247
47	-6964	-544	241
48	-7106	-489	249
49	-7144	-265	257
50	-7129	-6	265
51	-7371	25	275
52	-7624	66	289
53	-7890	-12	300
54	-8176	-141	303
55	-8393	-275	311
56	-8743	-497	311

Receptor Number	Coordinate Locations (m) of Receptors X-Coordinate	Y-Coordinate	Z-Coordinate
57	-9155	-731	302
58	-9390	-869	284
59	-9561	-1027	287
60	-9904	-1271	292
61	-10208	-1542	288
62	-10354	-1673	284
63	-10542	-1751	278
64	-10813	-1898	278
65	-11021	-2065	278
66	-11227	-2165	275
67	-11391	-2281	285
68	-11746	-2340	289
69	-12027	-2475	269
70	-12207	-2642	269
71	-12249	-2762	251
72	-12299	-2977	237
73	-12306	-3121	237
74	-12279	-3207	237
75	-11982	-3371	236
76	-11780	-3499	232
77	-11879	-3625	232
78	-12121	-3449	235
79	-12403	-3343	237
80	-12541	-3274	241
81	-12661	-3175	240
82	-12765	-3049	240
83	-12716	-3288	241
84	-12911	-3331	244

	Coordinate Locations (m) of Receptors		
Receptor Number	X-Coordinate	Y-Coordinate	Z-Coordinate
85	-13168	-3584	244
86	-13345	-3751	245
87	-13547	-3942	258
88	-13620	-3844	258
89	-14070	-4174	298
90	-14322	-4338	281
91	-14469	-4474	271
92	-14770	-4791	271
93	-15062	-5027	292
94	-15242	-5156	292
95	-15406	-5378	263
96	-15554	-5560	240
97	-15727	-5762	249
98	-15848	-5953	271
99	-15913	-6088	271
100	-15930	-6252	274
101	-15928	-6494	265
102	-15970	-6623	265
103	-16065	-6805	246
104	-15661	-7269	226
105	-15370	-6965	249
106	-15171	-6760	255
107	-14828	-6385	237
108	-14668	-6194	244
109	-14515	-6034	248
110	-14327	-5914	262
111	-14152	-5874	250
112	-14001	-5849	239

	Coordinate Locations (m) of Receptors		
Receptor Number	X-Coordinate	Y-Coordinate	Z-Coordinate
113	-13866	-5873	239
114	-13779	-6008	239
115	-13684	-6187	234
116	-13557	-6504	234
117	-13730	-6628	234
118	-13865	-6733	235
119	-14075	-6933	236
120	-14259	-7086	236
121	-14228	-7458	240
122	-14092	-7824	239
123	-13932	-7996	232
124	-13683	-8173	229
125	-13257	-8234	227
126	-12916	-8171	224
127	-12576	-8376	224
128	-12261	-8552	228
129	-12055	-8680	228
130	-11590	-8305	240
131	-11144	-7907	266
132	-10885	-7687	264
133	-10686	-7582	260
134	-10424	-7885	258
135	-10110	-8275	254
136	-9853	-8586	245
137	-9608	-8867	235
138	-9440	-9053	228
139	-9608	-9386	225
140	-9676	-9541	229

Receptor Number	Coordinate Locations (m) of Receptors X-Coordinate	Y-Coordinate	Z-Coordinate
141	-9361	-9523	230
142	-9097	-9524	231
143	-8705	-9521	231
144	-8343	-9469	231
145	-8033	-9428	226
146	-7713	-9561	230
147	-7223	-9670	230
148	-6804	-9862	233
149	-2410	-9913	256
150	-2271	-9547	248
151	-2076	-9300	251
152	-1772	-9284	242
153	-1417	-9594	249
154	-1142	-9861	266
155	-470	-9928	260
156	-459	-9753	260
157	-692	-9445	254
158	-903	-8963	240
159	-1103	-8627	234
160	-1086	-8356	237
161	-949	-8187	244
162	-683	-7945	263
163	-257	-7851	263
164	71	-7790	261
165	472	-7473	254
166	569	-7215	263
167	580	-7064	261
168	400	-6730	242

	Coordinate Locations (m) of Receptors		
Receptor Number	X-Coordinate	Y-Coordinate	Z-Coordinate
169	224	-6458	230
170	109	-6263	229
171	-310	-6096	230
172	-524	-6008	230
173	-766	-5796	230
174	-968	-5590	231
175	-1154	-5385	234
176	-1172	-5170	235
177	-1090	-4974	235
178	-913	-4888	240
179	-685	-4874	241
180	-432	-4889	243
181	-50	-5021	242
182	227	-5168	247
183	507	-5400	250
184	711	-5615	251
185	896	-5885	256
186	1151	-6190	266
187	1462	-6251	278
188	1761	-6224	276
189	2043	-6095	260
190	2146	-5831	249
191	2029	-5492	241
192	1871	-5113	237
193	1830	-4879	241
194	1888	-4581	246
195	1803	-4320	247
196	1741	-4196	243

Receptor Number	Coordinate Locations (m) of Receptors X-Coordinate	Y-Coordinate	Z-Coordinate
197	1448	-4173	262
198	1290	-4122	262
199	1210	-3918	262
200	1221	-3672	253
201	1372	-3479	243
202	1502	-3410	230
203	1711	-3458	236
204	1964	-3584	232
205	2235	-3776	235
206	2563	-4001	235
207	2901	-4240	236
208	2985	-4295	238
209	3258	-4385	241
210	3531	-4451	241
211	3848	-4346	240
212	4118	-4135	229
213	4051	-3721	227
214	4000	-3371	236
215	3766	-3092	239
216	3569	-2926	241
217	3464	-2703	250
218	3500	-2541	245
219	3688	-2259	247
220	3902	-1877	250
221	4031	-1509	241
222	4157	-1278	238
223	4338	-1078	250
224	4804	-989	279

	Coordinate Locations (m) of Receptors		
Receptor Number	X-Coordinate	Y-Coordinate	Z-Coordinate
225	5196	-941	274
226	5451	-874	282
227	5631	-656	264
228	5781	-359	242
229	5738	140	233
230	5720	439	243
231	5740	625	245
232	5456	697	258
233	5283	754	258
234	5159	637	262
235	5050	503	252
236	4878	394	257
237	4629	290	258
238	4295	158	270
239	4040	109	278
240	3813	70	278
241	3450	-225	260
242	3193	-441	258
243	2982	-523	258
244	2736	-668	261
245	2890	-889	267
246	2568	-1050	275
247	2198	-1325	274
248	1786	-1637	267
249	1432	-1839	256
250	1164	-1971	251
251	1012	-1714	258
252	1334	-1514	262

Coordinate Locations (m) of Receptors			
Receptor Number	X-Coordinate	Y-Coordinate	Z-Coordinate
253	1549	-1294	271
254	1814	-1054	282
255	2173	-860	277
256	2519	-673	266
257	2885	-468	261
258	3029	-379	258
259	3148	-266	258
260	2955	-3	267
261	2933	166	275
262	2735	363	283
263	2542	628	299
264	2271	836	311
265	1956	1045	305

APPENDIX C

SAMPLE INDUSTRIAL SOURCE COMPLEX INPUT FILES

Sample Input File: Industrial Source Complex Short-Term

```
CO STARTING
CO TITLEONE R.H. KINGREA M.S. THESIS
CO TITLETWO 1991 MET DATA FROM ORNL TOWER - 10m level
CO MODELOPT DFAULT CONC   RURAL
CO AVERTIME PERIOD
CO POLLUTID OTHER
CO DCAYCOEF     .000000
CO TERRHGTS ELEV
CO ELEVUNIT FEET
CO RUNORNOT RUN
CO ERRORFIL ERRORS.OUT
CO FINISHED


SO STARTING

** Source Location Cards:
**          SRCID SRCTYP        XS            YS          ZS

SO LOCATION  YPOINT POINT        0             0          286
SO LOCATION  XPOINT POINT    -4700         -6300          244
SO LOCATION  KPOINT POINT   -11800         -5400          247
SO LOCATION  KTSCA POINT    -11400         -5400          247

** Source Parameter Cards:
** POINT:   SRCID      QS           HS        TS          VS         DS
** VOLUME:  SRCID      QS           HS        SYINIT      SZINIT
** AREA:    SRCID      QS           HS        XINIT

SO SRCPARAM YPOINT     1            10        293         0          .5
SO SRCPARAM XPOINT     1            10        293         0          .5
SO SRCPARAM KPOINT     1            10        293         0          .5
SO SRCPARAM KTSCA      1            30.5      350         5.5        1.37
SO SRCGROUP KPOINT KPOINT
SO SRCGROUP KTSCA  KTSCA
SO FINISHED

NO ECHO
RE STARTING
RE DISCCART     1673.94   1250.71    976.96
RE DISCCART     1480.89   1334.44    993.94
RE DISCCART     1307.68   1511.29    938.07
RE DISCCART     1063.83   1422.04    896.73
RE DISCCART      784.62   1246.28    897.21
RE DISCCART      421.13   1068.09    954.36
RE DISCCART      122.04    819.14   1021.11
RE DISCCART     -183.76    618.93   1021.11
RE DISCCART     -321.17    549.89   1021.11
RE DISCCART     -558.45    531.57    965.79
RE DISCCART     -702.50    444.79    965.79
RE DISCCART     -988.48    355.43    951.36
RE DISCCART    -1294.28    159.65   1021.11
RE DISCCART    -1637.84      5.89   1021.11
RE DISCCART    -1983.56   -192.20   1021.11
RE DISCCART    -2473.62   -248.83   1021.11
RE DISCCART    -2877.25   -258.70    995.00
RE DISCCART    -2999.18   -294.46    995.00
RE DISCCART    -3273.99   -448.05    986.66
```

Sample Input File: Industrial Source Complex Short-Term

```
RE DISCCART     -3539.87     -645.94    1019.22
RE DISCCART     -3978.69     -886.37     962.22
RE DISCCART     -4273.37    -1106.50     920.02
RE DISCCART     -4543.63    -1353.16     884.22
RE DISCCART     -5017.78    -1708.91     927.09
RE DISCCART     -5341.25    -1966.78     944.83
RE DISCCART     -5531.80    -2109.08     924.19
RE DISCCART     -5709.08    -2218.11     899.67
RE DISCCART     -6070.35    -2396.30     919.89
RE DISCCART     -6418.25    -2632.07     994.29
RE DISCCART     -6690.76    -2843.27    1021.11
RE DISCCART     -6910.09    -3029.97    1018.13
RE DISCCART     -7056.38    -3096.82     994.57
RE DISCCART     -7178.63    -2875.51    1011.84
RE DISCCART     -7369.50    -2767.40     978.92
RE DISCCART     -7655.73    -2659.53     946.56
RE DISCCART     -7797.86    -2513.62     907.57
RE DISCCART     -7931.17    -2323.37     900.00
RE DISCCART     -8131.23    -1958.22     860.84
RE DISCCART     -7838.73    -1766.91     828.34
RE DISCCART     -7623.80    -1617.90     789.86
RE DISCCART     -7371.17    -1462.14     794.10
RE DISCCART     -7213.96    -1264.52     770.45
RE DISCCART     -7036.71    -1126.68     785.64
RE DISCCART     -7014.82     -902.81     780.78
RE DISCCART     -6833.17     -736.15     780.78
RE DISCCART     -6751.26     -618.49     811.24
RE DISCCART     -6964.27     -543.68     792.13
RE DISCCART     -7106.27     -488.63     816.32
RE DISCCART     -7144.26     -264.90     842.66
RE DISCCART     -7129.07       -5.59     867.91
RE DISCCART     -7370.85       24.84     902.38
RE DISCCART     -7623.73       66.31     947.89
RE DISCCART     -7889.76      -11.91     984.71
RE DISCCART     -8175.69     -141.16     994.43
RE DISCCART     -8392.86     -274.66    1021.11
RE DISCCART     -8742.99     -497.14    1021.11
RE DISCCART     -9155.20     -730.86     990.91
RE DISCCART     -9390.11     -868.84     931.35
RE DISCCART     -9560.68    -1026.61     943.09
RE DISCCART     -9904.12    -1271.23     958.00
RE DISCCART    -10207.61    -1542.35     945.89
RE DISCCART    -10353.82    -1673.46     932.14
RE DISCCART    -10542.23    -1751.49     912.21
RE DISCCART    -10812.62    -1898.43     912.68
RE DISCCART    -11020.88    -2065.15     911.47
RE DISCCART    -11227.00    -2165.39     901.50
RE DISCCART    -11390.97    -2281.03     936.29
RE DISCCART    -11745.74    -2339.53     948.77
RE DISCCART    -12027.23    -2475.41     880.97
RE DISCCART    -12206.66    -2642.07     880.97
RE DISCCART    -12248.64    -2761.84     823.18
RE DISCCART    -12299.38    -2976.92     777.34
RE DISCCART    -12305.84    -3120.98     777.34
RE DISCCART    -12279.12    -3207.34     777.76
RE DISCCART    -11981.73    -3370.59     775.00
RE DISCCART    -11779.75    -3498.62     760.03
RE DISCCART    -11879.39    -3625.18     760.03
RE DISCCART    -12121.35    -3448.50     770.86
```

```
RE DISCCART    -12403.14    -3342.83     777.76
RE DISCCART    -12540.73    -3274.48     789.53
RE DISCCART    -12660.62    -3175.05     786.91
RE DISCCART    -12765.02    -3049.00     786.91
RE DISCCART    -12715.92    -3288.21     789.53
RE DISCCART    -12911.03    -3330.80     800.00
RE DISCCART    -13167.97    -3584.07     801.00
RE DISCCART    -13345.18    -3750.72     804.62
RE DISCCART    -13546.76    -3941.81     847.82
RE DISCCART    -13620.07    -3844.48     847.82
RE DISCCART    -14069.86    -4173.58     977.12
RE DISCCART    -14322.48    -4338.20     922.99
RE DISCCART    -14468.68    -4473.75     890.37
RE DISCCART    -14769.89    -4791.39     888.59
RE DISCCART    -15062.34    -5027.02     959.55
RE DISCCART    -15241.82    -5156.00     959.55
RE DISCCART    -15405.65    -5378.02     863.42
RE DISCCART    -15554.01    -5560.11     787.70
RE DISCCART    -15726.74    -5762.20     817.14
RE DISCCART    -15848.47    -5953.08     887.96
RE DISCCART    -15912.62    -6088.42     887.96
RE DISCCART    -15930.15    -6252.46     900.00
RE DISCCART    -15927.62    -6494.00     870.64
RE DISCCART    -15969.60    -6622.64     870.64
RE DISCCART    -16064.73    -6804.59     806.43
RE DISCCART    -15660.50    -7268.96     742.09
RE DISCCART    -15370.36    -6964.63     818.05
RE DISCCART    -15171.02    -6760.26     837.14
RE DISCCART    -14827.74    -6384.89     778.00
RE DISCCART    -14668.30    -6193.91     801.03
RE DISCCART    -14515.48    -6033.97     812.73
RE DISCCART    -14327.12    -5913.83     859.01
RE DISCCART    -14151.97    -5873.51     820.09
RE DISCCART    -14001.19    -5848.76     782.74
RE DISCCART    -13865.88    -5872.80     782.74
RE DISCCART    -13779.21    -6007.76     784.97
RE DISCCART    -13683.62    -6187.02     767.73
RE DISCCART    -13556.80    -6503.60     766.06
RE DISCCART    -13729.63    -6628.13     766.06
RE DISCCART    -13864.78    -6732.63     769.86
RE DISCCART    -14075.21    -6932.60     773.95
RE DISCCART    -14259.09    -7085.96     773.88
RE DISCCART    -14227.57    -7458.19     786.97
RE DISCCART    -14091.82    -7823.50     784.78
RE DISCCART    -13931.92    -7995.95     762.14
RE DISCCART    -13683.30    -8172.62     749.88
RE DISCCART    -13257.41    -8233.61     745.36
RE DISCCART    -12915.95    -8170.71     735.77
RE DISCCART    -12576.37    -8375.95     736.15
RE DISCCART    -12261.22    -8552.45     747.09
RE DISCCART    -12054.80    -8680.47     747.09
RE DISCCART    -11589.54    -8304.79     788.70
RE DISCCART    -11144.28    -7907.01     873.69
RE DISCCART    -10885.07    -7686.97     867.33
RE DISCCART    -10685.61    -7582.32     852.30
RE DISCCART    -10423.52    -7885.27     845.06
RE DISCCART    -10110.32    -8274.51     832.66
RE DISCCART     -9852.66    -8586.34     803.59
RE DISCCART     -9608.34    -8867.17     772.26
```

Sample Input File: Industrial Source Complex Short-Term

```
RE DISCCART      -9439.55     -9052.90       746.92
RE DISCCART      -9607.68     -9385.73       737.99
RE DISCCART      -9676.23     -9541.02       751.88
RE DISCCART      -9361.33     -9522.51       753.93
RE DISCCART      -9097.41     -9524.07       758.99
RE DISCCART      -8704.87     -9520.87       758.02
RE DISCCART      -8343.44     -9469.00       757.36
RE DISCCART      -8033.00     -9428.34       740.02
RE DISCCART      -7713.47     -9560.50       753.97
RE DISCCART      -7223.20     -9670.09       754.41
RE DISCCART      -6803.79     -9861.84       763.58
RE DISCCART      -2410.29     -9912.93       840.82
RE DISCCART      -2271.04     -9546.94       813.68
RE DISCCART      -2076.19     -9300.47       823.69
RE DISCCART      -1772.37     -9284.20       792.35
RE DISCCART      -1417.13     -9593.56       816.46
RE DISCCART      -1141.78     -9861.02       871.57
RE DISCCART       -469.71     -9928.04       853.34
RE DISCCART       -458.84     -9752.94       853.34
RE DISCCART       -692.10     -9445.49       832.69
RE DISCCART       -903.41     -8962.92       788.91
RE DISCCART      -1103.44     -8626.57       767.09
RE DISCCART      -1086.04     -8356.17       777.32
RE DISCCART       -948.75     -8187.41       800.88
RE DISCCART       -682.93     -7945.19       861.60
RE DISCCART       -257.23     -7851.06       863.34
RE DISCCART         70.92     -7790.40       857.73
RE DISCCART        471.94     -7472.51       833.64
RE DISCCART        569.19     -7215.20       863.42
RE DISCCART        580.09     -7064.48       857.09
RE DISCCART        400.02     -6730.31       795.26
RE DISCCART        224.47     -6458.17       754.77
RE DISCCART        108.90     -6263.44       750.00
RE DISCCART       -310.48     -6096.06       754.71
RE DISCCART       -523.50     -6007.95       754.71
RE DISCCART       -765.51     -5795.81       755.81
RE DISCCART       -967.59     -5590.22       758.13
RE DISCCART      -1154.15     -5384.60       768.85
RE DISCCART      -1172.16     -5169.68       772.27
RE DISCCART      -1090.35     -4974.46       772.27
RE DISCCART       -913.04     -4887.60       787.65
RE DISCCART       -684.63     -4873.73       789.69
RE DISCCART       -431.78     -4888.61       798.43
RE DISCCART        -50.15     -5020.62       794.86
RE DISCCART        227.26     -5168.41       810.51
RE DISCCART        507.00     -5400.40       820.84
RE DISCCART        711.31     -5614.85       822.30
RE DISCCART        895.73     -5884.75       839.14
RE DISCCART       1151.16     -6189.93       871.38
RE DISCCART       1461.73     -6251.20       913.19
RE DISCCART       1761.10     -6223.86       903.98
RE DISCCART       2042.59     -6094.63       854.63
RE DISCCART       2146.49     -5830.66       817.71
RE DISCCART       2028.52     -5491.90       790.94
RE DISCCART       1870.57     -5113.34       778.51
RE DISCCART       1830.35     -4878.54       792.24
RE DISCCART       1887.63     -4581.44       806.14
RE DISCCART       1803.03     -4320.16       811.70
RE DISCCART       1740.77     -4196.21       795.71
```

Sample Input File: Industrial Source Complex Short-Term

```
RE DISCCART        1447.99    -4172.57       857.94
RE DISCCART        1290.46    -4121.99       857.94
RE DISCCART        1210.36    -3918.31       859.65
RE DISCCART        1221.14    -3672.30       830.12
RE DISCCART        1371.70    -3479.13       796.86
RE DISCCART        1502.46    -3410.10       755.91
RE DISCCART        1711.00    -3458.34       773.01
RE DISCCART        1963.98    -3584.02       760.58
RE DISCCART        2234.80    -3776.15       772.39
RE DISCCART        2563.32    -4001.37       770.97
RE DISCCART        2900.73    -4239.86       772.89
RE DISCCART        2985.07    -4295.05       781.00
RE DISCCART        3257.98    -4385.23       789.42
RE DISCCART        3530.85    -4451.03       791.46
RE DISCCART        3847.86    -4346.09       787.52
RE DISCCART        4118.16    -4134.88       751.34
RE DISCCART        4051.09    -3720.65       744.90
RE DISCCART        3999.64    -3370.64       775.00
RE DISCCART        3766.42    -3092.00       783.48
RE DISCCART        3568.82    -2926.28       790.81
RE DISCCART        3464.30    -2702.72       821.43
RE DISCCART        3499.58    -2540.86       803.65
RE DISCCART        3687.73    -2258.95       808.91
RE DISCCART        3902.37    -1877.25       819.56
RE DISCCART        4030.53    -1509.06       791.18
RE DISCCART        4156.65    -1278.28       781.00
RE DISCCART        4338.26    -1078.38       821.48
RE DISCCART        4803.88     -988.58       916.20
RE DISCCART        5196.37     -941.06       898.34
RE DISCCART        5451.33     -873.94       924.02
RE DISCCART        5630.69     -656.32       866.53
RE DISCCART        5781.12     -358.99       794.79
RE DISCCART        5738.35      139.51       764.43
RE DISCCART        5720.22      438.64       797.55
RE DISCCART        5739.94      624.84       802.32
RE DISCCART        5455.98      697.26       844.83
RE DISCCART        5282.92      754.45       844.83
RE DISCCART        5158.87      636.68       859.00
RE DISCCART        5050.37      503.45       828.38
RE DISCCART        4877.52      394.43       841.96
RE DISCCART        4629.26      289.66       845.15
RE DISCCART        4294.54      158.07       886.07
RE DISCCART        4039.56      108.69       912.89
RE DISCCART        3813.39       70.45       912.69
RE DISCCART        3450.05     -225.19       853.60
RE DISCCART        3193.07     -440.79       848.00
RE DISCCART        2982.48     -523.31       847.20
RE DISCCART        2736.49     -667.97       857.34
RE DISCCART        2889.80     -889.19       876.80
RE DISCCART        2568.43    -1049.55       902.82
RE DISCCART        2198.41    -1325.27       900.00
RE DISCCART        1786.30    -1636.54       874.39
RE DISCCART        1431.71    -1839.09       839.84
RE DISCCART        1163.52    -1970.51       822.92
RE DISCCART        1012.39    -1713.82       845.39
RE DISCCART        1333.71    -1513.57       860.40
RE DISCCART        1548.56    -1293.65       890.13
RE DISCCART        1814.38    -1053.65       925.16
RE DISCCART        2173.42     -859.96       908.67
```

Sample Input File: Industrial Source Complex Short-Term

```
RE DISCCART      2519.16      -672.94      873.03
RE DISCCART      2884.83      -468.15      857.34
RE DISCCART      3028.87      -379.15      848.00
RE DISCCART      3148.49      -265.83      848.00
RE DISCCART      2955.20        -2.61      875.65
RE DISCCART      2932.81       165.76      902.35
RE DISCCART      2735.18       362.50      929.57
RE DISCCART      2541.89       627.94      981.54
RE DISCCART      2271.06       835.58     1021.11
RE DISCCART      1955.86      1045.32     1001.62
RE FINISHED

ME STARTING
ME INPUTFIL C1091.BIN                   UNFORM
ME ANEMHGHT   10.000 METERS
ME SURFDATA      0  1991                SURFNAME
ME UAIRDATA      0  1991                UAIRNAME
ME WINDCATS    1.54      3.09     5.14     8.23     10.80
ME FINISHED

OU STARTING
** RECTABLE ALLAVE FIRST
OU PLOTFILE PERIOD  KPOINT      KMETK.DBF
** PLOTFILE PERIOD  ALL         KMET.DBF
OU PLOTFILE PERIOD  KTSCA       KMETT.DBF  50
** PLOTFILE PERIOD  KPOINT      KPOINT.Y12 50
** PLOTFILE PERIOD  KTSCA       KTSCA.Y12  50
** PLOTFILE 1       YPOINT      YPOINT
** PLOTFILE 1       ALL   FIRST Y9118.DBF  50
OU FINISHED
```

Sample Industrial Source Complex Long-Term Input File

```
CO STARTING
CO TITLEONE R.H. KINGREA M.S. THESIS
CO TITLETWO 1991 MET DATA FROM ORNL TOWER
CO MODELOPT DFAULT CONC   RURAL
CO AVERTIME ANNUAL
CO POLLUTID OTHER
CO DCAYCOEF    .000000
CO TERRHGTS ELEV
CO ELEVUNIT FEET
CO RUNORNOT RUN
CO ERRORFIL ERRORS.OUT
CO FINISHED


SO STARTING

** Source Location Cards:
**           SRCID SRCTYP         XS              YS           ZS

SO LOCATION  YPOINT POINT          0               0           286
SO LOCATION  XPOINT POINT      -4700           -6300           244
SO LOCATION  KPOINT POINT     -11800           -5400           247
SO LOCATION  KTSCA POINT      -11400           -5400           247

** Source Parameter Cards:
** POINT:    SRCID       QS              HS         TS          VS          DS
** VOLUME:   SRCID       QS               HS       SYINIT       SZINIT
** AREA:     SRCID       QS               HS        XINIT

SO SRCPARAM YPOINT       1               10         293         0           .5
SO SRCPARAM XPOINT       1               10         293         0           .5
SO SRCPARAM KPOINT       1               10         293         0           .5
SO SRCPARAM KTSCA        1               30.5       350         5.5       1.37
SO SRCGROUP KPOINT KPOINT
SO SRCGROUP KTSCA  KTSCA
SO FINISHED

NO ECHO
RE STARTING
RE DISCCART      1673.94    1250.71     976.96
RE DISCCART      1480.89    1334.44     993.94
RE DISCCART      1307.68    1511.29     938.07
RE DISCCART      1063.83    1422.04     896.73
RE DISCCART       784.62    1246.28     897.21
RE DISCCART       421.13    1068.09     954.36
RE DISCCART       122.04     819.14    1021.11
RE DISCCART      -183.76     618.93    1021.11
RE DISCCART      -321.17     549.89    1021.11
RE DISCCART      -558.45     531.57     965.79
RE DISCCART      -702.50     444.79     965.79
RE DISCCART      -988.48     355.43     951.36
RE DISCCART     -1294.28     159.65    1021.11
RE DISCCART     -1637.84       5.89    1021.11
RE DISCCART     -1983.56    -192.20    1021.11
RE DISCCART     -2473.62    -248.83    1021.11
RE DISCCART     -2877.25    -258.70     995.00
RE DISCCART     -2999.18    -294.46     995.00
RE DISCCART     -3273.99    -448.05     986.66
```

Sample Industrial Source Complex Long-Term Input File

```
RE DISCCART      -3539.87     -645.94     1019.22
RE DISCCART      -3978.69     -886.37      962.22
RE DISCCART      -4273.37    -1106.50      920.02
RE DISCCART      -4543.63    -1353.16      884.22
RE DISCCART      -5017.78    -1708.91      927.09
RE DISCCART      -5341.25    -1966.78      944.83
RE DISCCART      -5531.80    -2109.08      924.19
RE DISCCART      -5709.08    -2218.11      899.67
RE DISCCART      -6070.35    -2396.30      919.89
RE DISCCART      -6418.25    -2632.07      994.29
RE DISCCART      -6690.76    -2843.27     1021.11
RE DISCCART      -6910.09    -3029.97     1018.13
RE DISCCART      -7056.38    -3096.82      994.57
RE DISCCART      -7178.63    -2875.51     1011.84
RE DISCCART      -7369.50    -2767.40      978.92
RE DISCCART      -7655.73    -2659.53      946.56
RE DISCCART      -7797.86    -2513.62      907.57
RE DISCCART      -7931.17    -2323.37      900.00
RE DISCCART      -8131.23    -1958.22      860.84
RE DISCCART      -7838.73    -1766.91      828.34
RE DISCCART      -7623.80    -1617.90      789.86
RE DISCCART      -7371.17    -1462.14      794.10
RE DISCCART      -7213.96    -1264.52      770.45
RE DISCCART      -7036.71    -1126.68      785.64
RE DISCCART      -7014.82     -902.81      780.78
RE DISCCART      -6833.17     -736.15      780.78
RE DISCCART      -6751.26     -618.49      811.24
RE DISCCART      -6964.27     -543.68      792.13
RE DISCCART      -7106.27     -488.63      816.32
RE DISCCART      -7144.26     -264.90      842.66
RE DISCCART      -7129.07       -5.59      867.91
RE DISCCART      -7370.85       24.84      902.38
RE DISCCART      -7623.73       66.31      947.89
RE DISCCART      -7889.76      -11.91      984.71
RE DISCCART      -8175.69     -141.16      994.43
RE DISCCART      -8392.86     -274.66     1021.11
RE DISCCART      -8742.99     -497.14     1021.11
RE DISCCART      -9155.20     -730.86      990.91
RE DISCCART      -9390.11     -868.84      931.35
RE DISCCART      -9560.68    -1026.61      943.09
RE DISCCART      -9904.12    -1271.23      958.00
RE DISCCART     -10207.61    -1542.35      945.89
RE DISCCART     -10353.82    -1673.46      932.14
RE DISCCART     -10542.23    -1751.49      912.21
RE DISCCART     -10812.62    -1898.43      912.68
RE DISCCART     -11020.88    -2065.15      911.47
RE DISCCART     -11227.00    -2165.39      901.50
RE DISCCART     -11390.97    -2281.03      936.29
RE DISCCART     -11745.74    -2339.53      948.77
RE DISCCART     -12027.23    -2475.41      880.97
RE DISCCART     -12206.66    -2642.07      880.97
RE DISCCART     -12248.64    -2761.84      823.18
RE DISCCART     -12299.38    -2976.92      777.34
RE DISCCART     -12305.84    -3120.98      777.34
RE DISCCART     -12279.12    -3207.34      777.76
RE DISCCART     -11981.73    -3370.59      775.00
RE DISCCART     -11779.75    -3498.62      760.03
RE DISCCART     -11879.39    -3625.18      760.03
RE DISCCART     -12121.35    -3448.50      770.86
```

Sample Industrial Source Complex Long-Term Input File

```
RE DISCCART    -12403.14   -3342.83      777.76
RE DISCCART    -12540.73   -3274.48      789.53
RE DISCCART    -12660.62   -3175.05      786.91
RE DISCCART    -12765.02   -3049.00      786.91
RE DISCCART    -12715.92   -3288.21      789.53
RE DISCCART    -12911.03   -3330.80      800.00
RE DISCCART    -13167.97   -3584.07      801.00
RE DISCCART    -13345.18   -3750.72      804.62
RE DISCCART    -13546.76   -3941.81      847.82
RE DISCCART    -13620.07   -3844.48      847.82
RE DISCCART    -14069.86   -4173.58      977.12
RE DISCCART    -14322.48   -4338.20      922.99
RE DISCCART    -14468.68   -4473.75      890.37
RE DISCCART    -14769.89   -4791.39      888.59
RE DISCCART    -15062.34   -5027.02      959.55
RE DISCCART    -15241.82   -5156.00      959.55
RE DISCCART    -15405.65   -5378.02      863.42
RE DISCCART    -15554.01   -5560.11      787.70
RE DISCCART    -15726.74   -5762.20      817.14
RE DISCCART    -15848.47   -5953.08      887.96
RE DISCCART    -15912.62   -6088.42      887.96
RE DISCCART    -15930.15   -6252.46      900.00
RE DISCCART    -15927.62   -6494.00      870.64
RE DISCCART    -15969.60   -6622.64      870.64
RE DISCCART    -16064.73   -6804.59      806.43
RE DISCCART    -15660.50   -7268.96      742.09
RE DISCCART    -15370.36   -6964.63      818.05
RE DISCCART    -15171.02   -6760.26      837.14
RE DISCCART    -14827.74   -6384.89      778.00
RE DISCCART    -14668.30   -6193.91      801.03
RE DISCCART    -14515.48   -6033.97      812.73
RE DISCCART    -14327.12   -5913.83      859.01
RE DISCCART    -14151.97   -5873.51      820.09
RE DISCCART    -14001.19   -5848.76      782.74
RE DISCCART    -13865.88   -5872.80      782.74
RE DISCCART    -13779.21   -6007.76      784.97
RE DISCCART    -13683.62   -6187.02      767.73
RE DISCCART    -13556.80   -6503.60      766.06
RE DISCCART    -13729.63   -6628.13      766.06
RE DISCCART    -13864.78   -6732.63      769.86
RE DISCCART    -14075.21   -6932.60      773.95
RE DISCCART    -14259.09   -7085.96      773.88
RE DISCCART    -14227.57   -7458.19      786.97
RE DISCCART    -14091.82   -7823.50      784.78
RE DISCCART    -13931.92   -7995.95      762.14
RE DISCCART    -13683.30   -8172.62      749.88
RE DISCCART    -13257.41   -8233.61      745.36
RE DISCCART    -12915.95   -8170.71      735.77
RE DISCCART    -12576.37   -8375.95      736.15
RE DISCCART    -12261.22   -8552.45      747.09
RE DISCCART    -12054.80   -8680.47      747.09
RE DISCCART    -11589.54   -8304.79      788.70
RE DISCCART    -11144.28   -7907.01      873.69
RE DISCCART    -10885.07   -7686.97      867.33
RE DISCCART    -10685.61   -7582.32      852.30
RE DISCCART    -10423.52   -7885.27      845.06
RE DISCCART    -10110.32   -8274.51      832.66
RE DISCCART     -9852.66   -8586.34      803.59
RE DISCCART     -9608.34   -8867.17      772.26
```

Sample Industrial Source Complex Long-Term Input File

```
RE DISCCART      -9439.55     -9052.90      746.92
RE DISCCART      -9607.68     -9385.73      737.99
RE DISCCART      -9676.23     -9541.02      751.88
RE DISCCART      -9361.33     -9522.51      753.93
RE DISCCART      -9097.41     -9524.07      758.99
RE DISCCART      -8704.87     -9520.87      758.02
RE DISCCART      -8343.44     -9469.00      757.36
RE DISCCART      -8033.00     -9428.34      740.02
RE DISCCART      -7713.47     -9560.50      753.97
RE DISCCART      -7223.20     -9670.09      754.41
RE DISCCART      -6803.79     -9861.84      763.58
RE DISCCART      -2410.29     -9912.93      840.82
RE DISCCART      -2271.04     -9546.94      813.68
RE DISCCART      -2076.19     -9300.47      823.69
RE DISCCART      -1772.37     -9284.20      792.35
RE DISCCART      -1417.13     -9593.56      816.46
RE DISCCART      -1141.78     -9861.02      871.57
RE DISCCART       -469.71     -9928.04      853.34
RE DISCCART       -458.84     -9752.94      853.34
RE DISCCART       -692.10     -9445.49      832.69
RE DISCCART       -903.41     -8962.92      788.91
RE DISCCART      -1103.44     -8626.57      767.09
RE DISCCART      -1086.04     -8356.17      777.32
RE DISCCART       -948.75     -8187.41      800.88
RE DISCCART       -682.93     -7945.19      861.60
RE DISCCART       -257.23     -7851.06      863.34
RE DISCCART         70.92     -7790.40      857.73
RE DISCCART        471.94     -7472.51      833.64
RE DISCCART        569.19     -7215.20      863.42
RE DISCCART        580.09     -7064.48      857.09
RE DISCCART        400.02     -6730.31      795.26
RE DISCCART        224.47     -6458.17      754.77
RE DISCCART        108.90     -6263.44      750.00
RE DISCCART       -310.48     -6096.06      754.71
RE DISCCART       -523.50     -6007.95      754.71
RE DISCCART       -765.51     -5795.81      755.81
RE DISCCART       -967.59     -5590.22      758.13
RE DISCCART      -1154.15     -5384.60      768.85
RE DISCCART      -1172.16     -5169.68      772.27
RE DISCCART      -1090.35     -4974.46      772.27
RE DISCCART       -913.04     -4887.60      787.65
RE DISCCART       -684.63     -4873.73      789.69
RE DISCCART       -431.78     -4888.61      798.43
RE DISCCART        -50.15     -5020.62      794.86
RE DISCCART        227.26     -5168.41      810.51
RE DISCCART        507.00     -5400.40      820.84
RE DISCCART        711.31     -5614.85      822.30
RE DISCCART        895.73     -5884.75      839.14
RE DISCCART       1151.16     -6189.93      871.38
RE DISCCART       1461.73     -6251.20      913.19
RE DISCCART       1761.10     -6223.86      903.98
RE DISCCART       2042.59     -6094.63      854.63
RE DISCCART       2146.49     -5830.66      817.71
RE DISCCART       2028.52     -5491.90      790.94
RE DISCCART       1870.57     -5113.34      778.51
RE DISCCART       1830.35     -4878.54      792.24
RE DISCCART       1887.63     -4581.44      806.14
RE DISCCART       1803.03     -4320.16      811.70
RE DISCCART       1740.77     -4196.21      795.71
```

Sample Industrial Source Complex Long-Term Input File

```
RE DISCCART       1447.99    -4172.57      857.94
RE DISCCART       1290.46    -4121.99      857.94
RE DISCCART       1210.36    -3918.31      859.65
RE DISCCART       1221.14    -3672.30      830.12
RE DISCCART       1371.70    -3479.13      796.86
RE DISCCART       1502.46    -3410.10      755.91
RE DISCCART       1711.00    -3458.34      773.01
RE DISCCART       1963.98    -3584.02      760.58
RE DISCCART       2234.80    -3776.15      772.39
RE DISCCART       2563.32    -4001.37      770.97
RE DISCCART       2900.73    -4239.86      772.89
RE DISCCART       2985.07    -4295.05      781.00
RE DISCCART       3257.98    -4385.23      789.42
RE DISCCART       3530.85    -4451.03      791.46
RE DISCCART       3847.86    -4346.09      787.52
RE DISCCART       4118.16    -4134.88      751.34
RE DISCCART       4051.09    -3720.65      744.90
RE DISCCART       3999.64    -3370.64      775.00
RE DISCCART       3766.42    -3092.00      783.48
RE DISCCART       3568.82    -2926.28      790.81
RE DISCCART       3464.30    -2702.72      821.43
RE DISCCART       3499.58    -2540.86      803.65
RE DISCCART       3687.73    -2258.95      808.91
RE DISCCART       3902.37    -1877.25      819.56
RE DISCCART       4030.53    -1509.06      791.18
RE DISCCART       4156.65    -1278.28      781.00
RE DISCCART       4338.26    -1078.38      821.48
RE DISCCART       4803.88     -988.58      916.20
RE DISCCART       5196.37     -941.06      898.34
RE DISCCART       5451.33     -873.94      924.02
RE DISCCART       5630.69     -656.32      866.53
RE DISCCART       5781.12     -358.99      794.79
RE DISCCART       5738.35      139.51      764.43
RE DISCCART       5720.22      438.64      797.55
RE DISCCART       5739.94      624.84      802.32
RE DISCCART       5455.98      697.26      844.83
RE DISCCART       5282.92      754.45      844.83
RE DISCCART       5158.87      636.68      859.00
RE DISCCART       5050.37      503.45      828.38
RE DISCCART       4877.52      394.43      841.96
RE DISCCART       4629.26      289.66      845.15
RE DISCCART       4294.54      158.07      886.07
RE DISCCART       4039.56      108.69      912.89
RE DISCCART       3813.39       70.45      912.69
RE DISCCART       3450.05     -225.19      853.60
RE DISCCART       3193.07     -440.79      848.00
RE DISCCART       2982.48     -523.31      847.20
RE DISCCART       2736.49     -667.97      857.34
RE DISCCART       2889.80     -889.19      876.80
RE DISCCART       2568.43    -1049.55      902.82
RE DISCCART       2198.41    -1325.27      900.00
RE DISCCART       1786.30    -1636.54      874.39
RE DISCCART       1431.71    -1839.09      839.84
RE DISCCART       1163.52    -1970.51      822.92
RE DISCCART       1012.39    -1713.82      845.39
RE DISCCART       1333.71    -1513.57      860.40
RE DISCCART       1548.56    -1293.65      890.13
RE DISCCART       1814.38    -1053.65      925.16
RE DISCCART       2173.42     -859.96      908.67
```

Sample Industrial Source Complex Long-Term Input File

```
RE DISCCART      2519.16    -672.94     873.03
RE DISCCART      2884.83    -468.15     857.34
RE DISCCART      3028.87    -379.15     848.00
RE DISCCART      3148.49    -265.83     848.00
RE DISCCART      2955.20      -2.61     875.65
RE DISCCART      2932.81     165.76     902.35
RE DISCCART      2735.18     362.50     929.57
RE DISCCART      2541.89     627.94     981.54
RE DISCCART      2271.06     835.58    1021.11
RE DISCCART      1955.86    1045.32    1001.62
RE FINISHED

ME STARTING
ME INPUTFIL C1091.STR                   FREE
ME ANEMHGHT   10.000 METERS
ME SURFDATA       0  1991               SURFNAME
ME UAIRDATA       0  1991               UAIRNAME
ME STARDATA ANNUAL
ME AVETEMPS ANNUAL    6*287
ME AVEMIXHT ANNUAL 1 6*1962
ME AVEMIXHT ANNUAL 2 6*1308
ME AVEMIXHT ANNUAL 3 6*1308
ME AVEMIXHT ANNUAL 4 6*1308
ME AVEMIXHT ANNUAL 5 6*507
ME AVEMIXHT ANNUAL 6 6*507
ME FINISHED

OU STARTING
** MAXTABLE 5 INDSRC
OU PLOTFILE ANNUAL  KPOINT          C:\123R23\KPOINT.DBF
OU PLOTFILE ANNUAL  KTSCA           C:\123R23\KTSCA.DBF
** PLOTFILE ANNUAL  YPOINT          C:\123R23\YPOINT.DBF
** PLOTFILE ANNUAL  XPOINT          C:\123R23\XPOINT.DBF
OU FINISHED
```

VITA

Rodney Howard Kingrea was born in Roanoke, Virginia, on November 13, 1961. He graduated from high school in Greenfield, Indiana, and attended Purdue University in West Lafayette, Indiana, where he obtained Bachelor of Science degrees in atmospheric science (meteorology) and environmental engineering. In May 1993, he completed requirements for a Master of Science Degree in environmental engineering at the University of Tennessee, Knoxville.

Upon graduating from Purdue University in May 1984, he was employed by Martin Marietta Energy Systems, Inc., in Oak Ridge, Tennessee, as an Environmental Engineer until October 1987. Between 1987 and 1990, he was employed by Allied Signal in Elyria, Ohio, and Lexington, Kentucky, as a Senior Environmental Engineer and Manager of Health, Safety, and Environmental Protection, respectively. He is currently employed by Martin Marietta Energy Systems, Inc., in Oak Ridge, Tennessee, as Clean Air Act Compliance Program Manager.